

**Integrating Urban Hydrology, Social Vulnerability, and Fluvial  
Ecosystem Modeling into Green Infrastructure and Stream  
Restoration Planning**

---

A  
Dissertation  
Presented to  
the faculty of the School of Engineering and Applied Science  
University of Virginia

---

in partial fulfillment  
of the requirements for the degree

Doctor of Philosophy

by

Robert Seth Herbst

December 2023

# APPROVAL SHEET

This  
Dissertation  
is submitted in partial fulfillment of the requirements  
for the degree of  
Doctor of Philosophy

Author: Robert Seth Herbst

This Dissertation has been read and approved by the examining committee:

Advisor: Teresa B. Culver

Advisor: Lawrence E . Band

Committee Chair: Jonathan L. Goodall

Committee Member: Julianne D. Quinn

Committee Member: Bev Wilson

Accepted for the School of Engineering and Applied Science:



Jennifer L. West, School of Engineering and Applied Science

December 2023

## Dissertation Abstract

This dissertation details research that advances green infrastructure (GI) and stream restoration modeling by integrating an equity objective into GI optimization, experimenting with a novel method of assessing restoration effects on dissolved inorganic nitrogen (DIN) uptake, and developing an integrated model for assessing the impacts of GI on in-stream DIN processing. Urban development has intensified stormwater runoff, flow velocities, and nutrient loads in streams, degrading natural channels and water bodies. To address these issues, stormwater GI and stream restoration are often cited as viable solutions. This dissertation enhances modern GI and restoration modeling in three areas. Chapter 1 explains the research motivations of chapters 2,3, and 4. Chapter 2 details the integration of a spatial social equity objective (LID/GI-Social vulnerability (SVI) index correlation objective) into a GI optimization model, that promotes equitable GI implementation in socially vulnerable areas. Chapter 3 presents a novel adaptation of the Small Streams Hydro-Biochemistry Simulator (SSHBS) to assess the impact of various riffle, pool, and meander configurations on DIN uptake dynamics in an urban stream reach. Chapter 4 introduces a watershed-channel hydraulic stream-ecosystem model that is integrated into a single open-source Python notebook to evaluate the effects of GI on in-stream DIN processing.

Chapter 2's analysis details the development of the LID/GI-SVI correlation objectives, which directs optimization algorithms towards runoff management and equitable GI distribution goals and allows for tradeoff analyses between local hydrologic and equity goals. Chapter 3's findings show how SSHBS can be a promising option for process-based assessments of stream restoration designs and how benthic area augmentation, riparian canopy removal, and multi-feature channel designs can enhance simulated net DIN uptake in streams. Chapter 4 highlights the usefulness of an integrated model with results showing that: A relatively low percentage (0.86%) of DIN that enters a local urban stream from the watershed is retained or removed by the stream; Stream zones with higher light combined with lower leaf-litter have greater potential net DIN uptake; Higher groundwater DIN concentrations combined with infiltration-based GI could result in elevated in-stream concentrations and export of DIN.

# Table of Contents

Dissertation Abstract.....	iii
List of Figures .....	vii
List of Tables .....	xi
Acknowledgments.....	xiii
Related Publication and Presentations.....	xiv
<i>Chapter 1:Introduction.....</i>	<i>1</i>
1.0 Research Motivations.....	1
1.1 Chapter 1 Works Cited.....	6
<i>Chapter 2: Integrating Social Equity into Multi-Objective Optimization of Urban Stormwater Low Impact Development.....</i>	<i>9</i>
Chapter 2 Abstract .....	9
2.0 Introduction .....	10
2.1 Methods .....	15
2.1.1 Study Area Description.....	15
2.1.2 Calculating a social equity index for the Meadow Creek Subbasins .....	18
2.1.3 Feasible Area and Cost Constraints on LID/GI Distributions .....	20
2.1.4 The upper Meadow Creek SWMM Model .....	25
2.1.5 The Multi-Objective Optimization Formulation .....	26
2.1.6 Coupling SWMM and Borg.....	28
2.1.7 Tradeoff Analysis .....	31
2.2 Optimization Results .....	32
2.2.1 Quantifying the impact of integrating the LID/GI-vulnerability correlation on $\epsilon$ - nondominated LID/GI distributions and compositions with a forty-million- dollar cost constraint .....	32
2.2.2 Cost-Benefit analysis of the three formulations .....	37
2.2.3 Quantifying the sensitivity of hydrologic performance to changes in $\rho$ value choices.....	38
2.3 Discussion.....	40

2.3.1 The impacts of the LID/GI-equity correlation objective on LID/GI distributions, LID/GI type compositions, and equitability at the forty-million-dollar cost constraint.....	40
2.3.2 The impacts of the LID/GI-equity correlation objective on hydrologic performance and equity at multiple cost constraints.....	41
2.3.3 Recommendations and Insights.....	42
2.3.4 Scope and Limitations.....	43
2.4 Conclusions .....	45
2.5 Chapter 2 Works Cited.....	46
<i>Chapter 3: Simulating the Effects of Channel Restoration Designs on in-Stream Nitrogen Uptake.....</i>	<i>54</i>
Chapter 3 Abstract .....	54
3.0 Introduction .....	55
3.0.1 Study Area .....	58
3.1 Methods .....	59
3.1.1 Simulating in-stream flow with SSHBS.....	59
3.1.2 Simulating in-stream nutrient flux with SSHBS.....	60
3.1.3 Simulating N Uptake Rates for Riffle, Pool, and Meander Channel Restoration Scenarios Under Open and Closed Canopy Conditions.....	61
3.2 Results .....	66
3.3 Discussion .....	78
3.3.1 Case Study Outcomes .....	78
3.3.2 The Lessons, Limitations, and Future Work.....	80
3.4 Conclusions .....	83
3.5 Chapter 3 Works Cited.....	85
<i>Chapter 4: Estimating the Impacts of Green Infrastructure on Nitrogen Uptake in an Urban Stream through the Integration of Watershed, Channel Hydraulic, and Ecosystem models.....</i>	<i>88</i>
Chapter 4 Abstract .....	88
4.0 Introduction .....	89
4.0.1 Case Study Area .....	93
4.1 Methods .....	94

4.1.1 Developing an Integrated Ecosystem Service Model for Meadow Creek.....	94
4.1.2 Calibrating and Validating the Integrated Model.....	95
4.1.3 SWMM Model.....	99
4.1.4 HEC-RAS as the stream flow hydraulics module.....	101
4.1.5 STOICMOD-SSHBS as the stream nutrient processing module.....	102
4.1.6 GI Scenario Analysis.....	108
4.2 Results.....	110
4.2.1 Integrated Model Calibration and Validation.....	110
4.2.2 Simulated Stream Ecosystem DIN Processing Rates.....	114
4.2.3 Simulated Impacts of GI scenarios on in-stream N uptake.....	117
4.3 Discussion.....	124
4.3.1 Assessment of the Integrated Model.....	124
4.3.2 Simulated Impacts of Green Infrastructure on N Processing in the Stream.....	126
4.3.3 Reducing DIN Export: Terrestrial and Fluvial Environment Contributions.....	129
4.3.4 Simulated Impacts of Green Infrastructure on N Processing in the Stream.....	130
4.4 Conclusions.....	132
4.5 Data Availability Statement.....	133
4.6 Chapter 4 Works Cited.....	134
<i>Chapter 5: Concluding Remarks</i> .....	139
5.0 Dissertation Conclusions and Future Research Opportunities.....	140
Appendix A .....	144
Appendix B.....	148
Appendix C.....	153

## List of Figures

<b>Figure 2-1:</b> The upper Meadow Creek Watershed, Meadow Creek, and its restored reaches within the larger Rivanna River Watershed located in central Virginia, U.S.A (Source: ESRI World Topographic Map).....	18
<b>Figure 2-2:</b> Census Block Group Demographic Index Values (left) mapped to the Upper Meadow Creek Subbasins (right) using an area-weighted averaging approach.....	20
<b>Figure 2-3:</b> A simplified workflow diagram of the SWMM-BORG LID/GI optimization model.....	29
<b>Figure 2-4:</b> $\mathcal{E}$ -nondominated green LID/GI area distributions and performance summary for selected solutions at the forty-million-dollar cost constraint under the Hydrologic (a), Equitable (b), and Hydro-Equitable (c) formulations.....	34
<b>Figure 2-5.</b> Percentage of green LID/GI implemented within subbasins vs. subbasin SVI values.....	35
<b>Figure 2-6:</b> LID/GI type composition percentages (%) of selected solutions from each formulation under the forty-million-dollar cost constraint.....	36
<b>Figure 2-7:</b> Cost-Benefit Curve for average peak stream flow (left),total runoff export (middle), LID/GI-SVI correlation (right).....	38
<b>Figure 2-8:</b> Average hydrologic performance of $\mathcal{E}$ -nondominated solutions at each cost constraint according to $\rho$ interval.....	39
<b>Figure 3-1:</b> Scotts Level Branch study area and unrestored outlet reach.....	59
<b>Figure 3-2:</b> Flow diagram of ecosystem processes involved in modeling carbon, nitrogen, and phosphorus flux using SSHBS.....	61
<b>Figure 3-3:</b> The eight plan-view depiction of the channel restoration scenarios that were evaluated in this study. (Graph axes are not to-scale.) .....	65
<b>Figure 3-4:</b> Simulated whole reach DIN uptake and release rates in kilograms per day by season between 2012 – 2017 at SLB.....	67
<b>Figure 3-5:</b> Simulated PAR results from the RHESSys model at the SLB whole reach under closed and open canopy conditions.....	67
<b>Figure 3-6:</b> Changes in annual whole reach denitrification relative to the closed-canopy unrestored scenario.....	69
<b>Figure 3-7:</b> Dunn test for non-parametric pairwise comparison results for whole reach denitrification. Black squares indicate that there was not a significant difference between paired scenarios ( $p > 0.05$ ).....	69
<b>Figure 3-8:</b> Changes in annual whole reach algal DIN uptake relative to the closed-canopy unrestored scenario.....	71

<b>Figure 3-9:</b> Dunn test for non-parametric pairwise comparison results for whole reach algal DIN uptake and mineralization. Black squares indicate that there was not a significant difference between paired scenarios ( $p > 0.05$ ).....	71
<b>Figure 3-10:</b> Changes in whole reach annual DIN mineralization relative to the closed-canopy unrestored scenario.....	73
<b>Figure 3-11:</b> Changes in whole reach annual Net DIN uptake relative to the closed-canopy unrestored scenario.....	74
<b>Figure 3-12:</b> Dunn test for non-parametric pairwise comparison results for whole reach net DIN uptake. Black squares indicate that there was not a significant difference between paired scenarios ( $p > 0.05$ ).....	75
<b>Figure 3-13:</b> Simulated daily DIN uptake per square meter and release rates by season between 2012 – 2017 at SLB .....	77
<b>Figure 3-14:</b> Benthic area by season for each of the channel restoration scenarios.....	78
<b>Figure 4-1:</b> The upper Meadow Creek study area location (A), land cover (B), and zoning (C).93	
<b>Figure 4-2:</b> Integrated Watershed-Stream Ecosystem Model Diagram.....	95
<b>Figure 4-3:</b> The upper Meadow Creek reach zones, subbasins, major tributaries, and nutrient grab sampling points at each zone.....	99
<b>Figure 4-4:</b> The 1m DEM used in the HEC-RAS model for Meadow Creek with cross-sections at 30m intervals.....	102
<b>Figure 4-5:</b> Carbon, nitrogen, and phosphorus processing pathways as modeled with STOICMOD-SSHBS equations.....	103
<b>Figure 4-6:</b> Time series graphs for daily flow calibration (upper graph) and validation (lower graph).....	111
<b>Figure 4-7:</b> Time series showing observed and modeled DIN concentrations for each reach zone during the calibration and validation periods .....	112
<b>Figure 4-8:</b> Measured (blue) and simulated (orange) DIN loads from zone 3 over the simulation period.....	113
<b>Figure 4-9:</b> Monthly primary production and ecosystem respiration at each section as modeled with BASE and our integrated model.....	114
<b>Figure 4-10:</b> Modeled algal DIN uptake, denitrification, immobilizer N assimilation, and N mineralization daily rates for reach zones 1, 2, and 3. Net mineralization is graphed and tabulated as a negative value since it adds N back into the water column, counter to the other simulated processes.....	115
<b>Figure 4-11:</b> Daily standing stocks of algal and detritus biomass per square meters of benthic area at each zone over the two-year simulation period.....	117

**Figure 4-12:** Simulated percent changes in daily DIN spiraling variables at the three zones under the nine rain garden scenarios. Raingarden scenarios are numbered at the bottom according to the subbasin where single 10 x 10-meter raingardens were implemented at all residential parcels. The numbers in brackets on the left indicate the zone.....118

**Figure 4-13:** Simulated percent changes in daily DIN spiraling variables at the three zones under the eight green roof scenarios. Green roof scenarios are numbered at the bottom according to the subbasin where commercial roof areas were converted to green roofs in SWMM. The numbers in brackets on the left indicate the zone.....120

**Figure 4-14:** Simulated percent changes in daily DIN spiraling variables at the three zones under the nine impervious conversions to green space scenarios. Impervious conversion scenarios are numbered at the bottom according to the subbasin where 25% of the impervious surfaces were converted to tree canopy and grasses. The numbers in brackets on the left indicate the zone...121

**Figure 4-15:** Hydrograph for stormflow and post-stormflow illustrating the impact of GI scenarios at subbasin 1 on peak flow within zone reach 1. Note that green roofs do not appear to be the best option for peak flow reduction but may be best for reducing DIN input into the stream.....132

**Figure A-1:** Hydrograph and hyetograph for 8/9 April 2021 calibration storm event.....144

**Figure A-2:** Hydrograph and hyetograph for 3/4 June 2021 validation storm event 1.....145

**Figure A-3:** Hydrograph and hyetograph for 10/11 June 2021 validation storm event 2.....145

**Figure A-4:** Hydrograph and hyetograph for 22/23 June 2021 validation storm event 3.....146

**Figure A-5:** Hydrograph and hyetograph for 22/23 Mar 2022 validation storm event 4.....146

**Figure A-6:** Hydrograph and hyetograph for 22/23 June 2022 validation storm event 5.....147

**Figure C-1:** Distribution of  $\delta^{15}\text{N}$  and  $\delta^{18}\text{O}$  from different nitrate sources. Figure created by de Azevedo Torrellas (2021).The isotope ranges and denitrification lines were taken from Zhang et al., 2019. This figure shows that the most significant source of nitrate in the upper Meadow Creek watershed is likely leaky sewage and sanitary systems. MC1 -7 (seen on the right) are the 7 different sampling points along upper Meadow Creek from upstream to downstream. Point MC4 corresponds to the sampling point at zone reach 1 at this paper and MC7 corresponds to the sampling point at zone 3.....153

**Figure C-2:** Sampling points for isotope analysis. Note: These points are more numerous than the sampling points used in chapter 4.....154

**Figure C-3:** Dissolved inorganic nitrogen (DIN) Concentration vs. Discharge at Zone 3 of Upper Meadow Creek at baseflow. This graph suggests a slightly negative relationship between DIN concentrations and discharge at Meadow Creek.....154

**Figure C-4:** Leaf-litter C inputs per square meter at each reach zone. Webster et. al (2016) leaf-litter inputs include a spike in leaf-litter fall during the October leaf-out period each year. Zone 2

leaf-litter fall is 50% of the other zone reaches due to its relatively lack in tree-  
canopy.....155

**Figure C-5:** Simulated percent changes in daily DIN spiraling variables at the three zones under the nine rain garden scenarios on a per hectare implemented basis. Raingarden scenarios are numbered at the bottom according to the subbasin where single 10 x 10-meter raingardens were implemented at all residential parcels. The numbers in brackets on the left indicate the zone...156

**Figure C-6:** Simulated percent changes in daily DIN spiraling variables at the three zones under the nine impervious conversions to green space scenarios on a per hectare implemented basis. Impervious conversion scenarios are numbered at the bottom according to the subbasin. The numbers in brackets on the left indicate the zone.....157

## List of Tables

<b>Table 2-1:</b> GIS layers and physical criteria of feasible areas for each LID type.....	21
<b>Table 2-2:</b> Land uses used to approximate the feasible areas for each LID type.....	22
<b>Table 2-3:</b> Total Allowable Area for each LID Type.....	23
<b>Table 2-4:</b> Estimated Construction Costs for each LID type.....	24
<b>Table 2-5:</b> Chosen $\epsilon$ values for each objective.....	31
<b>Table 2-6:</b> Percentage of green LID area implementation by SVI percentile for the three formulations.....	36
<b>Table 3-1:</b> Slopes and Mannings N values for each of the reach features.....	63
<b>Table 3-2:</b> Channel Restoration Scenarios and Feature Lengths.....	64
<b>Table 3-3:</b> Changes in median denitrification rates by season in grams per day for each reach scenario relative to the closed canopy unrestored scenario.....	70
<b>Table 3-4:</b> Changes in median algal DIN uptake by season in grams per day for each reach scenario relative to the closed canopy unrestored scenario.....	72
<b>Table 3-5:</b> Changes in median mineralization rates by season in grams per day for each reach scenario relative to the closed canopy unrestored scenario.....	73
<b>Table 3-6:</b> Changes in the median net DIN uptake by season in grams per day for each reach scenario relative to the closed canopy unrestored scenario.....	75
<b>Table 3-7:</b> Expected percent reductions in net DIN uptake if riparian canopy regrows for the eight channel restoration scenarios.....	76
<b>Table 4-1:</b> Land use composition for each subbasin.....	98
<b>Table 4-2:</b> Calibrated groundwater and event mean dissolved inorganic nitrogen concentration.....	101
<b>Table 4-3:</b> Number of rain garden parcels, commercial green roof area, and impervious conversions areas for each of the 26 GI scenarios.....	110
<b>Table 4-4:</b> Mean absolute error values for daily DIN concentrations for the calibration and validation periods.....	111
<b>Table 4-5:</b> Primary Production and Ecosystem Respiration MAE values between BASE and our integrated model.....	113
<b>Table 4-6:</b> Simulated average daily velocity and DIN concentrations for the status-quo and the GI scenarios at subbasin 1 at the four flow quantiles.....	123
<b>Table A-1:</b> Summary of individual storm event calibration and validation results for chapter 2.....	144

**Table C-1:** STOICMOD-SSHBS in-stream ecosystem parameters. Asterisks (\*) by the value indicate that it is a calibrated value. Otherwise, values were obtained by Lin et al. (2021) and Webster et al. (2016).....158

**Table C-2:** Minimum, mean, and maximum simulated uptake rates at each zone.....158

**Table C-3:** Minimum, mean, and maximum benthic algae and detritus mass at each zone.....159

**Table C-4:** N inputs into the stream from the subbasin, total uptake from each zone reach, and the total % uptaken by the stream ecosystem under the status quo scenario.....159

**Table C-5:** N inputs into the stream from the subbasin, total uptake from each zone reach, and the total % uptake by the stream ecosystem under the rain garden scenarios.....159

**Table C-6:** N inputs into the stream from the subbasin, total uptake from each zone reach, and the total % uptake by the stream ecosystem under the green roof scenarios.....160

**Table C-7:** N inputs into the stream from the subbasin, total uptake from each zone reach, and the total % uptake by the stream ecosystem under the impervious surface conversion scenarios.....160

## Acknowledgements

Funding for this dissertation was graciously provided by the University of Virginia through several sources, including the "3-Cavaliers" grant, Dean's Scholar Fellowship funding, the Graduate Assistance in Areas of National Need (GAANN) grant, and the Virginia Water Resources Research Center (VWRRC) 2022 competitive grant. I extend my gratitude to Research Computing (RC) at the University of Virginia for their invaluable support and access to computational resources, which significantly contributed to the outcomes of this dissertation (URL: <https://rc.virginia.edu>). Special thanks to Computational Hydraulics International (CHI) for granting access to PCSWMM through their educational grant program.

My dissertation committee played a pivotal role in shaping my PhD journey and facilitating the completion of this dissertation. I am deeply thankful to Dr. Teresa Culver for introducing me to optimization techniques in water resources, guiding me through the complexities of graduate school administration, and encouraging the development of my grant writing skills. Dr. Lawrence Band's unwavering support, provision of fieldwork resources, and weekly guidance in improving my dissertation projects have been instrumental. Dr. Julianne Quinn's dedicated assistance in overcoming challenging programming issues has been invaluable, and Dr. Bev Wilson's collaboration on local social equity matters has been enlightening. Dr. Jonathan Goodall imparted essential GIS analysis skills that underpin my dissertation projects.

I extend my appreciation to Kazi Tamaddun, Zach Perkins, Emilia Torrellas, Ruoyu Zhang, Meredith Hoos, and other post-doctoral staff and graduate students at the University of Virginia for their valuable contributions in field monitoring and GIS support. Additionally, I am grateful to Greg Harper, Chief of Environmental Services for Albemarle County, and Andrea Henry, PE, Water Resources Protection Administrator from the Public Works Department in the City of Charlottesville, for providing essential information on local GI planning, preliminary model data, and drainage documentation for the study area.

Finally, I would like to express my heartfelt thanks to my wife who helped me navigate the trials and tribulations of being a PhD graduate student and for being an exemplary hard-working scientist and professional. I also want to thank her along with my friends and family for their unwavering support, especially during the challenges posed by the pandemic years and throughout my graduate studies. This achievement would not have been possible without your presence and encouragement.

## Related Publications

**Chapter 1:** Herbst, R. Seth., Culver, Teresa. B., Band, Lawrence. E., Wilson, Bev., & Quinn, Julianne D. (2023). Integrating Social Equity into Multiobjective Optimization of Urban Stormwater Low-Impact Development. *Journal of Water Resources Planning and Management*, 149(8).

**Chapter 2:** Herbst, R. Seth., Band, Lawrence. E., Culver, Teresa. B., Simulating the Effects of Channel Restoration Designs on in-Stream Metabolism and Nitrogen Uptake. (\*Manuscript almost prepared for submission)

**Chapter 3:** Herbst, R. Seth., Band, Lawrence. E., Culver, Teresa. B. Estimating the Impacts of Green Infrastructure on Nitrogen Uptake in an Urban Stream through the Integration of Watershed, Channel Hydraulic, and Ecosystem models. (\*Manuscript almost prepared for submission)

### Other Publications:

Saby, Linnea., Herbst, R. Seth., Goodall, Jonathan., Nelson D. Jacob., Culver, Teresa. B., Stephens, Emma., Marquis, M. Caroline., Lawrence E. Band. (2023). Assessing and improving the outcomes of nonpoint source water quality trading policies in urban areas: A case study in Virginia. *Journal of Environmental Management*, 345(August)

## Related Presentations

1. Herbst, R. Seth., Culver, Teresa, B., Band, Lawrence, E. “Integrating Social Equity into Multi-objective Optimization for Low Impact Development. Abstract for oral presentation. Environmental & Water Resources Institute Congress, June 2022.
2. Herbst, R. Seth., Culver, Teresa, B., Band, Lawrence, E. “Integrating Social Equity in Multi objective Optimization for Low Impact Development. Abstract for poster presentation, Council of Engineering Systems Universities Engineering Systems Symposium, October 2021.
3. Herbst, R. Seth. Band, Lawrence, E. , Culver, Teresa, B. “Comparing stream metabolism and ecosystem health in restored and unrestored reaches of Meadow Creek.” Abstract for oral presentation, Environmental & Water Resources Institute Congress, June 2021

# **Chapter 1: Introduction**

## **1.0 Research Motivations**

The expansion and concentrated development of impervious surfaces has presented a number of problems for local stream ecosystems as well as human inhabitants. Not only has increased urbanization facilitated the impairment of local streams through the intensification of stormwater runoff and elevated nutrient loads (USEPA, 2023), but it has also contributed to the decline in human livability, especially for socially vulnerable communities, by elevating temperatures due to the urban heat island effect (Sekertekin & Zadbagher, 2021), reducing green space and recreational opportunities (Gerecke et al., 2019), and increased flooding (Zhang et al., 2018) among other drawbacks. Civil and environmental engineers have a prominent role in shaping the development of urban areas and have promoted the expansion of green infrastructure (GI) and stream restoration projects to regain some of the ecosystem services that have been lost. Although there are myriads of analytical tools and techniques that can help city planners estimate the potential benefits of GI and stream restoration projects before they take place, there is a pronounced lack of integrated models that account for more than just a single component of the urban system. GI modeling tools typically only consider hydrologic aspects of the watershed without considering the distribution of social benefits that could arise from city-scale GI implementation, nor have these models assumed the ability to quantify the impacts to in-stream ecosystem functionality that can arise from the urban GI. In addition, stream restoration project plans are generally not assessed with process-based models of their potential benefits to in-stream ecosystem functionality or within the context of the larger terrestrial watershed, but

instead, have almost strictly considered physical corrections to the channel form with the assumption that ecosystem functional restoration will follow.

Green infrastructure (GI) is frequently lauded for its capacity to address stormwater-related challenges in communities. However, it has also gained recognition for its potential to provide a range of ecosystem services to the areas where it is implemented (Madureira & Andresen, 2014; Scott et al., 2016). For instance, specific types of GI have demonstrated their effectiveness in mitigating the urban heat island effect (Block et al., 2014; Santamouris, 2014). GI generally leads to increased property values in accessible regions (Du & Zhang, 2020; Mazzotta et al., 2014) and can contribute to energy conservation and the generation of green employment opportunities (Celik & Binatli, 2018). Furthermore, GI has the potential to enhance the visual appeal of urban landscapes and play a role in enhancing the mental well-being and safety of the local community (Kondo et al., 2015; Roe et al., 2013; Wolch et al., 2014). However, it's important to acknowledge GI and its associated benefits are often distributed inequitably within cities (Keeler et al., 2019; Mell & Whitten, 2021; Porse, 2018). In the United States, urban inequality is closely tied to factors like race and poverty rates. Historically, African Americans and other ethnic minorities have deliberately faced marginalization concerning neighborhood investment, infrastructure planning processes, and other aspects of public decision-making (Wright, 2021).

To devise strategic and efficient distributions of Green Infrastructure (GI), engineering researchers have combined advanced heuristic multi-objective optimization tools with hydrologic models. This approach helps identify near-optimal GI configurations that not only minimize costs but also reduce the impact of urban development on runoff (Eckart et al., 2018; Giacomoni et al., 2017; Sebti et al., 2016; Zhang & Chui, 2018). Chapter 2 of this dissertation

addresses a specific gap in the existing GI-optimization literature. While several studies have focused on GI optimization, there has been little consideration of the equity implications of these optimal distributions or how including an equity objective might alter optimization outcomes. Enhancing access to GI benefits in socially vulnerable communities is now a key priority for local policymakers and infrastructure planners. Chapter 2 explores the consequences of integrating a novel spatial social equity objective into an urban GI optimization model.

The fundamental concept behind the widely used stream restoration method known as "Natural Channel Design" (NCD) is the close interconnection between the physical structure of stream channels and their ecological functionality (Rosgen, 1998), including in-stream nutrient retention. Consequently, most assessments and models related to stream restoration have primarily focused on understanding the relationship between modifications to channel form and their effects on in-stream flow dynamics and sediment patterns. However, there have been notable objections to this perspective, particularly from academics critical of NCD. These critics argue that solely manipulating channel form is insufficient for restoring the ecological function of rivers without considering ecological, chemical, and biological processes (Wohl et al., 2015; Palmer et al., 2014; Simon et al., 2007). They advocate for the integration of ecosystem process-based approaches to assess the effectiveness of stream restoration designs. As highlighted by Wohl et al. (2015), there is a growing demand for a deeper understanding of how various aspects of physical complexity contribute to biogeochemical processes influencing nutrient retention, stream ecosystem productivity, and the degradation of contaminants.

Since the late 20th century, designers of stream restoration projects have had access to various modeling tools to predict the effects of channel modifications on streamflow and sediment patterns. However, these models often lack the capability to account for integrated

hydraulic and ecosystem processes involved in nutrient transport and retention. More recently, process-based models have emerged to help estimate the nutrient retention and removal that can result from different stream restoration designs. Chapter 3 details a novel application of such a model, the Small Streams Hydro-Biogeochemistry Simulator (SSHBS – Lin et al., 2021), by testing its ability to evaluate potential impacts to the rates of dissolved inorganic nitrogen (DIN) uptake and retention in an urban stream that can arise from a variety of riffle, pool, and meandering channel configurations. Although it's important to note that while SSHBS has been validated with detailed in-stream measurements in our experimental stream reach, our specific simulation results lack empirical validation. However, the study underscores the practicality of employing SSHBS as a modeling tool for stream restoration designers and how it can be valuable for estimating the impacts of geomorphic restoration features on net DIN uptake rates, which suggests strong potential for enhancing current methodologies for stream restoration design.

Typically, assessments of urban landscape restoration plans focus on model simulations to gauge the benefits of GI, such as managing stormwater runoff, reducing pollutants, and mitigating urban heat (Fletcher et al., 2013; Pataki et al., 2011). However, these modeling studies often lack the capability to shed light on the potential impacts of watershed GI on stream ecosystem processes by regulating upland runoff and nutrient loading regimes. Grimm et al. (2003) highlighted a persistent gap in the coupling of stream-reach models with watershed models, a situation that remains unchanged today. They argued that addressing management challenges like eutrophication necessitates comprehensive analytical tools that encompass both terrestrial and fluvial components.

While various models exist for assessing GI's effects on stormwater runoff and groundwater, and for estimating alterations in channel hydraulics due to different runoff and baseflow conditions, and even the evaluation of in-stream ecosystem processes, no model to date has treated these elements as an interconnected system. As such, chapter 4 addresses the lack of accessible modeling tools that mechanistically link watershed runoff, nutrient sources, channel hydraulics, and aquatic ecosystems to evaluate GI's impact on nutrient reduction and urban stream dynamics. It details the development and calibration of an integrated watershed-channel hydraulic stream-ecosystem model, packaged into a single open-source Python notebook. The novel integrated model couples the Stormwater Management Model (SWMM), Hydrologic Engineering Center's River Analysis System (HEC-RAS), and stream channel metabolism modules from Stream Model Based on Spiraling and Ecological Stoichiometry Specific Fluxes (STOICMOD) and Small Streams Hydro Biogeochemistry Simulator (SSHBS). Chapter 4 shows the integrated model's utility and limitations in assessing GI's effects on urban streams and provides insights applicable to local watershed management and suggests future development of the integrated modeling goal.

In summary, this dissertation explores new methods for modeling GI and stream restoration, integrating urban social vulnerability and stream ecosystem dynamics. These approaches enhance conventional practices, typically focused on isolated elements within urban hydrology. Adopting these methods allows for more flexible strategies applicable to diverse areas, surpassing current limitations and seeking a comprehensive understanding of urban water environments.

## 1.1 Chapter 1 Works Cited

- Block, A. H., Livesley, S. J., & Williams, N. S. G. (2014). *Responding to the Urban Heat Island: A Review of the Potential of Green Infrastructure Literature Review*. [www.vcccar.org.au](http://www.vcccar.org.au)
- Celik, S., & Binatli, A. O. (2018). Energy Savings and Economic Impact of Green Roofs : A Pilot Study Energy Savings and Economic Impact of Green Roofs : A Pilot Study. *Emerging Markets Finance and Trade*, 54(8), 1778–1792. <https://doi.org/10.1080/1540496X.2018.1434620>
- Du, M., & Zhang, X. (2020). Land Use Policy Urban greening : A new paradox of economic or social sustainability ? *Land Use Policy*, 92(December 2019), 104487. <https://doi.org/10.1016/j.landusepol.2020.104487>
- Eckart, K., McPhee, Z., & Bolisetti, T. (2018). Multiobjective optimization of low impact development stormwater controls. *Journal of Hydrology*, 562, 564–576. <https://doi.org/10.1016/j.jhydrol.2018.04.068>
- Fletcher, T. D., Andrieu, H., & Hamel, P. (2013). Understanding, management and modelling of urban hydrology and its consequences for receiving waters: A state of the art. *Advances in Water Resources*, 51, 261–279. <https://doi.org/10.1016/j.advwatres.2012.09.001>
- Gerecke, M., Hagen, O., Bolliger, J., Hersperger, A. M., Kienast, F., Price, B., & Pellissier, L. (2019). Assessing potential landscape service trade-offs driven by urbanization in Switzerland. *Palgrave Communications*, 5(1), 1–13. <https://doi.org/10.1057/s41599-019-0316-8>
- Giacomoni, M. H., & Joseph, J. (2017). Multi-objective evolutionary optimization and Monte Carlo simulation for placement of low impact development in the catchment scale. *Journal of Water Resources Planning and Management*, 143(9). [https://doi.org/10.1061/\(ASCE\)WR.1943-5452.0000812](https://doi.org/10.1061/(ASCE)WR.1943-5452.0000812)
- Grimm, N. B., Gergel, S. E., McDowell, W. H., Boyer, E. W., Dent, C. L., Groffman, P., Hart, S. C., Harvey, J., Johnston, C., Mayorga, E., McClain, M. E., & Pinay, G. (2003). Merging aquatic and terrestrial perspectives of nutrient biogeochemistry. *Oecologia*, 137(4), 485–501. <https://doi.org/10.1007/s00442-003-1382-5>
- Keeler, B. L., Hamel, P., McPhearson, T., Hamann, M. H., Donahue, M. L., Meza Prado, K. A., Arkema, K. K., Bratman, G. N., Brauman, K. A., Finlay, J. C., Guerry, A. D., Hobbie, S. E., Johnson, J. A., MacDonald, G. K., McDonald, R. I., Neverisky, N., & Wood, S. A. (2019). Social-ecological and technological factors moderate the value of urban nature. In *Nature Sustainability* (Vol. 2, Issue 1, pp. 29–38). Nature Publishing Group. <https://doi.org/10.1038/s41893-018-0202-1>
- Kondo, M. C., Low, S. C., Henning, J., & Branas, C. C. (2015). *The Impact of Green Stormwater Infrastructure Installation on Surrounding Health and Safety*. 105(3), 114–121. <https://doi.org/10.2105/AJPH.2014.302314>
- Lin, L., Reisinger, A. J., Rosi, E. J., Groffman, P. M., & Band, L. E. (2021). Evaluating Instream Restoration Effectiveness in Reducing Nitrogen Export from an Urban Catchment with a Data-Model Approach. *Journal of the American Water Resources Association*, 57(3), 449–

473. <https://doi.org/10.1111/1752-1688.12922>

- Madureira, H., & Andresen, T. (2014). Planning for multifunctional urban green infrastructures: Promises and challenges. *Urban Design International*, 19(1), 38–49. <https://doi.org/10.1057/udi.2013.11>
- Mazzotta, M. J., Besedin, E., & Speers, A. E. (2014). A meta-analysis of hedonic studies to assess the property value effects of low impact development. In *Resources* (Vol. 3, Issue 1). <https://doi.org/10.3390/resources3010031>
- Mell, I., & Whitten, M. (2021). Access to nature in a post covid-19 world: Opportunities for green infrastructure financing, distribution and equitability in urban planning. *International Journal of Environmental Research and Public Health*, 18(4), 1–16. <https://doi.org/10.3390/ijerph18041527>
- Palmer, M. A., Hondula, K. L., & Koch, B. J. (2014). Ecological restoration of streams and rivers: Shifting strategies and shifting goals. *Annual Review of Ecology, Evolution, and Systematics*, 45(1), 247–269. <https://doi.org/10.1146/annurev-ecolsys-120213-091935>
- Pataki, D. E., Carreiro, M. M., Cherrier, J., Grulke, N. E., Jennings, V., Pincetl, S., Pouyat, R. V., & Whitlow, T. H. (2011). Coupling biogeochemical cycles in urban environments: ecosystem services, green solutions. In *Ecology and the Environment* (Vol. 9, Issue 1).
- Porse, E. (2018). Open data and stormwater systems in Los Angeles: applications for equitable green infrastructure. *Local Environment*, 23(5), 505–517. <https://doi.org/10.1080/13549839.2018.1434492>
- Roe, J. J., Ward Thompson, C., Aspinall, P. A., Brewer, M. J., Duff, E. I., Miller, D., Mitchell, R., & Clow, A. (2013). Green space and stress: Evidence from cortisol measures in deprived urban communities. *International Journal of Environmental Research and Public Health*, 10(9), 4086–4103. <https://doi.org/10.3390/ijerph10094086>
- Rosgen, D. (1998). The reference reach: A blueprint for natural channel design. *Engineering Approaches to Ecosystem Restoration*, 1009–1016. [https://doi.org/10.1061/40382\(1998\)166](https://doi.org/10.1061/40382(1998)166)
- Santamouris, M. (2014). Cooling the cities - A review of reflective and green roof mitigation technologies to fight heat island and improve comfort in urban environments. *Solar Energy*, 103, 682–703. <https://doi.org/10.1016/j.solener.2012.07.003>
- Scott, M., Lennon, M., Haase, D., Kazmierczak, A., Clabby, G., & Beatley, T. (2016). "Nature-based solutions for the contemporary city/Re-naturing the city/Reflections on urban landscapes, ecosystems services and nature- based solutions in cities/Multifunctional green infrastructure and climate change adaptation: brownfield greening as an adaptation strategy for vulnerable communities?/Delivering green infrastructure through planning: insights from practice in Fingal, Ireland/Planning for biophilic cities: from theory to practice". *Planning Theory and Practice*, 17(2), 267–300. <https://doi.org/10.1080/14649357.2016.1158907>
- Sebti, A., Aceves, M. C., Bennis, S., & Fuamba, M. (2016). Improving nonlinear optimization algorithms for BMP implementation in a combined sewer system. *Journal of Water Resources Planning and Management*, 142(9). [https://doi.org/10.1061/\(ASCE\)WR.1943-](https://doi.org/10.1061/(ASCE)WR.1943-)

5452.0000669

Sekertekin, A., & Zadbagher, E. (2021). Simulation of future land surface temperature distribution and evaluating surface urban heat island based on impervious surface area. *Ecological Indicators*, 122(November 2020), 107230.  
<https://doi.org/10.1016/j.ecolind.2020.107230>

## **Chapter 2: Integrating Social Equity into Multi-Objective Optimization of Urban Stormwater Low Impact Development**

This chapter resulted in one publication in the Journal of Water Resources Planning and Management in June 2023.

### **Chapter 2 Abstract**

Recent studies have demonstrated some advantages of using advanced heuristic algorithms to identify near-Pareto-optimal future locations, types, and sizes for stormwater low-impact development and green infrastructure (LID/GI) across a given urban landscape. However, previous optimization studies did not consider social equity as an objective, which poses problems because urban green infrastructure often is distributed inequitably. Increasing access to LID/GI in historically marginalized areas is a prominent environmental justice issue, and increasingly is becoming a primary consideration when prioritizing future locations, types, and sizes of urban LID/GI. This study integrated a novel spatial social equity objective [LID/GI–Social Vulnerability Index (SVI) correlation objective,  $\rho$ ] into a multiobjective LID/GI optimization model. The LID/GI-SVI correlation is an objective that directs the optimization algorithm to search for LID/GI distributions that maximize the linear correlation between LID/GI implementation and subbasins with higher estimated percentages of historically marginalized people. Our analysis focused on understanding the impacts of the LID/GI-SVI correlation objective on a LID/GI optimization model. This modeling study demonstrates that (1) the LID/GI-SVI correlation objective can be used to direct optimization algorithms to search for LID/GI distributions that can achieve runoff management objectives, increase green LID/GI implementation in more marginalized areas, and explore the potential trade-offs or synergies between hydrologic and equity goals; (2) LID/GI optimization formulations that consider only hydrologic objectives likely will not result in equitable LID/GI distributions; (3) LID/GI distributions that perform well on the LID/GI-SVI correlation may be composed of different types of LID/GI than less-equitable but more hydrologically favorable LID/GI distributions; and (4) for our study area, including spatial equity as an objective resulted in modest reductions in the hydrologic performance of near-Pareto-optimal LID/GI distributions.

## 2.0 Introduction

Low impact development (LID) is a collection of structures or practices that are designed to mimic natural hydrologic processes such as infiltration, storage, and evapotranspiration. The U.S Environmental protection agency (USEPA) uses the term green infrastructure (GI) to describe specific stormwater control measures as components of the overall LID concept (USEPA, 2022a). Common LID/GI types include but are not limited to raingardens, bioretention cells, green roofs, permeable pavement, grass swales, and green space.

Many cities in the U.S. and globally have been active in implementing LID/GI in the face of increased impervious surfaces, aging infrastructure, elevated stormwater runoff due to climate change, and to meet federal non-point source discharge permit requirements (Chini et al., 2017; Copeland, 2013; Hopkins et al., 2018). In the U.S., under the Clean Water Act (CWA) and other state laws, municipalities are required to control stormwater discharges as combined sewer overflows (CSO) or as discharge from municipal separate sewer systems (MS4). Though USEPA endorses the use of LID/GI to control nonpoint source stormwater discharges, there is no national set of standards or codes for LID/GI and so the extent of implementation is largely subject to local government policies and budgeting. Political barriers that exist to prevent or slow the transition to LID/GI include a lack of motivation from decision makers, community acceptance, limited or no incentives to private landowners and developers, and entrenched preferences for gray infrastructure in local policy (Dhakal & Chevalier, 2017; Johns, 2019). Many of the major cities in the U.S. that are most active in implementing LID/GI have been CSO municipalities which are subjected to more substantial fines when stormwater discharge requirements are not met (USEPA, 2022b). In areas with fewer regulatory motivations to implement LID/GI, like many MS4 municipalities, successful efforts to increase implementation of LID/GI have often

coincided with an institution of a local stormwater utility fee (Allen, 2020) and the establishment of strong partnerships between local government and/or non-government organizations that work to link the stormwater control goals of LID/GI to other public priorities (Harrington & Hsu, 2018).

Stormwater LID/GI has been promoted for its potential to provide multiple benefits to communities where they are implemented (Madureira & Andresen, 2014; Scott et al., 2016). Though less well understood than the hydrologic benefits (Venkataramanan et al., 2019), LID/GI does coincide with a range of social amenities and advantages. For example, some LID/GI types have shown promise in mitigating the urban heat island effect (Block et al., 2014; Santamouris, 2014). LID/GI generally increases property values in accessible areas (Du & Zhang, 2020; Mazzotta et al., 2014) and could contribute to energy savings and the creation of green jobs (Celik & Binatli, 2018). LID/GI also can enhance the natural aesthetic of urban landscapes and contribute to improving the mental health and safety of a community (Kondo et al., 2015; Roe et al., 2013; Wolch et al., 2014).

LID/GI and the associated benefits are often distributed inequitably within cities (Keeler et al., 2019; Mell & Whitten, 2021; Porse, 2018). In the U.S., race and rates of poverty are major indicators of urban inequity, as African Americans, ethnic minorities, and low-income households have historically been intentionally disenfranchised from neighborhood investment, infrastructure planning processes, and other arenas of public decision making (Wright, 2021). There is a clear need within the engineering community and beyond to put forth a conscious effort to correct past practices and to prevent future harm caused by inequitable green infrastructure planning (Anguelovski et al., 2020). Increasing access to LID/GI within minority and low-income communities has become a prominent environmental justice issue and is a major

priority in the planning of future locations of urban LID/GI (Garcia-Cuerva et al., 2018; Heck, 2021; Luan et al., 2019; Mason et al., 2019; Meerow & Newell, 2017; Zhu et al., 2019). As of 2021, federal infrastructure initiatives such as Justice40 have been introduced in the U.S. and have emphasized increasing infrastructure investment in historically marginalized communities (U.S. Executive Office of the President, 2021).

In response to inequitable distributions of green infrastructure in urban areas, researchers and urban planners have been mapping indicators of social vulnerability to help identify priority locations for future LID/GI implementation. A Social Vulnerability Index (SVI) typically includes at minimum, census demographic and other publicly available socioeconomic data. SVIs can serve as visual aids for LID/GI planners by revealing distributions of historically marginalized populations within different areas of a city (Heckert & Rosan, 2016; Mandarano & Meenar, 2017). For example, Mandarano and Meenar (2017) developed a stormwater LID/GI priority census tract map for Philadelphia, Pennsylvania, by ordinally ranking census tracts for future LID/GI consideration based on multiple factors such as race, income, parental status, education level, along with the current extent of LID/GIs. Heckert and Rosan (2016) describe an index method that consolidates census block group data and other environmental justice indicators into a composite score to identify areas of relatively high levels of environmental inequity. Even local governments such as Montgomery County, Maryland, have begun to use vulnerability indicators for LID/GI planning (DEP, 2022). The USEPA Environmental Justice Screening tool (EJST) is a valuable resource for those interested in mapping potential equity voids and vulnerability indicator data within areas of the U.S. (USEPA, 2014).

Determining optimal locations for future LID/GI can be a complex process. If placed in strategic locations throughout a given urban watershed, stormwater LID/GI can mitigate the

destruction of urban streams by reducing excess erosion, sedimentation, and pollution caused by runoff (Bernhardt, 2011; Dietz, 2007; Palmer et al., 2014). Within a given urban area, there can exist a vast number of feasible spaces or possible spatial distributions of LID/GI. Trial-and-error exploration of the vast decision space of possible LID/GI distributions, requiring modeling the hydrologic impacts of each distribution, can be impractical and ineffective. To address this challenge, engineering researchers have coupled advanced heuristic multi-objective optimization tools with hydrologic models to efficiently identify near Pareto-optimal spatial LID/GI distributions that minimize the cost and the impacts of development on runoff within a given urban area (Eckart et al., 2018; Giacomoni et al., 2017; Sebti et al., 2016; Zhang & Chui, 2018). Sebti et al. (2016) analyzed three different optimization methods by comparing the LID/GI distribution results and performances on a set of runoff management objectives, finding that non-linear methods such as genetic algorithms and simulated annealing have the potential to outperform linear programming methods for LID/GI spatial optimization. Giacomoni et al. (2017) coupled a stormwater management model (SWMM) with the Non-Dominated Sorting Genetic Algorithm-II (NSGA-II) and introduced a new hydrologic objective into their formulation to help identify optimal local subbasins where green roofs and permeable pavement could be implemented within a small watershed. Eckart et al. (2018) was the first to demonstrate the coupling of the stormwater management model (SWMM) to the Borg evolutionary algorithm (Hadka & Reed, 2013) to search for optimal LID/GI distributions that would best treat total and peak runoff within a small urban area in Windsor, Ontario. Past optimization studies such as these have demonstrated the usefulness of applying heuristic algorithms for locating near Pareto-optimal locations, sizes, and LID/GI types that minimize the impacts of stormwater runoff and cost. However, no LID/GI optimization study has considered the equity implications of optimal

LID/GI distributions and how an equity objective can change optimization results. Improving access to the benefits of LID/GI within socially vulnerable communities is becoming a clear goal for local policy makers and infrastructure planners. The purpose of this study is to gain an understanding of the impacts of integrating a novel spatial social equity objective into an urban LID/GI optimization model.

In this study, a storm water management model (SWMM) has been coupled to the Borg multi-objective evolutionary algorithm to search for Pareto-optimal LID/GI distributions (subbasin locations, sizes, and types) that differentially favor multiple conflicting objectives. We combine a state-of-the-art optimization algorithm with the social vulnerability index mapping concept by introducing a novel objective function (the LID/GI – Social Vulnerability Index (SVI) correlation,  $\rho$ ) that directs the optimization model to search for LID/GI distributions that maximize the linear relationship between implementation and subbasin SVI values. Note that the authors do not view linearization of this relationship as the preeminent form of an equity objective, just one of many that could be used to enhance equitable LID/GI implementation within optimization models. We analyze and compare results for three sets of optimization formulations. The first formulation searches for optimal LID/GI distributions using two hydrologic goals: minimization of average peak stream flow and minimization of total runoff exported from the watershed. The second formulation solely searches for distributions with a strong positive linear relationship between LID/GI implementation and socioeconomic indicators of historic marginalization. The third formulation considers both the hydrologic objectives and the correlation between LID/GI placement and subbasin SVI values by considering all objectives in the first and second formulations; that is the third formulation has two hydrologic objectives and the objective of correlation between LID/GI placement and socioeconomic indicators of

historic marginalization. We produce maps of near Pareto-optimal LID/GI area distributions and quantify the potential impacts of a unique optimization objective on both hydrologic and equity outcomes.

## **2.1 Methods**

In this section we introduce the study area and provide the optimization formulation details. We explain three key methods that were involved in constructing our LID/GI optimization model. First, an SVI was developed from census block group socio-economic data and was used to estimate the location of preferred subbasins for future LID/GI implementation and greening in the upper Meadow Creek watershed. Second, using LID/GI Virginia design and placement recommendations, we approximated the feasible LID/GI areas within each subbasin using simple GIS methods. Finally, we coupled a SWMM model to the Borg multi-objective evolutionary algorithm. We then explain our approach to the tradeoff analyses of the optimization results.

### **2.1.1 Study Area Description**

An optimal distribution of LID/GI should strive to compensate for past racial injustices that have occurred locally, particularly in areas that have a history of discrimination and exclusionary infrastructure policies against socially vulnerable groups. Our case study area is the upper Meadow Creek watershed located in Charlottesville and Albemarle County, Virginia. Unlike Philadelphia, the Charlottesville area was not redlined (Hillier, 2003) by the Home Owners' Loan Corporation (HOLC) (Klosterwill et al. 2020). However, the same social imperatives that reproduced residential segregation based on race during the period of post-WWII suburbanization through selective access to mortgage credit were present. The primary

mechanism through which existing patterns of racial segregation were maintained involved legal restrictions on who could purchase and hold a title to a home (Yager, 2017). These racial covenants typically barred non-whites and were permanent fixtures of residential properties in exclusive neighborhoods. Following the 1948 Shelley v. Kramer decision, racial covenants were no longer legally enforceable and the loss of this tool for maintaining residential segregation contributed to the creation of public housing developments in Charlottesville to receive African Americans displaced by urban renewal (Harris et al. 1991; Dukes 2019). A 2007 report published by the National Community Reinvestment Coalition (NCRC) found that the Charlottesville area ranked 251<sup>st</sup> (last) among the metropolitan areas examined in terms of “lending disparities between African-American borrowers and white borrowers” (p. 11) underscoring the influence of race on access to mortgage credit despite a lack of official HOLC “redlining” maps locally. The 2017 Unite the Right rally and ensuing violence focused national attention on the Charlottesville area and the considerable work that remains to address and redress past injustices.

The upper Meadow Creek watershed is within three separate MS4 jurisdictions- the City of Charlottesville, Albemarle County, and the University of Virginia. The primary motivation for implementing LID/GI in the study area is to satisfy MS4 and Chesapeake Bay Program total maximum daily load (TMDL) requirements (Albemarle County, 2022; Charlottesville, 2019). There currently is no formal, centralized process for planning, identifying, and implementing LID/GI in the study area, though all three jurisdictions are evolving their stormwater programs to incorporate more LID/GI to mitigate flood risks and to enhance the quality of life of those living and working in the area. Immediately prior to urbanization, agricultural and reforestation practices dominated the local landscape of Meadow Creek while mill ponds were constructed on many of the rivers in the upper James River watershed, of which Meadow Creek is a part

(Rivanna Conservation Society, 1996; Mattson et al. 1995). Like other areas in the Chesapeake Bay watershed, the agricultural era resulted in the mobilization of a substantial amount of sediment. The expansion of urban impervious surfaces, which now cover approximately 40% of the study area (Chesapeake Conservancy, 2019), increased volumes and velocities of stormwater runoff, eroded the built-up alluvial sedimentation, incised the streams, and exposed steep banks of erodible sediment. This ultimately resulted in the acceleration of erosion, sedimentation, pollutant loading, and the destruction of aquatic habitat leading the Virginia Department of Environmental Quality to officially add Meadow Creek to its list of impaired waters (VDEQ, 2020). After the original impairment designation in 2006, major stream restoration activities followed (The Nature Conservancy, 2013), but future upland LID/GI is needed to prevent future degradation of Meadow Creek and facilitate addressing TMDL impairments in the local and larger watersheds.

Figure 2-1 shows the upper Meadow Creek watershed, its subbasins, and their location within the larger Rivanna watershed and Central Virginia. Our hydrologic model of the 1415-hectare, upper Meadow Creek watershed is composed of twenty-six subbasins, ranging in size from 31 to 118 hectares that serve as the possible locations for future LID/GI within our model.

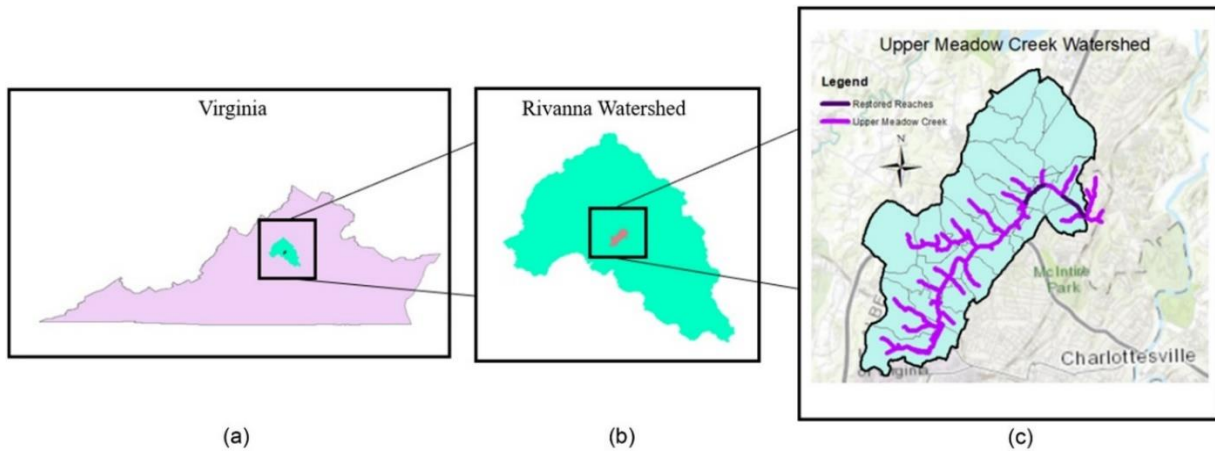


**Figure 2-1:** The upper Meadow Creek Watershed within the Rivanna River Watershed located in central Virginia, U.S.A (Source: ESRI World Topographic Map).

### 2.1.2 Calculating a social equity index for the Meadow Creek Subbasins

Marginalized populations within the Meadow Creek watershed were mapped at the subbasin level with the demographic index equation described by the USEPA Environmental Justice Screening Tool (EJST) technical documentation (USEPA, 2014) as the social vulnerability index (SVI) in this study:

$$SVI = \frac{(\% \text{ minority} + \% \text{ low income})}{2} \quad (1)$$

Note that the demographic index and other data can be extracted directly from the EJST web interface, but we extracted the raw percent minority and percent low-income data directly from the American Community Survey database (U.S. Census Bureau, 2019) and calculated the demographic index values within the upper Meadow Creek watershed at the census block group level. On average, the census block groups in the upper Meadow Creek area contain 1,340 residents. The simple demographic index was deemed sufficient to use as an SVI for this study since it is positively correlated with other potential social vulnerability indicators, such as no

high school diploma (%), children (%), and linguistically isolated (%), and it is negatively correlated with median income for the study area. The demographic index metric is used as a minimal form of an SVI that can be calculated at the census block group scale for areas within the U.S. An alternative, more tailored vulnerability index for the upper Meadow Creek watershed could be constructed through further community discussion and input.

Since our model subbasins do not spatially align with the census block groups, the subbasins were assigned SVI values by calculating an area-weighted average of the census block group SVI values. Figure 2-2 illustrates the area-weighted average SVI values for the twenty-six Meadow Creek subbasins derived from the census block group data. As census block groups are developed to partition areas towards more homogeneous socioeconomic characteristics, remapping census information to sub-census block group levels introduces local uncertainty. However, considering the ubiquitous absence of finer resolution sociodemographic survey data, such as how the population is distributed within each census block group to enable population-weighting, the area-weighted averaging method for assigning SVI values to the local subbasins has been judged to be sufficient for the purposes of this study.

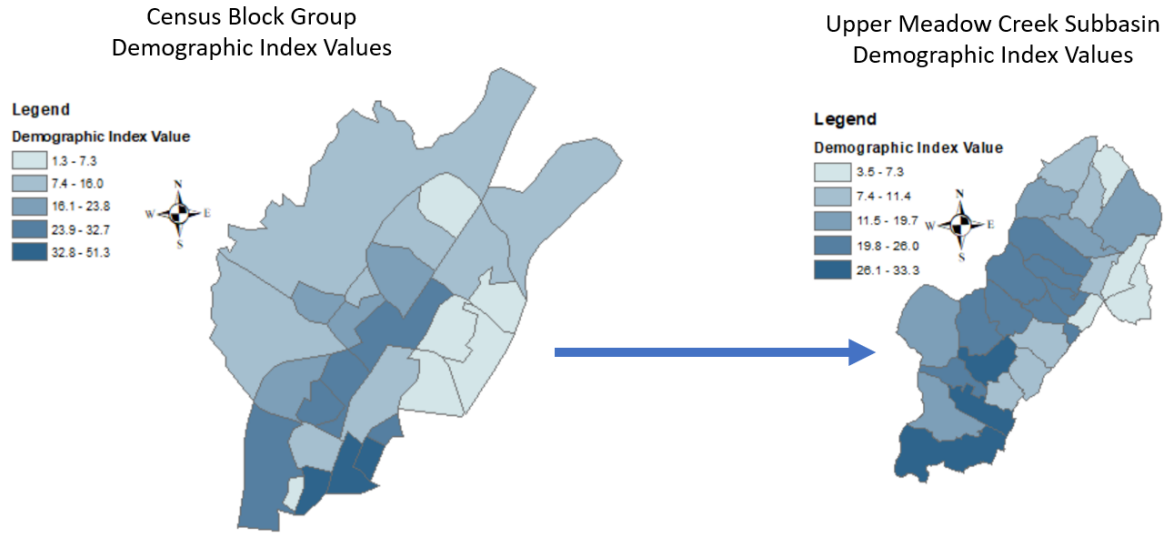


**Figure 2-2:** Census Block Group Demographic Index Values (left) mapped to the Upper Meadow Creek Subbasins (right) using an area-weighted averaging approach.

### 2.1.3 Feasible Area and Cost Constraints on LID/GI Distributions

Major constraints within our LID/GI optimization model are the feasible areas where each LID/GI type can be placed within the urban watershed and the maximum LID/GI construction costs. Feasible areas for rain gardens, bioretention, green roofs, grass swales, permeable pavement, and impervious conversion were determined in this study based on five criteria primarily in accordance with Virginia BMP clearinghouse (VDEQ & VWRRC, 2013). Four of the five criteria include: building setback which is the minimum distance between a structure and various LID/GI types, drainage area size which refers to the land area that drains stormwater to a specific LID/GI, slope of the drainage area, the hydrologic soil group (HSG) which is a classification of the runoff potential of a given soil type.

Raster data included products from a 10-meter digital elevation model downloaded from the U.S. geological survey’s National Map database (USGS, 2019), soil hydrologic group data from the soil survey geographic database (ESRI & SSURGO, 2021), and the Chesapeake Bay

Conservancy’s land use raster (Chesapeake Conservancy, 2019) resampled to a 10-meter resolution. A binary threshold filter was applied to the data to convert the raster spaces to Boolean matrices of the same dimension. For each data set, raster spaces that met major Virginia BMP clearinghouse recommendations (VDEQ & VWRRC, 2013) were mapped to a value of 1 and spaces that did not meet a specific criterion to a value of 0. We then multiplied all the binary matrices together for each LID/GI type to obtain final feasibility maps that included only spaces that met all criteria.

Table 2-1 summarizes most of the criteria used to determine the feasible areas for permeable pavement, grass swales, rain gardens and bioretention within the Meadow Creek watershed. Land use was another criterion that was used to approximate the feasible areas for each LID/GI type. Using the Chesapeake Conservancy land use 1-meter raster data, we assumed that grass swales, rain gardens, and bioretention cells were only feasible in pervious areas without canopy cover. Permeable pavement, green roofs, and impervious conversion were assumed to be feasible only in specific impervious areas. Table 2-2 shows which land covers corresponded to feasible areas for each LID/GI type in this study.

**Table 2-1:** GIS layers and physical criteria of feasible areas for each LID type.

LID Type	GIS Layer Criteria			
	Building Setback (m)	Drainage Area (ha)	Slope (%)	Hydrologic Soil Group
Permeable Pavement	15.24	0.05	<1	A,B,C,D
Grass Swale	15.24	< 2.02	<4	A,B
Rain Garden	3.048	< 0.20	1 to 5	A,B
Bioretention	15.24	0.2 to 2.02	1 to 5	A,B

**Table 2-2:** Land uses used to approximate the feasible areas for each LID type.

LID Type	Land Use						
	Turf Grass	Pervious Developed	Cropland	Pasture/Hay	Parking/Drive ways	Commercial Buildings	Impervious (No roads or buildings)
Permeable Pavement					X		
Grass Swale	X	X	X	X			
Green Roof						X	
Rain Garden	X	X	X	X			
Bioretention	X	X	X	X			
Impervious Conversion							X

The authors chose to apply additional constraints to impervious surface conversion and the green roof space because they are relatively expensive and/or require significant land use changes to implement. The feasible areas for green roofs and impervious conversion are much greater than the feasible areas for the other LID/GI types and utilizing all that area for LID/GI would likely be economically unfavorable to commercial property owners. Thus, replacing all commercial building roofs with green roofs and replacing all sidewalks and parking lots with green space was judged to be impractical in this study area, so, to ensure that green roof and impervious surface conversion would not be overrepresented in the near optimal solutions we reduced the feasible space to 1% of the total subbasin area for impervious conversion and reduced the overall available feasible green roof space by two-thirds. Ideally, deciding what is practical in terms of LID/GI implementation values would be determined by decision makers and property owners in the design process. The total maximum areas allowed by the optimization model account for all the modifications to the feasible areas and are summarized in table 2-3 for each LID/GI type.

**Table 2-3:** Total Allowable Area for each LID Type.

<b>LID Type</b>	<b>Total Feasible Area (ha)</b>
Permeable Pavement	2.4
Grass Swale	3.5
Green Roof	24.3
Rain Garden	9.9
Bioretention	0.1
Impervious Conversion	12.9

It is possible that two different LID/GI types can be feasible in a single location but to simplify the optimization model and to help prevent unreasonable exclusion of any single LID/GI approach, we developed an LID/GI implementation hierarchy that is based on total maximum allowable area. If the space for two LID/GI types overlap, the optimizer will only consider the LID/GI type with the least overall allowable area for that space. For example, if a single space was found to be feasible for both permeable pavement and impervious removal, then the optimizer will recognize it as only a permeable pavement space. Likewise, if a space was found to be feasible for a rain garden and a grass swale, the optimizer will only consider grass-swailes for that space.

Table 2-4 summarizes the estimated LID/GI costs used in this study. To estimate the construction cost of different LID/GI types, we primarily relied on a few publicly available sources, while the price of impervious surface removal was estimated based on a local consulting firm quote. The construction cost values are estimates and do not include maintenance, land, opportunity costs or any other costs. This is particularly relevant to impervious surface conversion where economic value may be lost due to a reduction in activities such as parking.

Green roofs, permeable pavement, and impervious removal costs were assumed to be dependent on total implemented area while the other LID/GI types were priced based on the impervious area treated.

**Table 2-4:** Estimated Construction Costs for each LID type.

<b>LID TYPE</b>	<b>Construction Cost</b>	<b>Source</b>
Permeable Pavement	\$26.77/m <sup>2</sup>	(VDEQ & VWRRC, 2013)
Grass Swale	\$18.15/ m <sup>2</sup> impervious treated	(Maryland DOE, 2016)
Green Roof	\$102.92/m <sup>2</sup>	(VDEQ & VWRRC, 2013)
Rain Garden	\$10.73/ m <sup>2</sup> impervious treated	(Maryland DOE, 2016)
Bioretention	\$15.32/ m <sup>2</sup> impervious treated	(Maryland DOE, 2016)
Impervious Removal	\$16.41/m <sup>2</sup>	Local Consulting Sources

To further streamline the computation process, a few additional constraints were programmed into our LID/GI optimization model regarding feasibility and the decision variables. All LID/GI were programmed with default design parameters. When user input was required for design parameters, we referenced design recommendations from the Virginia BMP clearinghouse design specifications. The drainage areas within the optimization models and the percentages of impervious surfaces of those drainage areas are assumed to be constants that fall within VDEQ & VWRRC recommendations. Rain gardens and bioretention drainage areas are assumed to be twenty times greater than their surface areas while grass swale drainage areas were set to be twenty-five times greater. Grass swales, raingardens, and bioretention drainage areas were

assumed to be 25% impervious while permeable pavement drainage areas were assumed to be 100% impervious within our LID/GI optimization model.

#### **2.1.4 The upper Meadow Creek SWMM Model**

The runoff reduction performance of LID/GI distributions was quantified using an USEPA SWMM model for the upper Meadow Creek watershed. The SWMM model used in this study is a modified version of a model that was constructed in 2010 through a collaboration between the U.S. Army Corp of Engineers, URS Corporation, and the city of Charlottesville (Charlottesville et. al 2008, 2009). The original model included eighty-seven subbasins for upper Meadow Creek. To meaningfully simplify the decision space of the optimization model, the original subbasin model was converted to a twenty-six subbasin model by merging adjacent subbasins that drained to common junctions within the model. Impervious surface information as well as infiltration parameters were updated in the twenty-six-subbasin model using the sensitivity-based radio tuning calibration (SRTC) tool available in the PCSWMM software. After the SWMM model updates, there were no major differences in the calibration results of the two models. The twenty-six subbasin SWMM model in this study has been calibrated using one local rain event and validated using five later events. The calibration and validation events were observed in the spring and summer of 2021 and spring of 2022. For each recorded rain event, the rainfall was recorded using a HOBO® Pendant Event data logger tipping-bucket rain gauge located in the center of the upper Meadow Creek watershed approximately 100 meters from the stream. Stream stage was recorded using a HOBO U20L-01 transducer. Stage measurements were converted to discharge using a rating curve developed over a period of 18 months. Discharge was recorded at the upper Meadow Creek outlet using a SonTek Flow Tracker 2 acoustic velocimeter and depth was recorded using a staff gage and pressure transducer. The

calibrated Nash-Sutcliffe Efficiency (NSE) was 0.84 and the average NSE across four validation rain events was 0.76, indicating an acceptably calibrated hydrologic model. Further details on the SWMM model calibration can be found in appendix A on table A-1 and figures A-1 to A-6.

### 2.1.5 The Multi-Objective Optimization Formulation

To quantify LID/GI hydrologic performance, we simulated an SCS type II 24-hour design storm with a 1-year return period (3.04 inches per day for Charlottesville, Virginia) using the upper Meadow Creek SWMM Model. Our LID/GI optimization model consists of 156 decision variables with continuous values between 0 and 1 that represent the fraction of the feasible LID/GI area for the 6 LID/GI options in each of the twenty-six subbasins. We compared results from three optimization formulations that we will refer to as the Hydrologic, Equitable, and Hydro-Equitable formulations. The mathematical objectives for the three optimization formulations are described below.

Formulation 1: The Hydrologic Formulation identifies LID/GI distributions that minimize the total runoff volume exported from the upper Meadow Creek watershed and peak stream flow averaged over ten restored reaches of Meadow Creek. The ten restored reaches span the restored sections of Meadow Creek, which go as far downstream as the outlet. These reaches were chosen because maintaining the integrity of previously restored areas is a major local stormwater management goal within the study area. The objective function for the first formulation can be summarized with equation 2 below.

$$\min (Q_p, V_{runoff}) \quad (2)$$

$Q_p$  is the average peak stream flow rate at ten restored stream reach locations and  $V_{runoff}$  denotes the total volume of runoff exported from the watershed.

Formulation 2: The Equitable Formulation searches for LID/GI distributions that maximize the linear relationship between subbasin SVI values and green LID/GI area implemented as a ratio of subbasin area:

$$\max (\rho_{X,Y}) \quad (3)$$

Equation 3 is the Pearson correlation coefficient between subbasin SVI values  $X$  and the green LID/GI area ratios (green LID/GI area divided by total subbasin area)  $Y$ . Green LID/GI area includes all LID/GI types except for permeable pavement. Higher amounts of LID/GI per subbasin area were assumed to increase the likelihood of local resident access to the LID/GI and thus greenery. Equation 3 is referred to as the “LID/GI-SVI correlation” or simply “ $\rho$ ” (we use “ $R$ ” to refer to any other correlation coefficient). The maximum value for the LID/GI-SVI correlation equals 1, though there may only exist solutions that approach 1 depending on the problem definition and constraints of the model. We round the correlation coefficient to two decimals, which makes a  $\rho$  value of 1 achievable.

It should be noted that while this metric prioritizes implementing LID/GIs in direct proportion to vulnerability as desired by an equity metric, it does not specify what that proportion should be. As such, multiple LID/GI distributions could achieve similar values of  $\rho$  with different slopes between LID/GI area ratio and demographic index scores. What an appropriate slope might be is likely location-dependent, and perhaps nonlinear. Other equity objective forms such as categorical, exponential, piecewise etc. could be explored instead of a linear function in future work.

Formulation 3: The Hydro-Equitable Formulation searches for LID/GI distributions that minimize the average peak stream flow and total runoff exported from Meadow Creek while also

maximizing the linear dependence between subbasin SVI values and green LID/GI implementation.

$$\mathbf{min} (Q_p, V_{runoff}, -\rho_{X,Y}) \quad (4)$$

The three formulations were optimized given different cost constraints ranging from five to forty-million dollars. A forty-million-dollar limit is a reasonable upper threshold to explore given a multiple year investment in LID/GI that, theoretically, could be funded through stormwater utility taxes levied within the study area. Unlike the city of Charlottesville, Albemarle County does not currently have a stormwater utility tax based on impervious surface area that could help fund LID/GI projects in the study area, but if the county did adopt the same stormwater utility tax policy as Charlottesville, a total of 1.8 million dollars could potentially be raised annually in the upper Meadow Creek watershed. If loftier stormwater policies were adopted (Arlington County, 2022), such as those of Arlington, Virginia, up to six million dollars could be raised each year within the upper Meadow Creek Watershed.

Before optimization trials were run, SWMM simulations were conducted to obtain baseline results for the scenario with no LID/GI added. The hydrologic performance of different LID/GI distributions on peak and total runoff are reported in percentage reductions in runoff from the baseline scenario. To examine the impact of  $\rho$  on LID/GI distributions and compositions produced using our optimization model, we focus on results from the forty-million-dollar construction cost constraint. To examine the influence of  $\rho$  on runoff reduction performance, we examine the near Pareto-optimal LID/GI distributions across a range of cost constraints.

### **2.1.6 Coupling SWMM and Borg**

Optimization of the LID/GI distributions was performed by a master-worker parallelization of the Borg algorithm (Hadka & Reed, 2015). Borg is a multi-objective

evolutionary algorithm that seeks to find a set of non-dominated solutions across multiple objectives, meaning no solution in the set outperforms another on all objectives. This set of solutions is also called the Pareto frontier. For a given optimization trial, Borg will generate a random initial set of LID/GI distributions as depicted in figure 2-3. Once LID/GI distributions were generated in a Python data frame, the fitness of LID/GI distributions was quantified using open-source Python libraries including the combination of two SWMM application programming interface (API) libraries. We developed Python code that allows for the rapid generation and testing of a vast number of individual LID/GI distributions. SWMMIO (Erispaha, 2022) and pySWMM (McDonnell et al., 2020) were used to update the SWMM input files of newly generated LID/GI scenarios, implement LID/GI within the model, execute SWMM simulations, and to evaluate results entirely in Python. When our SWMM model was coupled to Borg using the Python wrappers, the evolutionary algorithm took control of scenario generation, model simulation, results evaluation, and the optimal sorting of different LID/GI distributions.

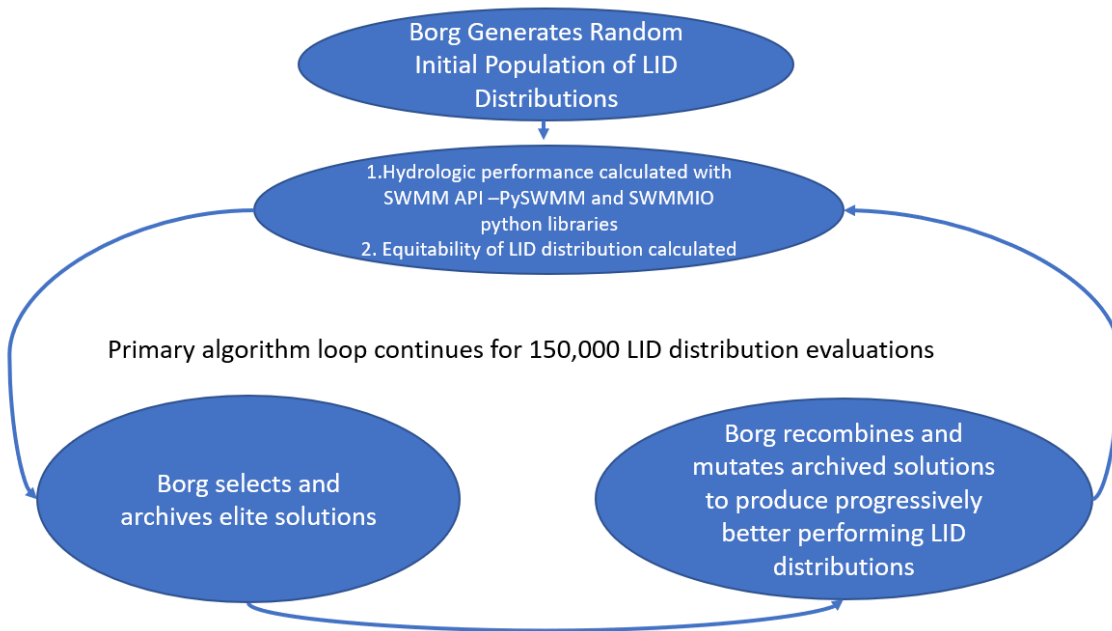


**Figure 2-3:** A simplified workflow diagram of the SWMM-BORG LID optimization model.

After the initial LID/GI distribution set is generated and tested, the main algorithm loop continues as the non-dominated LID/GI distributions are archived for recombination to produce new sets of solutions to be evaluated. To find the best approximation of the Pareto frontier, Borg deploys an elitist selection strategy, where only the most fit or best performing LID/GI distributions survive. This algorithmic recombination is analogous to “mating” the LID/GI distribution decision variables of the elite LID/GI distributions. The main loop seen in figure 3 continues for a user specified number of LID/GI distribution evaluations. We executed the optimization model using the University of Virginia’s high-performance computing system and ran 150,000 LID/GI distribution evaluations. This took 20 hours using 3 cores.

It should be noted that evolutionary algorithms such as Borg are not guaranteed to converge to the global non-dominated set given a finite number of evaluations (Laumanns et al., 2002), but they represent the current state of the art for high-dimensional, nonlinear, multi-objective optimization problems. Borg utilizes a combination of techniques such as randomized restarts and auto-adaptive multi-operator recombination within a single optimization framework that can produce sets of  $\epsilon$ -nondominated solutions.  $\epsilon$  values are domain-specific thresholds of indifference on each objective defined by the Borg user. That is, a user is indifferent to improvements  $< \epsilon_i$  on objective  $i$ .  $\epsilon$  values organize the objective space into hypercubes of side length  $\epsilon$ , called  $\epsilon$ -boxes, and the non-dominated sort is performed over the  $\epsilon$ -boxes rather than the solutions themselves. If multiple solutions reside in the same  $\epsilon$ -box, only that closest to the ideal point of the box is retained, and in the case of ties, only the first evaluated solution is kept. This limits the size of the archive and speeds up convergence. We use the terms  $\epsilon$ -nondominated

and near Pareto-optimal interchangeably in this study. The  $\epsilon$  values used for the objectives in our study are provided in table 2-5.

**Table 2-5:** Chosen  $\epsilon$  values for each objective

$Q_p$ (m <sup>3</sup> /s)	$R$ (m <sup>3</sup> )	$\rho$
0.000283 (0.01 CFS)	0.283 (10 ft <sup>3</sup> )	0.01

Because the Equitable Formulation was only composed of a single objective, we used Pareto sorting instead of  $\epsilon$ -non-dominance sorting for this formulation. In Pareto sorting, solutions within the same  $\epsilon$ -box, including ties, are archived. This allows the Borg algorithm to store alternative sets of LID/GI distributions that produce the same  $\rho$  value. Without this modification, only a single LID/GI distribution would be archived under the Equitable Formulation.

### 2.1.7 Tradeoff Analysis

The primary analytical goal of this study is to examine the potential impact of  $\rho$  on  $\epsilon$ -nondominated distributions, compositions, hydrologic performances, and equity. We hypothesize that the Hydro-Equitable Formulation will discover near Pareto-optimal LID/GI distributions that are more equitable but less hydrologically optimal than those found under the Hydrologic Formulation but more hydrologically optimal and less equitable than the LID/GI distribution produced under the Equitable Formulation. This should occur based on the definition of non-dominance; however, it is possible that more equitable but equally hydrologically favorable solutions to those from the Hydrologic Formulation could be discovered by adding an equity objective if improving equity does not strongly conflict with reducing peak and total runoff. To

test our first hypothesis, we conducted Wilcoxon rank sum tests to determine if median nondominated performance is significantly different between the three formulations.

Depending on the problem formulation and chosen  $\epsilon$  values, by the end of an optimization trial Borg may archive dozens to hundreds of  $\epsilon$ -nondominated solutions that span a range of objective value combinations. For  $\epsilon$ -nondominated solutions produced under the Hydro-Equitable Formulation, we quantified the expected tradeoffs between  $\rho$  values and runoff reduction performance at multiple cost constraints. If the strictly equitable distributions are expected to underperform compared to the "Hydrologic" distributions on runoff objectives, as we state in the first hypothesis, then we should expect a tradeoff between those two objectives under the same formulation and cost constraint. Therefore, our second hypothesis is that choosing an LID/GI distribution with a higher  $\rho$ -value will result in a decline in hydrologic performance. To test this hypothesis,  $\epsilon$ -nondominated solutions with  $\rho$  values from 0.6 to 0.7, 0.7 to 0.8, 0.8 to 0.9, and 0.9 to 1 were categorized into four respective bins and the average hydrologic performance of each bin was compared across all cost constraints.

## **2.2 Optimization Results**

### **2.2.1 Quantifying the impact of integrating the LID/GI-vulnerability correlation on $\epsilon$ -nondominated LID/GI distributions and compositions with a forty-million-dollar cost constraint.**

At each cost constraint, the Hydrologic Formulation produced relatively few  $\epsilon$ -nondominated distributions, all with similar hydrologic performances. This suggests peak flow reduction and total runoff reduction are not strongly conflicting. Under the Pareto-sorting method, the Equitable Formulation archived up to tens of thousands of non-dominated LID/GI distributions at each cost constraint. Since the Equitable Formulation nondominated sets were so

large, we randomly sampled 1000 distributions to analyze. Under the Hydro-Equitable formulation, between 100 and approximately 1000 LID/GI distributions were archived as an  $\epsilon$ -nondominated set at each cost constraint, suggesting stronger conflicts between equity and hydrologic performance. To compare the performance of solutions across these formulations, we selected one representative solution from each. For the Hydrologic and Hydro-Equitable formulations, we chose the solution with the lowest Mahalanobis distance (Encyclopedia of Mathematics, 2020) from the mean objective values across all nondominated solutions in their respective Pareto sets. The Equitable Formulation did not consider hydrologic objectives and produced nondominated solutions with identical  $\rho$  objective values, so we chose the solution with the shortest Mahalanobis distance from the mean cost and mean linear slope of LID/GI area ratios vs. SVI among the nondominated equitable solutions. We refer to these as the Hydrologic Solution, Hydro-Equitable Solution, and the Equitable Solution. Figure 2-4 shows the LID/GI area distributions for the three selected solutions under the forty-million-dollar-cost constraint. Most of the subbasins across all three solutions exhibited green LID/GI area ratios between 0.00 and 0.024; exceptions occurred under the Hydrologic Solution (panel a), which resulted in green LID/GI area ratios between 0.024 and 0.039 in four separate subbasins that are located in the central part of the study area. Under this solution, the green LID/GI area ratios were not significantly correlated with the SVI values ( $\rho = 0.13$ ,  $p > 0.05$ ) but were significantly correlated with feasible raingarden area ( $R = 0.7$ ,  $p < 0.05$ ). Hydrologic performance is greatest under this solution, which led to a 10.6% reduction in the average peak streamflow in restored reaches of the stream and 13.6% reduction in total runoff.

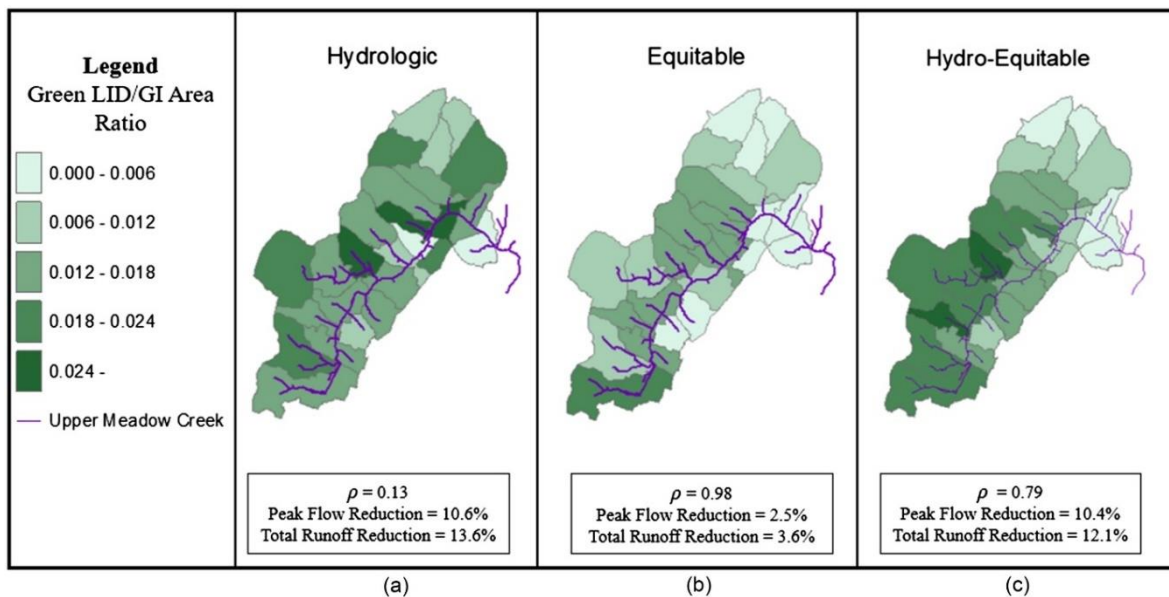


**Figure 2-4:**  $\epsilon$ -nondominated green LID area distributions and performance summary for selected solutions at the forty-million-dollar cost constraint under the Hydrologic (a), Equitable (b), and Hydro-Equitable (c) formulations.

Map b of figure 2-4 shows the selected green LID/GI area ratios of the Equitable Solution. This green LID/GI area ratio map resembles the SVI map since the green LID/GI area ratios are dependent on individual subbasin SVI values ( $\rho = 0.98$ ,  $p < 0.05$ ). The Equitable Solution green LID/GI area ratios were also most highly correlated with percent impervious conversion ( $R = 0.8$ ,  $p < 0.05$ ), feasible green roof areas ( $R = 0.54$ ,  $p < 0.05$ ), and percent impervious ( $R = 0.47$ ,  $p < 0.05$ ). Hydrologic performance was poorest under the Equitable Solution, which only reduced the average peak stream flow in restored reaches of the stream by 2.5% and total runoff export by 3.6%.

Map c in figure 2-4 shows the green LID/GI area ratios under the selected solution from the Hydro-Equitable Formulation. The green LID/GI area ratios produced under this solution are greatest in the central and southwest subbasins while there were two subbasins where green LID/GI area ratio was above 0.024. The green LID/GI area ratio implementations are significantly correlated with the subbasin SVI values ( $\rho = 0.79$ ,  $p < 0.05$ ) and with feasible impervious conversion area ( $R = 0.39$ ,  $p < 0.05$ ). The hydrologic performance under the Hydro-Equitable Solution was more similar to that of the Hydrologic Solution than to the Equitable

Solution, resulting in reductions of the average peak stream flow in restored reaches of the stream by 10.4% and total runoff export by 12.1%.

The distribution of total green LID/GI area (not ratio) has also been analyzed in relation to the SVI values. Figure 2-5 shows the cumulative percentage of total green LID/GI area that was implemented for each of the above solutions from the three formulations versus subbasin SVI values. The Hydrologic Solution implemented more green LID/GI area in the subbasins with lower SVI values compared to the selected solutions from other two formulations. For example, the Hydrologic Solution resulted in the implementation of approximately 54% of the green LID/GI to subbasins within the upper half of the SVI values, as compared to over 67% for the other two solutions. Table 2-6 summarizes the green LID/GI area distributions between different percentiles of SVI values for each of the selected solutions.

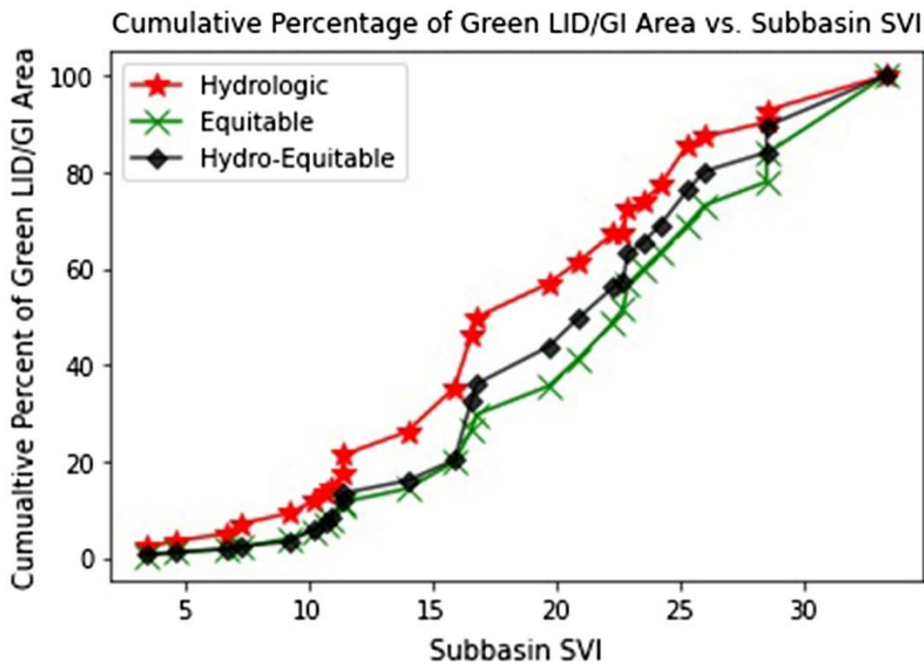


**Figure 2-5:** Percentage of Green LID implemented within subbasins vs. subbasin SVI values.

**Table 2-6:** Percentage of green LID area implementation by SVI percentile for the three formulations.

<b>SVI Percentile</b>	<b>Hydrologic (%)</b>	<b>Equitable (%)</b>	<b>Hydro-Equitable (%)</b>
Top 5 <sup>th</sup>	14.4	30.9	23.8
Top 3 <sup>rd</sup>	32.5	48.5	42.5
Top 50 <sup>th</sup>	53.7	73.3	67.2
Bottom 50 <sup>th</sup>	46.3	26.7	32.8
Bottom 3 <sup>rd</sup>	17.3	10.7	11.8
Bottom 5 <sup>th</sup>	9.2	4.0	3.3

The LID/GI type composition was another significant decision variable change that occurred between the three solutions at the forty-million-dollar cost limit constraint. These solutions' LID/GI distributions were composed of different amounts of LID/GI types depending on the formulation. Figure 2-6 illustrates the overall LID/GI type composition differences for each of the three solutions considered. Bioretention, which is not depicted in figure 2-6, composed a relatively negligible share of the total LID/GI implemented under all three formulations.

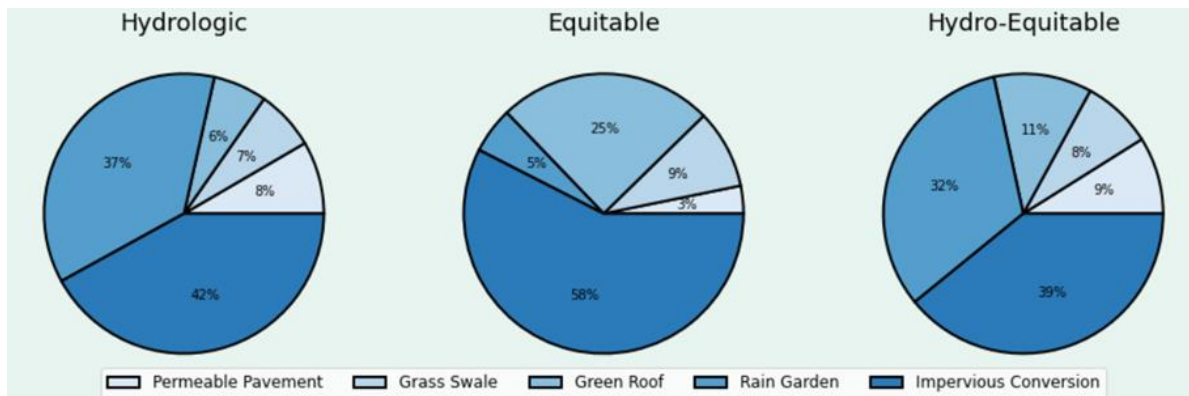


**Figure 2-6:** LID type composition percentages (%) of selected solutions from each formulation under the forty-million-dollar cost constraint.

Under the Hydrologic Solution, the LID/GI types that were implemented most extensively were impervious conversion (42%), impervious surface conversion (37%), and permeable pavement (8%). Under the Equitable Solution, impervious surface conversion was the

most extensive LID/GI type with 58% of the total LID/GI area share. Other than the impervious surface conversion, this solution's LID/GI composition was more diverse than the selected solutions from the other formulations, with green roofs (25%) and grass swales (9%) composing a greater share of total LID/GI area implemented. The LID/GI composition of the Equitable Solution was more predictable in this study area, as the demographic index values were found to be significantly correlated with the total feasible areas of impervious surface conversion ( $R = 0.47$ ,  $p < 0.05$ ) and green roofs ( $R = 0.56$ ,  $p < 0.05$ ) within each subbasin. The LID/GI type composition under the Hydro-Equitable Solution was similar to both of the other solutions with impervious surface conversion (39%), raingardens (32%), and permeable pavement (9%) being the top LID/GI type choices like the Hydrologic solution but with elevated green roof (11%) and grass swale (8%) implementation like the Equitable Solution. Note that figure 2-6 does not include drainage area treated by each of the LID/GI types.

### **2.2.2 Cost-Benefit analysis of the three formulations**

Figure 2-7 shows the performance of nondominated LID/GI distributions versus cost constraint limits. We plotted the average values for peak streamflow on the left panel and total runoff reduction on the middle panel. Error bars were added to all points to show the range in hydrologic performance across all the  $\epsilon$ -nondominated distributions, though they may not be visible if the ranges are very small. Increasing the cost limit under the Equitable Formulation did not improve hydrologic performance much compared to the other two formulations, as peak streamflow and total runoff export was only reduced by about 1.5% and 2.2% respectively from the lowest to the highest cost constraint. The Equitable Formulation also resulted in LID/GI distributions that were significantly under the cost constraints, which also explains the lowered performance. The hydrologic performances under the Hydrologic and Hydro-Equitable

Formulations improved at a similar rate with peak streamflow being reduced between the highest and lowest constraint by 8.3% under the Hydrologic Formulation and the Hydro-Equitable Formulation. Total runoff export was reduced by approximately 10.0% under the Hydrologic formulation and by 10.1% under the Hydro-Equitable formulation. Two-sample Wilcoxon Rank Sum test results reveal that the median hydrologic performance and  $\rho$  values of  $\mathcal{E}$ -nondominated distributions were significantly different at all cost constraints for all formulations ( $p < 0.05$ ).

The right plot in figure 2-7 is the LID/GI-SVI correlation versus cost constraint for nondominated LID/GI distributions which illustrates the difference in the spatial equity of LID/GI distributions under each of the formulations. According to the LID/GI-SVI correlation, the Hydro-Equitable formulation does produce LID/GI distributions that are more equitable than those produced under the Hydrologic Formulation but less equitable than those produced under the Equitable Formulation.

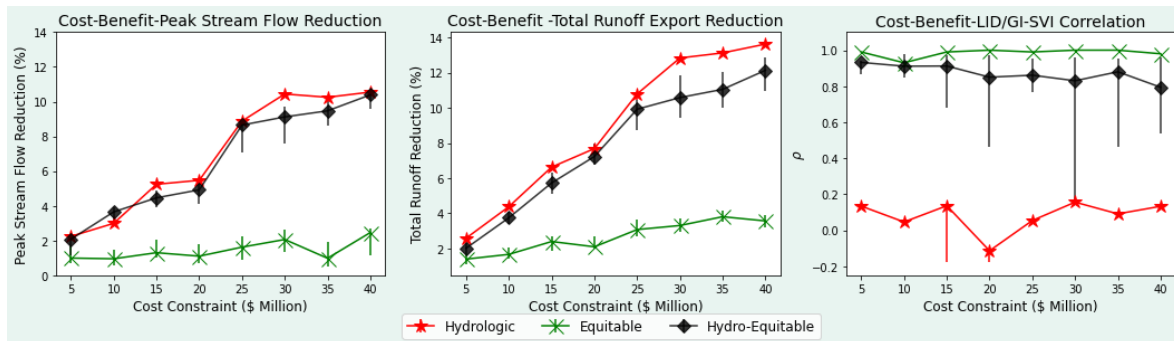


**Figure 2-7:** Cost-Benefit Curve for average peak stream flow (left), total runoff export (middle), LID-SVI correlation (right).

### 2.2.3 Quantifying the sensitivity of hydrologic performance to changes in $\rho$ value choices.

The potential to discover multiple  $\mathcal{E}$ -nondominated LID/GI distributions is one advantage of using Borg in this type of optimization study. As mentioned earlier, the Hydro-Equitable Formulation archived between 100 and approximately 1000 LID/GI distributions in the  $\mathcal{E}$ -nondominated set at each cost constraint. For example, optimization under this formulation with

a forty-million-dollar cost constraint resulted in the production of 114  $\epsilon$ -nondominated archived LID/GI distributions with  $\rho$  values ranging from 0.54 to 0.96. To quantify the possible tradeoffs between  $\rho$  values and hydrologic performance at multiple cost intervals under the Hydro-Equitable formulation,  $\epsilon$ -nondominated solutions were sorted into four bins at 0.1 increment  $\rho$  values from 0.6-0.7 to 0.9-1. The average hydrologic performance is plotted for each  $\rho$  value interval category at each cost constraint in figure 2-8.

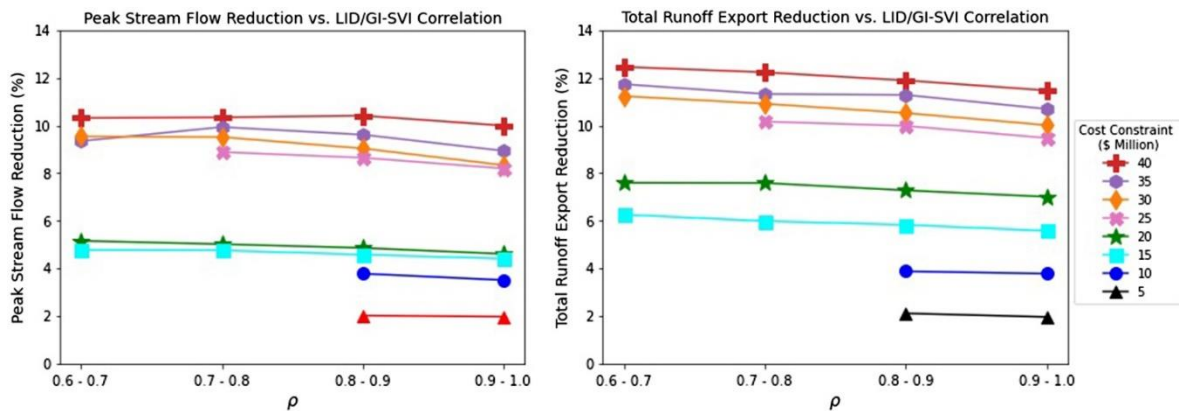


**Figure 2-8:** Average hydrologic performance of  $\epsilon$ -nondominated solutions at each cost constraint according to  $\rho$  interval.

Overall, choosing a near Pareto-optimal LID/GI distribution with a higher  $\rho$  value is expected to result in a loss in hydrologic performance, confirming our first hypothesis. However, the tradeoff is minor compared to that between cost and hydrologic performance. On average, choosing a solution in the next highest  $\rho$  value interval category among other  $\epsilon$ -nondominated solutions at a given cost constraint will result in only a loss of 0.2% in peak stream flow reduction and 0.3% in total runoff export reduction on average. This suggests that one could always choose the most equitable LID/GI distribution at a particular cost constraint, without significantly sacrificing hydrologic performance in the upper Meadow Creek watershed.

## 2.3 Discussion

### 2.3.1 The impacts of the LID/GI-equity correlation objective on LID/GI distributions, LID/GI type compositions, and equitability at the forty-million-dollar cost constraint.

Our results at the forty-million-dollar cost constraint show that an objective such as the LID/GI-equity correlation may be a necessary component of LID/GI-optimization models of similar scales if local management goals include both runoff management and maximizing green LID/GI implementation in more marginalized areas. Each formulation produced solutions with major differences in green LID/GI distributions and LID/GI type compositions. We have shown that under the Hydrologic Formulation at a forty-million-dollar cost constraint, the greatest green LID/GI implementation rates occurred in four subbasins in the central part of the study area, whereas under the Equitable Formulation the green LID/GI distributions were dependent on the subbasin SVI values. The Hydrologic and the Hydro-Equitable Solutions consisted of mostly rain gardens and impervious surface conversion. The Equitable Solution resulted in impervious surface conversion implementation with the remainder being mostly shared by a combination of green roofs, grass swales, and permeable pavements. The highest green LID/GI area ratios were implemented in subbasins at the central and southeast parts of the upper Meadow Creek watershed under the selected solution from the Hydro-Equitable Formulation which are composed of mostly residential areas surrounded by commercial and university districts.

Because  $\rho$  was not included as an objective in the Hydrologic Formulation, it is not surprising that the LID/GI distribution in the selected solution from this formulation had a  $\rho$  value that was insignificant ( $\rho=0.13$ ,  $p > 0.05$ ) and that LID/GI distribution of the selected solution from the Hydrologic Formulation was slightly skewed towards subbasins with lower SVI values. The solution from the Equitable Formulation produced more equitable green LID/GI

distributions but at great sacrifice to hydrologic performance. As hypothesized, the selected solution from the Hydro-Equitable formulation did result in hydrologic performance that was similar to that of the solution selected from the Hydrologic Formulation but with an LID/GI distribution that was significantly more equitable.

### **2.3.2 The impacts of the LID/GI-equity correlation objective on hydrologic performance and equity at multiple cost constraints.**

Recall our first hypothesis that the Hydro-Equitable formulation will produce  $\epsilon$ -nondominated LID/GI distributions with objective values that are between those of solutions from the other formulations. The median hydrologic performance was found to be statistically different between all formulations at all cost constraints as revealed through two-sample Wilcoxon rank sum tests. The median hydrologic performance of solutions from the Hydrologic Formulation was superior to that of the Hydro-Equitable Formulation for all but one scenario. Likewise, the Hydro-Equitable Formulation produced improved hydrologic performance compared to the Equitable Formulation at all costs constraints. Two-sample Wilcoxon rank sum tests also revealed that the Hydro-Equitable  $\rho$  values were significantly lower than the Equitable  $\rho$  values ( $p < 0.05$ )

Though our results mostly confirm our first hypothesis, there are a few notable caveats. As mentioned above, results showed a single scenario where the median peak streamflow reduction of solutions in the Hydro-Equitable Formulation was better than that of the Hydrologic Formulation. Furthermore, the peak streamflow reduction performance was just 0.5% greater on average for the Hydrologic versus the Hydro-Equitable Formulation across all cost constraints and 1.3% greater for total runoff export reduction. In terms of how equity is defined in this study, the Hydro-Equitable Formulation produces LID/GI distributions that are significantly more

equitable than the Hydrologic Formulation. According to our results, and depending on the perspective of local stakeholders, integrating the  $\rho$  objective into similarly scaled optimization models could improve the equity of LID/GI distributions with minimal sacrifice to hydrologic performance.

A simple sensitivity analysis revealed that, out of the two hydrologic objectives, total runoff export reduction was slightly more sensitive to incremental changes in  $\rho$  than total runoff reduction across  $\epsilon$ -nondominated LID/GI distributions in the Hydro-Equitable Formulation. The sensitivity analysis also provided evidence that allows for the confirmation of our second hypothesis, that hydrologic performance will decline with increasing  $\rho$  values. Though, there are a few specific instances where peak stream flow reduction improved with increasing  $\rho$ , total runoff reduction was found to decline over all  $\rho$  intervals at each cost constraint.

### **2.3.3 Recommendations and Insights**

Maps produced using the methods in this study can be used in the planning of local LID/GI expansion to areas with higher percentages of historically marginalized populations. The maps should not be intended for final design recommendations but could be used for strategic LID/GI planning on a city-wide scale. The maps of nondominated LID/GI distributions like those produced in figure 2-4, could represent LID/GI implementation targets for each of the subbasins under consideration and could be used to help inform local stormwater LID/GI awareness, outreach, and implementation campaigns.

Combining SVI mapping and LID/GI optimization methods offers advantages over using either approach individually. This integration allows for a comprehensive analysis of tradeoffs between traditional hydrologic goals and socially desirable objectives specific to an area. Solely relying on SVI maps for increasing implementation in marginalized communities doesn't provide

insights into how LID/GI performs relative to optimal conditions in that area. As demonstrated in this study, implementing LID/GI in marginalized areas led to suboptimal runoff management when compared to what's achievable at Meadow Creek. Similarly, solely emphasizing hydrologic objectives doesn't ensure equitable LID/GI distribution. The multi-objective optimization approach generates solutions that can align with multiple LID/GI implementation goals, harmonizing various objectives effectively.

Numerous studies have shown that socially vulnerable communities tend to inhabit areas with the highest temperatures in urban environments, which are often associated with increased impervious surfaces and reduced vegetation (Huang et al., 2011; Mitchell & Chakraborty, 2018; Saverino et al., 2021). Additionally, research has indicated that impervious surfaces and reduced vegetation are key factors influencing urban runoff generation (Bera et al., 2022; Moglen, 2009). It might seem logical to assume that prioritizing runoff management in LID/GI planning would naturally lead to greater implementation in marginalized communities. However, this study highlights that this assumption doesn't always hold true, as the outcome depends on the specific runoff management goals of the area in question.

#### **2.3.4 Scope and Limitations**

We acknowledge that the equity objective chosen here is simply an example of an equity metric that would favor increasing LID/GI implementation in areas of greater social vulnerability, but that there could be many alternative formulations that better reflect an equitable distribution of LID/GI benefits. Future work should iteratively explore alternative formulations with the community to identify what social equity indicators are most acceptable and quantifiable for their area (Fletcher et al., 2022). For the purposes of this study, we assumed that the LID/GI implementation was a sufficient surrogate metric for increasing LID/GI access, as is

a common assumption among green LID/GI planners. The optimization objectives can be altered to include different runoff management and LID/GI implementation goals and constraints. For example, the equity objective could be modified to include other specific ecosystem services provided by LID/GIs, and the costs could be quantified differently. But the basic methodology can handle a wide range of alternative formulations to allow customization to each local watershed and community.

There are some important limitations to consider when using LID/GI optimization results produced using methods described in this study. Site-scale LID/GI design that is smaller than the upper Meadow Creek subbasins is beyond the scope of this study and would require more detailed design practices. To conduct an optimization study that was replicable by others, we chose spatial data that was likely to be available at most locations across the U.S. We recommend that these methods be applied only with the highest resolution socioeconomic data that is available to minimize the error introduced into the chosen social vulnerability index.

As the expansion of LID/GI may result in increasing property values within LID/GI accessible areas, the displacement or migration of marginalized people out of implementation areas is a viable concern that is not addressed by our algorithm. It is not enough to strategically place LID/GI in more marginalized communities. New urban LID/GI plans must also coincide with local policies that limit green gentrification (Anguelovski et al., 2020).

Where implemented, it is important for city managers and property owners to ensure that all stormwater facilities are maintained. If facilities are not maintained, then they can have Net Negative impacts on nearby communities. It is important that individual communities both support and understand future LID/GI plans before implementation (Dean et al., 2021) and that

these communities have the capacity to maintain stormwater facilities either through funding of resources and/or volunteer participation (Mandarano & Meenar, 2017).

## **2.4 Conclusions**

The primary objective of this study was to integrate a novel spatial social equity objective, constructed using modern social vulnerability mapping concepts, into a multi-objective optimization model for stormwater low impact development (LID/GI). This objective successfully maximized the linear correlation between green-LID/GI implementation and areas with higher percentages of historically marginalized people with small sacrifices in hydrologic performance under most cost constraints. Major conclusions that can be drawn from the results of this study include the following: 1) The LID/GI-SVI correlation objective can be used to direct optimization algorithms to search for LID/GI distributions that can achieve runoff management objectives, increase green LID/GI implementation in more marginalized areas, and explore the potential tradeoffs between hydrologic and equity goals. 2) LID/GI optimization formulations that only consider hydrologic objectives will likely not result in equitable LID/GI distributions. 3) LID/GI distributions performing well on the LID/GI-SVI correlation may be composed of different types of LID/GI compared to less equitable but more hydrologically favorable LID/GI distributions. 4) Integrating the LID/GI-SVI correlation objective slightly impaired runoff objectives, which suggests that these objectives moderately conflict with each other in our study area. Replication of these methods in other study areas is necessary to draw further conclusions regarding the integration of similar social equity objectives into urban stormwater LID/GI optimization models and to further test the hypotheses explored in this study.

## 2.5 Chapter 2 Works Cited

- Albemarle County. 2023. "Albemarle County Local TMDL Action Plan : 22902(434)".
- Albemarle County. 2022. "Local TMDL action plan: Sediment TMDLs for moores creek, lodge creek, meadow creek, and schenks branch." Accessed September 1, 2022.  
<https://www.albemarle.org/home/showpublisheddocument/8776/637553903498430000>.
- Allen, L. J. 2020. "Factors influencing the establishment of stormwater utilities in the United States." *J. Urban Environ. Eng.* 14 (1): 3–31.  
<https://doi.org/10.4090/juee.2020.v14n1.003031>.
- Anguelovski, I., Brand, A. L., Connolly, J. J. T., Corbera, E., Kotsila, P., Steil, J., Garcia-Lamarca, M., Triguero-Mas, M., Cole, H., Baró, F., Langemeyer, J., del Pulgar, C. P., Shokry, G., Sekulova, F., & Argüelles Ramos, L. 2020. "Expanding the Boundaries of Justice in Urban Greening Scholarship: Toward an Emancipatory, Antisubordination, Intersectional, and Relational Approach." *Annals of the American Association of Geographers*, 110(6), 1743–1769. <https://doi.org/10.1080/24694452.2020.1740579>
- Arlington County. 2022 . "Stormwater utility fee estimator". Retrieved November 21, 2022, from: <https://www.arlingtonva.us/Government/Programs/Sustainability-and-Environment/Stormwater/Stormwater-Utility-Feasibility-Study/Stormwater-Utility-Fee-Estimator>
- Bera, D., Kumar, P., Siddiqui, A., & Majumdar, A. (2022). Assessing impact of urbanisation on surface runoff using vegetation-impervious surface-soil (V-I-S) fraction and NRCS curve number (CN) model. *Modeling Earth Systems and Environment*, 8(1), 309–322.  
<https://doi.org/10.1007/s40808-020-01079-z>
- Bernhardt, E. 2011. "River restoration : the fuzzy logic of repairing reaches to reverse catchment scale degradation." *Ecological Applications*, 21(6), 1926–193.1 <https://doi.org/10.1890/10-1574.1>.
- Block, A. H., Livesley, S. J., & Williams, N. S. G. 2014." Responding to the Urban Heat Island: A Review of the Potential of Green Infrastructure Literature Review. " Victorian Center Climate Change Adaptation Research.
- Celik, S., & Binatli, A. O. 2018. "Energy Savings and Economic Impact of Green Roofs : A Pilot Study Energy Savings and Economic Impact of Green Roofs : A Pilot Study." *Emerging Markets Finance and Trade*, 54(8), 1778–1792.  
<https://doi.org/10.1080/1540496X.2018.1434620>
- Charlottesville. 2021. "Local TMDL action plan: Sediment TMDLs for moores creek, lodge creek, meadow creek, and schenks branch." Accessed September 1, 2022.  
<https://www.charlottesville.gov/DocumentCenter/View/5468/City-of-Charlottesville-Local-TMDL-Action-Plan---Moores-Lodge-Meadow-Schenks-Sediment-TMDL---April-2021-PDF>.
- Charlottesville, U.S. Army Corp of Engineers, & URS Corporation. 2008. *Technical Report: Charlottesville Stormwater Master Plan*. Charlottesville, VA

- Charlottesville, U.S. Army Corp of Engineers, & URS Corporation. 2010. *Technical Report: Charlottesville Stormwater Services*. Charlottesville, VA
- Charlottesville. 2019. "Chesapeake Bay TMDL Phase II Action Plan".
- Chesapeake Conservancy. 2019. "Chesapeake Bay Program Land Use/Land Cover Data Project." Chesapeake Conservancy Database. Accessed June 23, 2022, from <https://www.chesapeakeconservancy.org/conservation-innovation-center/high-resolution-data/lulc-data-project-2022/>
- Chini, C. M., J. F. Canning, K. L. Schreiber, J. M. Peschel, and A. S. Stillwell. 2017. "The green experiment: Cities, green stormwater infrastructure, and sustainability." *Sustainability (Switzerland)* 9 (1): 1–21. <https://doi.org/10.3390/su9010105>.
- Copeland, C. 2013. "Green infrastructure and issues in managing urban stormwater." In *Selected issues in water resources and management*, 79–113. Washington, DC: Federation of American Scientists.
- Dean, A. J., Newton, F. J., Gulliver, R. E., Fielding, K. S., & Ross, H. 2021. "Accelerating the adoption of water sensitive innovations: community perceptions of practices and technologies to mitigate urban stormwater pollution." *Journal of Environmental Planning and Management*, 0(0), 1–20. <https://doi.org/10.1080/09640568.2021.200229>
- Department of Environmental Protection (DEP), Montgomery County, Maryland. 2022. "Watershed Restoration Suitability & Equity Mapping Tools." Accessed March 12, 2022, from <https://www.montgomerycountymd.gov/water/restoration/equity.html>
- Dhakal, K. P., and L. R. Chevalier. 2017. "Managing urban stormwater for urban sustainability: Barriers and policy solutions for green infrastructure application." *J. Environ. Manage.* 203 (Dec): 171–181. <https://doi.org/10.1016/j.jenvman.2017.07.065>.
- Dietz, M. E. 2007. Low impact development practices: "A review of current research and recommendations for future directions." *Water, Air, and Soil Pollution* 186(1-4), 351–363. <https://doi.org/10.1007/s11270-007-9484-z>
- Du, M., & Zhang, X. 2020. "Urban greening: A new paradox of economic or social sustainability?" *Land Use Policy*, 92, 1-11. <https://doi.org/10.1016/j.landusepol.2020.104487>
- Dukes, E. F. 2019. "Trauma, History and Resilience: A Charlottesville Story." *Ohio State Journal on Dispute Resolution*, 34(5), 753-776.
- Eckart, K., McPhee, Z., & Bolisetti, T. 2018. "Multiobjective optimization of low impact development stormwater controls." *Journal of Hydrology*, 562, 564–576. <https://doi.org/10.1016/j.jhydrol.2018.04.068>
- Encyclopedia of Mathematics. 2020. "Mahalanobis distance". Retrieved November 29, 2022, from [https://encyclopediaofmath.org/index.php?title=Mahalanobis\\_distance](https://encyclopediaofmath.org/index.php?title=Mahalanobis_distance)

- Entzminger, Brielle. 2017. "Uncovered: How racist redlining shaped our urban forest." *Cville Weekly*, October 14, 2020. <https://www.c-ville.com/uncovered-how-racist-redlining-shaped-our-urban-forest/>
- Erispaha, A. (2022). "Swmmio.". Accessed April 4, 2022. <https://pypi.org/project/swmmio/0.1.0/>
- ESRI (Environmental Systems Research Institute). 2021. "Soil survey geographic (SSURGO) database mapviewer." Accessed August 8, 2021. <https://www.arcgis.com/apps/mapviewer/index.html?layers=34dacdf1af5a40cda9e0c14ac4e16aba>.
- Executive Office of the President, Young, S. D., Mallory, B., & McCarthy, G. 2021. "Memorandum for the Heads of Departments and Agencies: Interim Implementation Guidance for the Justice40 Initiative". Accessed June 30, 2022. <https://www.whitehouse.gov/wp-content/uploads/2021/07/M-21-28.pdf>
- Ferguson, M., Roberts, H. E., McEachan, R. R. C., & Dallimer, M. 2018. "Contrasting distributions of urban green infrastructure across social and ethno-racial groups." *Landscape and Urban Planning*, 175, 136–148. <https://doi.org/10.1016/j.landurbplan.2018.03.020>
- Fletcher, S., A. Hadjimichael, J. Quinn, K. Osman, M. Giuliani, D. Gold, A. J. Figueroa, and B. Gordon. 2022. "Equity in water resources planning: A path forward for decision support modelers" *J. Water Resour. Plann. Manage.* 148 (7): 104–115. [https://doi.org/10.1061/\(asce\)wr.1943-5452.0001573](https://doi.org/10.1061/(asce)wr.1943-5452.0001573).
- Garcia-Cuerva, L., Berglund, E. Z., & Rivers, L. 2018. An integrated approach to place Green Infrastructure strategies in marginalized communities and evaluate stormwater mitigation. *Journal of Hydrology*, 559, 648–660. <https://doi.org/10.1016/j.jhydrol.2018.02.066>
- Giacomoni, M. H., & Joseph, J. 2017. "Multi-objective evolutionary optimization and Monte Carlo simulation for placement of low impact development in the catchment scale." *J. Water Resour. Plan. Manag.* 143(9), 1-15. [https://doi.org/10.1061/\(ASCE\)WR.1943-5452.0000812](https://doi.org/10.1061/(ASCE)WR.1943-5452.0000812)
- Hadka, D., & Reed, P. 2013. "Borg: An Auto-Adaptive Many-Objective Evolutionary Computing Framework." *Evolutionary Computation* 21(2), 231-259. [https://doi.org/10.1162/EVCO\\_a\\_00075](https://doi.org/10.1162/EVCO_a_00075)
- Hadka, D., & Reed, P. 2015. "Large-scale parallelization of the Borg multiobjective evolutionary algorithm to enhance the management of complex environmental systems." *Environmental Modelling and Software*, 69, 353–369. <https://doi.org/10.1016/j.envsoft.2014.10.014>
- Harrington, E., and D. Hsu. 2018. "Roles for government and other sectors in the governance of green infrastructure in the U.S." *Environ. Sci. Policy* 88 (Jun): 104–115. <https://doi.org/10.1016/j.envsci.2018.06.003>.
- Harris Sr, W. M., & Olmsted, N. 1991. "Public housing in Charlottesville: The black experience in a small Southern City." *The Review of Black Political Economy*, 19(3-4), 161-174

- Heck, S. 2021. "Greening the color line: historicizing water infrastructure redevelopment and environmental justice in the St. Louis metropolitan region." *Journal of Environmental Policy and Planning*. <https://doi.org/10.1080/1523908X.2021.1888702>
- Heckert, M., & Rosan, C. D. 2016. "Urban Forestry & Urban Greening Developing a green infrastructure equity index to promote equity planning." *Urban Forestry & Urban Greening*, 19, 263–270. <https://doi.org/10.1016/j.ufug.2015.12.011>
- Hillier, A. E. 2003. "Redlining and the home owners' loan corporation." *Journal of Urban History*, 29(4), 394–420. <https://doi.org/10.1177/0096144203029004002>
- Hopkins, K. G., Grimm, N. B., & York, A. M. 2018. "Influence of governance structure on green stormwater infrastructure investment." *Environmental Science and Policy*, 84, 124–133. <https://doi.org/10.1016/j.envsci.2018.03.008>
- Huang, G., Zhou, W., & Cadenasso, M. L. (2011). Is everyone hot in the city? Spatial pattern of land surface temperatures, land cover and neighborhood socioeconomic characteristics in Baltimore, MD. *Journal of Environmental Management*, 92(7), 1753–1759. <https://doi.org/10.1016/j.jenvman.2011.02.006>
- Johns, C. M. 2019. "Understanding barriers to green infrastructure policy and stormwater management in the City of Toronto: A shift from grey to green or policy layering and conversion?" *J. Environ. Plann. Manage.* 62 (8): 1377–1401. <https://doi.org/10.1080/09640568.2018.1496072>.
- Keeler, B. L., Hamel, P., McPhearson, T., Hamann, M. H., Donahue, M. L., Meza Prado, K. A., Arkema, K. K., Bratman, G. N., Brauman, K. A., Finlay, J. C., Guerry, A. D., Hobbie, S. E., Johnson, J. A., MacDonald, G. K., McDonald, R. I., Neverisky, N., & Wood, S. A. 2019. "Social-ecological and technological factors moderate the value of urban nature." *Nature Sustainability*, 2(1), 29–38). <https://doi.org/10.1038/s41893-018-0202-1>
- Klosterwill, K. J., Diamond, A. U., Wilson, B. B., & Ripple, J. 2020. "Constructing Health: Representations of Health and Housing in Charlottesville's Urban Renewals." *Journal of Architectural Education*, 74(2), 222-236.
- Kondo, M. C., Low, S. C., Henning, J., & Branas, C. C. 2015. "The Impact of Green Stormwater Infrastructure Installation on Surrounding Health and Safety." *American Journal of Public Health*, 105(3), 114–121. <https://doi.org/10.2105/AJPH.2014.302314>
- Laumanns, M., Thiele, L., Deb, K., & Zitzler, E. 2002. "Combining convergence and diversity in evolutionary multiobjective optimization." *Evolutionary Computation*, 10(3), 263–282. <https://doi.org/10.1162/106365602760234108>
- Luan, B., Yin, R., Xu, P., Wang, X., Yang, X., Zhang, L., & Tang, X. 2019. "Evaluating Green Stormwater Infrastructure strategies efficiencies in a rapidly urbanizing catchment using SWMM-based TOPSIS." *Journal of Cleaner Production*, 223, 680–691. <https://doi.org/10.1016/j.jclepro.2019.03.028>
- Madureira, H., & Andresen, T. 2014. "Planning for multifunctional urban green infrastructures: Promises and challenges." *Urban Design International*, 19(1), 38–49. <https://doi.org/10.1057/udi.2013.11>

- Mandarano, L., & Meenar, M. 2017. "Equitable distribution of green stormwater infrastructure: a capacity-based framework for implementation in disadvantaged communities." *Local Environment*, 22(11), 1338–1357. <https://doi.org/10.1080/13549839.2017.1345878>
- Maryland Department of the Environment (DOE). 2016. "BMP Cost Estimates Spreadsheet". Accessed: June 1, 2022. [https://mde.maryland.gov/programs/Water/TMDL/TMDLImplementation/Documents/Data\\_and\\_Tools/BMP\\_Unit\\_Cost\\_Estimates\\_12.23.2016.pdf](https://mde.maryland.gov/programs/Water/TMDL/TMDLImplementation/Documents/Data_and_Tools/BMP_Unit_Cost_Estimates_12.23.2016.pdf)
- Mason, L. R., Ellis, K. N., Hathaway, J. M., Reyes, L., Ellis, K. N., Hathaway, J. M., & Mason, L. R. 2019. "Urban flooding , social equity , and “ backyard ” green infrastructure : An area for multidisciplinary practice infrastructure : An area for multidisciplinary practice." *Journal of Community Practice*, 27(3–4), 334–350. <https://doi.org/10.1080/10705422.2019.1655125>
- Mattson, R., Alexander, F., Cassedy, D., & Henry, G. 1995." From the Monacans to Monticello and Prehistoric and Historic Contexts for Albemarle County, Virginia." Accessed April 12, 2022. [https://www.albemarle.org/upload/images/Forms\\_Center/Departments/Community\\_Development/Forms/Historic\\_Preservation/AB-060\\_Monicans\\_to\\_Monticello\\_Prehistoric&Historic\\_Contexts\\_Albemarle\\_1995\\_TRC\\_report.pdf](https://www.albemarle.org/upload/images/Forms_Center/Departments/Community_Development/Forms/Historic_Preservation/AB-060_Monicans_to_Monticello_Prehistoric&Historic_Contexts_Albemarle_1995_TRC_report.pdf)
- Mazzotta, M. J., Besedin, E., & Speers, A. E. 2014. "A meta-analysis of hedonic studies to assess the property value effects of low impact development." *Resources* 3(1), 31-61. <https://doi.org/10.3390/resources3010031>
- McDonnell, Bryant E., Ratliff, Katherine M., Tryby, Michael E., Wu, Jennifer Jia Xin, & Mullapudi, Abhiram. 2020. "PySWMM: The Python Interface to Stormwater Management Model (SWMM)." *Journal of Open Source Software*, 5(52), 2292, <https://doi.org/10.21105/joss.02292>
- Meerow, S., & Newell, J. P. 2017. "Spatial planning for multifunctional green infrastructure: Growing resilience in Detroit." *Landscape and Urban Planning*, 159, 62–75. <https://doi.org/10.1016/j.landurbplan.2016.10.005>
- Mell, I., & Whitten, M. 2021." Access to nature in a post covid-19 world: Opportunities for green infrastructure financing, distribution and equitability in urban planning." *International Journal of Environmental Research and Public Health*, 18(4), 1–16. <https://doi.org/10.3390/ijerph18041527>
- Mitchell, B. C., & Chakraborty, J. (2018). Exploring the relationship between residential segregation and thermal inequity in 20 U.S. cities. *Local Environment*, 23(8), 796–813. <https://doi.org/10.1080/13549839.2018.1474861>
- Mitchell, R. J., Richardson, E. A., Shortt, N. K., & Pearce, J. R. 2015. "Neighborhood Environments and Socioeconomic Inequalities in Mental Well-Being." *American Journal of Preventive Medicine*, 49(1), 80–84. <https://doi.org/10.1016/j.amepre.2015.01.017>
- [Moglen, G. E. \(2009\). Hydrology and Impervious Areas. \*Journal of Hydrologic Engineering\*, 14\(4\), 303–304. \[https://doi.org/10.1061/\\(asce\\)1084-0699\\(2009\\)14:4\\(303\\)\]\(https://doi.org/10.1061/\(asce\)1084-0699\(2009\)14:4\(303\)\)](https://doi.org/10.1061/(asce)1084-0699(2009)14:4(303))

- Montgomery County, Maryland DEP (Department of Environmental Protection). 2022. "Watershed restoration suitability & equity mapping tools." Accessed March 12, 2022. <https://www.montgomerycountymd.gov/water/restoration/equity.html>.
- National Community Reinvestment Coalition (NCRC). 2007. "Income is No Shield Against Racial Differences in Lending: A Comparison of High-cost Lending in America's Metropolitan Areas." *Washington, DC: National Community Reinvestment Coalition*.
- Nature Conservancy and Charlottesville. 2013. "Meadow creek stream restoration project fact sheet." Accessed September 9, 2021. <https://www.charlottesville.gov/DocumentCenter/View/531/Meadow-Creek-Restoration-Project-Fact-Sheet-PDF>.
- Palmer, M. A., Hondula, K. L., & Koch, B. J. 2014. "Ecological restoration of streams and rivers: Shifting strategies and shifting goals." *Annual Review of Ecology, Evolution, and Systematics*, 45(1), 247–269. <https://doi.org/10.1146/annurev-ecolsys-120213-091935>
- Porse, E. 2018. "Open data and stormwater systems in Los Angeles: applications for equitable green infrastructure." *Local Environment*, 23(5), 505–517. <https://doi.org/10.1080/13549839.2018.1434492>
- Rivanna Conservation Society. 1996. Rivanna river history. Accessed December 1, 2021. <http://www.rivannariver.org/wp-content/uploads/2015/02/RCS-Rivanna-River-History.pdf>
- Roe, J. J., Ward Thompson, C., Aspinall, P. A., Brewer, M. J., Duff, E. I., Miller, D., Mitchell, R., & Clow, A. 2013. "Green space and stress: Evidence from cortisol measures in deprived urban communities." *International Journal of Environmental Research and Public Health*, 10(9), 4086–4103. <https://doi.org/10.3390/ijerph10094086>
- Santamouris, M. 2014. "Cooling the cities - A review of reflective and green roof mitigation technologies to fight heat island and improve comfort in urban environments." *Solar Energy*, 103, 682–703. <https://doi.org/10.1016/j.solener.2012.07.003>
- Saverino, K. C., Routman, E., Lookingbill, T. R., Eanes, A. M., Hoffman, J. S., & Bao, R. (2021). Thermal inequity in richmond, va: The effect of an unjust evolution of the urban landscape on urban heat islands. *Sustainability (Switzerland)*, 13(3), 1–18. <https://doi.org/10.3390/su13031511>
- Scott, M., Lennon, M., Haase, D., Kazmierczak, A., Clabby, G., & Beatley, T. 2016. "Nature-based solutions for the contemporary city/Re-naturing the city/Reflections on urban landscapes, ecosystems services and nature-based solutions in cities/Multifunctional green infrastructure and climate change adaptation: brownfield greening as an adaptation strategy for vulnerable communities?/Delivering green infrastructure through planning: insights from practice in Fingal, Ireland/Planning for biophilic cities: from theory to practice". *Planning Theory and Practice*, 17(2), 267–300. <https://doi.org/10.1080/14649357.2016.1158907>
- Sebti, A., Aceves, M. C., Bennis, S., & Fuamba, M. 2016. "Improving nonlinear optimization algorithms for BMP implementation in a combined sewer system." " *J. Water Resour. Plan. Manag.*, 142(9). [https://doi.org/10.1061/\(ASCE\)WR.1943-5452.0000669](https://doi.org/10.1061/(ASCE)WR.1943-5452.0000669)

- U.S. Census Bureau. 2019. "Tiger/line with selected demographic and Economic Data." Census.gov. Accessed September 30, 2021. <https://www.census.gov/geographies/mapping-files/time-series/geo/tiger-data.html>
- U.S. Environmental Protection Agency (USEPA). 2022a. "Urban Runoff: Low Impact Development". Retrieved November 20, 2022, from <https://www.epa.gov/nps/urban-runoff-low-impact-development>
- U.S. Environmental Protection Agency (USEPA). 2022b. "Civil Cases and Settlements by Statute". Retrieved November 20, 2022, from <https://cfpub.epa.gov/enforcement/cases/index.cfm?templatePage=12&ID=3&sortBy=&stat=Clean%20Water%20Act>
- U.S. Environmental Protection Agency (USEPA). 2014. "EJSCREEN technical documentation 2014 - US EPA. EJSCREEN Technical Documentation 2014." Retrieved June 14, 2022, from [https://www.epa.gov/sites/default/files/2021-04/documents/ejscreen\\_technical\\_document.pdf](https://www.epa.gov/sites/default/files/2021-04/documents/ejscreen_technical_document.pdf)
- U.S. Geological Survey (USGS). 2019. "1/3 Arc-Second Resolution Digital Elevation Model" . Accessed February 19, 2021. <https://www.usgs.gov/the-national-map-data-delivery>
- Virginia Department of Environmental Quality (VDEQ). 2020. "2020 Impaired Waters - 303(d) List 2020 Impaired Waters - 303(d) List Category 5 - Waters needing Total Maximum Daily Load Study Aquatic Life 303(d)". Accessed January 1, 2022. <https://www.deq.virginia.gov/home/showpublisheddocument/2251/637436331811570000>
- Virginia Water Resources Research Center (VWRRC), & Virginia Department of Environmental Quality (VDEQ). 2013. "Virginia Stormwater BMP Clearinghouse Draft Design Specifications." Accessed Dec 30, 2020. <https://swbmp.vwrcc.vt.edu/>
- The Nature Conservancy. 2013. "Meadow Creek Stream Restoration Project Fact Sheet." Accessed September 9, 2021. [www.charlottesville.org/meadowcreek](http://www.charlottesville.org/meadowcreek)
- Venkataramanan, V., Packman, A. I., Peters, D. R., Lopez, D., McCuskey, D. J., McDonald, R. I., Miller, W. M., & Young, S. L. 2019. "A systematic review of the human health and social well-being outcomes of green infrastructure for stormwater and flood management." *Journal of Environmental Management*, 246(June), 868–880. <https://doi.org/10.1016/j.jenvman.2019.05.028>
- Wolch, J. R., Byrne, J., & Newell, J. P. 2014. "Urban green space, public health, and environmental justice: The challenge of making cities "just green enough."" *Landscape and Urban Planning*, 125, 234–244. <https://doi.org/10.1016/j.landurbplan.2014.01.017>
- Wright, W. J. 2021. "As Above, So Below : Anti-Black Violence as Environmental Racism." *Antipode*, 53(3), 791–809. <https://doi.org/10.1111/anti.12425>
- Yager, Jordy. 2017. "A new page: Longtime 10th & Page residents are seeing a shift in the neighborhood". Cville Weekly, December 1, 2017. <https://www.c-ville.com/new-page->

[longtime-10th-page-residents-seeing-shift-neighborhood/](#)

Zhang, K., & Chui, T. F. M. 2018. "A comprehensive review of spatial allocation of LID/GI-BMP-GI practices: Strategies and optimization tools." In *Science of the Total Environment* (Vol. 621, pp. 915–929). Elsevier B.V. <https://doi.org/10.1016/j.scitotenv.2017.11.281>

Zhu, Z., Ren, J., & Liu, X. 2019. "Urban Forestry & Urban Greening Green infrastructure provision for environmental justice: Application of the equity index in Guangzhou , China." *Urban Forestry & Urban Greening*, 46, 126443. <https://doi.org/10.1016/j.ufug.2019.12644>

## **Chapter 3: Simulating the Effects of Channel Restoration Designs on in-Stream Nitrogen Uptake**

This chapter is currently being prepared for publication.

### **Chapter 3 Abstract**

The proliferation of impervious development in urban areas has intensified stormwater runoff, increased flow velocities, and elevated nutrient loads. This has caused degradation in natural channels and receiving water bodies through processes like erosion, scouring, sedimentation, and eutrophication. Channel restoration, a prevalent engineering practice, is employed to rectify deteriorated streams. Environmental scientists and aquatic ecologists contend that effective restoration should augment stream functions, boosting assimilative and nutrient retention capabilities. In this study, we have used the Small Streams Hydro-Biogeochemistry Simulator (SSHBS) to assess a variety of configurations of riffles, pools, and meanders along an unrestored stream segment in an urban watershed within Baltimore County. SSHBS has previously been used and validated with empirical observations on our study stream. Our objective is to address the following research questions: How do geomorphic restoration alterations impact the rates of dissolved inorganic nitrogen (DIN) uptake in an urban stream? Our findings indicate the following: 1) Enhanced benthic area, especially from pools and meandering features, increased simulated whole Reach net DIN uptake through amplified denitrification under closed-canopy conditions; 2) The removal of riparian canopy, often coinciding with channel restoration efforts, boosted net DIN uptake most significantly, via increased algal DIN uptake; 3) The pool (P) and riffle-meander (RM) scenarios showcased similar rates of simulated net DIN uptake under both canopy conditions; 4) Designs combining riffle, pool, and meander features performed better compared to those with fewer features; 5) The return of tree canopy growth is expected to reduce the overall increase in net DIN uptake for all restoration designs, primarily due to reduced algal activity from lower levels of photosynthetically active radiation reaching the stream. Restorations with a combination of features, particularly those incorporating a pool, could be more effective in sustaining net DIN uptake rates compared to single-feature channel scenarios upon the return of tree canopy growth. Although the specific simulation outcomes lack field validation, our study demonstrates the viability of SSHBS as a modeling tool for stream restoration designers seeking to estimate the effects of geomorphic restoration features on net DIN uptake rates. This research has the potential to enrich prevailing methodologies for stream restoration design.

### 3.0 Introduction

Over the past century, land in the United States has become increasingly developed for commercial, industrial, residential, and other anthropogenic purposes. Impervious land development has elevated volumes and velocities of stormwater runoff and nutrient loadings in urban areas, causing the degradation of naturally formed channels and benthic habitat through erosion, scouring, sedimentation, and eutrophication. Stream restoration has become a common engineering practice deployed to repair degraded streams. Common goals of stream restoration include improving water quality, increasing biodiversity, improving riparian and in-stream habitat, stabilizing the channel, protecting proximal infrastructure, and enhancing aesthetics. Stream restoration often requires a variety of manipulations of the riparian ecosystem and the stream geomorphology, such as: planting native riparian vegetation; structural alteration of the channel with the creation of meanders, riffles, and pools to regulate flow; and the reconnection of the streambank to the floodplain (Bennett et al., 2011).

In the Chesapeake Bay area, there is increased pressure to design stream restorations that aim to improve water quality and to reduce nitrogen (N) and phosphorus (P) daily loads (Williams et al., 2017). Hall et al. (2014) concludes that meeting total maximum daily load (TMDL) requirements with in-stream restoration practices must include enhancing stream functions that increase assimilative and retention capacity of the entire ecosystem. Other researchers have pointed to the importance of stream ecotones such as the stream-floodplain-connection and benthic transient storage zones as opportunities to enhance denitrification (Kaushal et al., 2008; Klockner et al., 2009; Lawrence et al., 2013; Roley et al., 2012). Additionally, algal assimilation of  $\text{NO}_3\text{-N}$  and  $\text{NH}_4\text{-N}$  has been found to provide significant but temporary reductions of inorganic nitrogen export from streams (Crumpton & Isenhardt, 1987;

Hall & Tank, 2003; Webster et al., 2003). Reisinger et al. (2019) showed that stream restorations can enhance nitrogen uptake in the stream, but these enhancements can be mostly attributed to the removal of tree canopy which increases the available light for primary production.

Stream restoration is a multi-billion-dollar industry in the United States (Bernhardt et al., 2005) that has become more commonplace with the advent of a compensatory stream mitigation program vis-a-vis section 404 of the Clean Water act (Doyle & Douglas Shields, 2012; Lave et al., 2010). The largely private practice industry and applied science of stream restoration has been dominated by the “Natural Channel Design” (NCD) approach (D. Rosgen, 1998). The NCD method is a multi-step stream engineering design process involving the restoration of a degraded stream’s sediment and streamflow regimes towards that of a natural reference stream through manipulation and maintenance of channel geomorphology. A central tenet of NCD is that stream form and function are highly interrelated. Critics of NCD have often cited a high failure rate and have found it questionable to assume that channel form manipulation alone can restore fluvial ecological functioning without accounting for ecological, chemical, and biological processes (Wohl et al., 2015; Palmer et al., 2014; Simon et al., 2007). In response to this criticism, Rosgen (2011) emphasized the importance of including physical, biological, chemical, aesthetic, social, and economic goals in sustainable NCD projects (D. L. Rosgen, 2011). Nevertheless, the academic community has proceeded to advocate for the integration of more ecosystem process-based approaches to evaluate the efficacy of stream restoration designs.

As summarized by Wohl et al. (2015), there is increasing demand for a better understanding of how various aspects of physical complexity can assist biogeochemical function, stream ecosystem productivity, and contaminant degradation, and how small alterations in stream forms can make a difference to instream nutrient spiraling. Nutrient spiraling is a concept

that describes how nutrients move, cycle, and transform within stream ecosystems as they travel downstream. It is a useful concept related to modeling how nutrients transform between different biogeochemical species and how they are retained within in-stream ecosystems. Nutrient spiraling lengths are related to how well a stream retains nutrients and is impacted by physical characteristics of a stream channel along with many other anthropogenically affected variables (Newbold et al., 1982). Nutrient spiraling length is the expected distance a nutrient molecule travels down a stream before uptake occurs. Nutrient spiraling lengths increase with stream depth, where the surface water volume to benthic area is increased, and with stream velocity, where the hydraulic residence times are reduced (Peters et al., 2011). Process-based modeling tools that can simulate the effects of a variety of different stream restoration designs on in-stream ecological functioning and DIN spiraling are especially useful since physical experimentation with stream channels is expensive and rare.

Since the late 20<sup>th</sup> century, stream restoration designers have had access to an array of modeling tools that can help to estimate the impacts of channel alterations on the streamflow and sediment regimes. However, these models typically lack functions for integrated hydraulic and ecosystem processes. Recently, more process-based models have been developed that can assist in the estimation of nutrient retention and removal resulting from different stream restoration designs that are responsive to altered stream hydraulics. Though the model is not fully process-based, Calfe et al. (2022) coupled HEC-RAS with an R script model for nitrate removal to analyze the cumulative effects of restoration scenarios on a full stream network with a water and solute mass balance approach. At a smaller scale, Lin et al. (2021) developed the Small Stream Hydro-Biogeochemistry Simulator (SSHBS) and used it to compare ecological processing rates between two reach segments, one restored and one unrestored, at Scott's Level Branch (SLB) in

Baltimore County, Maryland. As will be demonstrated in this study, SSHBS can also be used to simulate a variety of ecological effects of different channel designs and to analyze the key relationships between simulated in-stream ecological and nutrient retention processes.

We conduct a channel restoration scenario analysis and answer the following research questions: 1) How do channels with simulated riffle, pool, and meandering features impact DIN uptake rates at an unrestored reach at SLB? 2) How does the removal of canopy influence net DIN uptake across a variety of channel restoration designs? 3) What are the most significant differences in DIN uptake rates between different restoration designs? We adapted a version of the SSHBS model that was first deployed by Lin et al. (2021) at paired restored and unrestored reaches at SLB to answer these questions. We carry out a set of numerical experiments, varying channel restoration features to estimate the impacts on DIN ( $\text{NO}_3\text{-N}$  and  $\text{NH}_4\text{-N}$ ) uptake rates and evaluate the individual and integrated impacts of the different restoration features.

### **3.0.1 Study Area**

In this study we test how various riffle, pool, and meander restoration designs impact simulated DIN dynamics at a 133-meter-long reach at SLB within the Gwynn's Falls watershed. This site, because of prior stream restorations in the area and field monitoring (Reisinger et al 2019), has been modeled before using SSHBS (Lin et al 2021). This reach that is the subject of our numerical experiments was unrestored prior to 2019 but has since undergone restoration that are unrelated to this study. Figure 3-1 depicts our study area which consists of 72 hectares of suburban land cover. The catchment area is approximately 40% impervious surface and 32% turfgrass that mostly consists of lawn (Chesapeake Conservancy, 2019). A set of the streams within the Scotts Level Branch watershed have undergone restorations since 2014 with the USEPA touting the effort as a “non-point source success story” (EPA, 2022) for sediment and

nutrient reduction. To protect the downstream Chesapeake Bay, Baltimore County has planned to reduce nutrient load reductions (as compared to the 2009 levels) for the SLB restoration by 29% for total nitrogen and by 41.5% for total phosphorus (Baltimore County, 2013a, 2013b).

## Scott's Level Branch Unrestored Basin

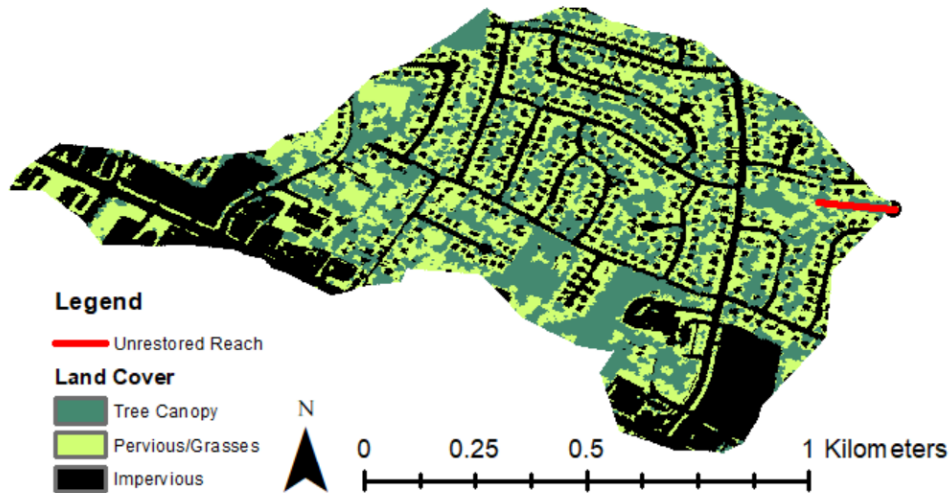


**Figure 3-1:** Scotts Level Branch Study Area and Unrestored Outlet Reach

### 3.1 Methods

#### 3.1.1 Simulating in-stream flow with SSHBS.

SSHBS is a hybrid process and data-driven stream ecosystem model that can be used to evaluate in-stream nutrient processing (Lin et al., 2021), including the potential impacts of different stream restoration designs. SSHBS partitions a study stream into longitudinally connected geomorphic zones that receive lateral water and nutrient inputs from upstream and terrestrial hillslopes. SSHBS simulates daily average hydraulic parameters at different cross-sections along the study reach using a combination of observed discharge data and a lookup table for key stream hydraulic parameters generated by a routing model. Observed flow data was

retrieved from the SLB USGS stream gage at Rockdale, MD (USGS, 2023), which is downstream of our study reach. Flow was estimated at each point along the study reach by scaling the observed discharge to drainage area. Using the area-weighted flow, Manning Equation parameters (slope, Manning n, hydraulic radius, cross-sectional area, and volume) are back-calculated using the lookup table. We use the unrestored Manning's equation cross-section data obtained by Lin et al. (2021) in the study as the base case scenario. The modeling period spans the time period between January 2012 to December 2017. The in-stream flow model is explained in more detail by Lin et al. (2021) and in appendix B of this paper. The Manning equation lookup tables are included in the supplementary information.

### **3.1.2 Simulating in-stream nutrient flux with SSHBS.**

In addition to flow, SSHBS input data also includes lateral water input concentrations of nitrogen and phosphorus, photosynthetically active radiation (PAR), water temperature, and organic detritus (leaf litter) loadings. Lin et al. (2021) estimated PAR at the stream and leaf litter loadings for the unrestored reach using the Regional Hydro-Ecological Simulation System (RHESSys). Daily nitrogen and phosphorus concentrations at this reach were estimated using the Weighted Regressions on Time, Discharge, and Season (WTRDS) method (Hirsch et al., 2010), calibrated with weekly concentration and discharge measurements in an adjacent, similar watershed that were conducted as part of the Baltimore Ecosystem study since 1998 (Baltimore Ecosystem Study, 2019) and by in-stream measurements at SLB by Reisinger et al. (2019). RHESSys is a Geographic Information System (GIS)- based model that employs mathematical functions to simulate a range of biogeochemical and hydrological processes, encompassing surface/subsurface hydrologic flows, microclimate variations, canopy radiation interactions, and the cycling of carbon and nitrogen within vegetation and soil. Within each stream reach zone,

SSHBS computes fluxes and transformations of carbon, nitrogen, and phosphorus between the water column, algae and benthic microbes, and organic detritus. These fluxes are governed by flow conditions, temperature, light, and ecological processes occurring within each reach zone including algal uptake, denitrification, nitrification, immobilization, and mineralization. Figure 3-2 is a conceptual diagram of the nutrient fluxes that are simulated by SSHBS. The setup of the in-stream ecosystem model used in this study is explained in more detail by Lin et al. (2021) with key functions briefly explained in appendix B.

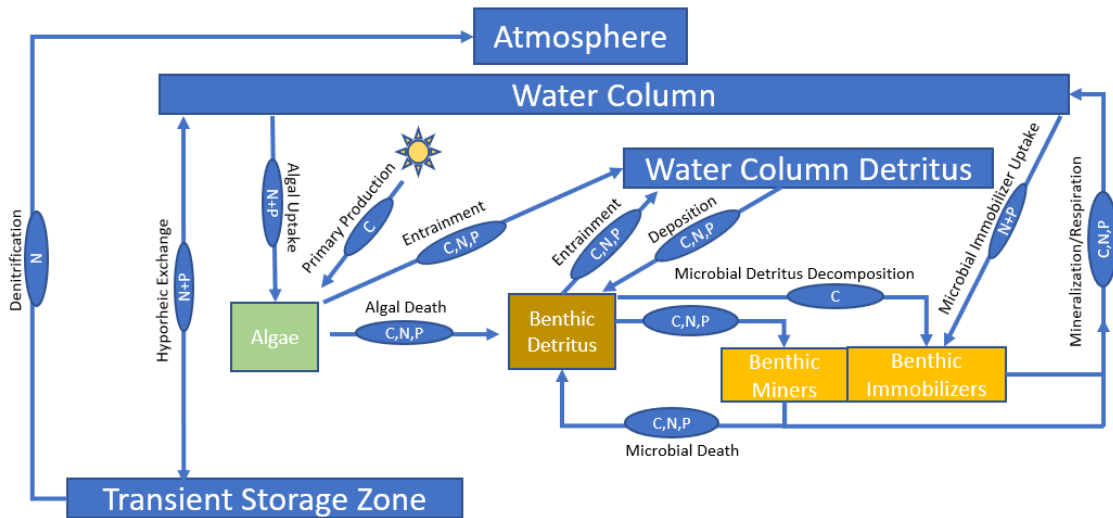


**Figure 3-2:** Flow diagram of ecosystem processes involved in modeling carbon, nitrogen, and phosphorus flux using SSHBS.

### 3.1.3 Simulating N Uptake Rates for Riffle, Pool, and Meander Channel Restoration Scenarios Under Open and Closed Canopy Conditions

The 133-meter-long unrestored SLB reach has been divided into 20 sections, each 6.66 meters in length in longitudinal order under unrestored non-meandered conditions. We implement riffles and pools by adjusting Manning’s *n* values and the slopes at specified channel sections. Riffle reaches were adjusted to have increased slopes and Mannings *n* values, which

resulted in a decreased hydraulic radius. Pools were set to have nearly flat slopes which increased the hydraulic radius of the cross-section. Modifications to these parameters alter the stream benthic area and the hydraulic residence times of the different zones of the stream which directly impacts the magnitude of nutrient spiraling lengths and uptake of nutrients (Cunha et al., 2018). Meandering cross-sections were lengthened, and the slopes were decreased accordingly to account for longitudinal elevation changes. All tested channel configurations maintain a consistent net elevation change with the longitudinal distance of the unrestored stream. For example, with the implementation of a riffle with an increased slope, the slope of the downstream reaches was decreased so that the net elevation change of the stream does not change over the length of the stream with all of the tested restoration scenarios.

By manipulating the slopes, Manning's  $n$  values, and reach lengths of the original look-up table information provided by (Lin et. al 2021), we created ten different reach features: a riffle, a pool, a post-riffle, a post-pool, a meander, a meandered-riffle, a meandered-pool, a meandered-post-riffle, a meandered-post-pool, and a meandered-post-riffle-pool reach to model along with the unrestored reaches. Table 3-1 summarizes the slopes and Manning's  $N$  values that were changed accordingly to create the different reach features.

**Table 3-1:** Slopes and Mannings N values for each of the reach features.

<b>Scenario</b>	<b>Slope (%)</b>	<b>Manning's N</b>
<b>Unrestored</b>	1.16	0.035
<b>Riffle</b>	2.28	0.055
<b>Pool</b>	1.00E-04	0.035
<b>Post-Riffle</b>	0.60	0.035
<b>Post-Pool</b>	1.74	0.035
<b>Meander</b>	0.81	0.035
<b>Meandered-Riffle</b>	2.28	0.055
<b>Meandered Pool</b>	1.00E-04	0.035
<b>Meandered-Post-Riffle</b>	0.07	0.035
<b>Meandered-Post-Riffle-Pool</b>	1.21	0.035
<b>Meandered-Post-Pool</b>	0.41	0.035

Meandering features were implemented in SSHBS by modeling the reach as a sinusoidal equation ( $w$ ) that increases the length of the unrestored reach:

$$w = A * \sin(0.19 * x) \tag{1}$$

where  $x$  is the downstream longitudinal distance from 0 to 133-meters and  $A$  is the meander amplitude or the maximum lateral distance that the stream deviates from the original unrestored centerline as a result from the simulated meandering pattern, which was set to 1.5 meters. By measuring the distance of the stream centerline to nearby vegetation using Google Earth Pro, 1.5 meters was judged to be a feasible upper threshold for an engineered sinusoidal meandering pattern at SLB. The authors of this paper did not consider underground piping or other infrastructure when deciding to test a 1.5-meter amplitude. However, implementing a sinusoidal pattern would necessitate obtaining data about these elements. The parameters seen in equation 1 produce meanders with four complete periods over the centerline of the original 133-meter reach

length. The new length of the stream as a result of meandering patterns was found with the arclength formula for w applied over the longitudinal length of the reach.

$$L = \int_0^{133} \sqrt{1 + (1.5 * \cos (0.19 * x))^2} \quad (2)$$

A total of eight channel restoration scenarios were explored to evaluate the potential impacts that restoration features could have on DIN uptake (table 3-2). Plan-views of the 8 scenarios are shown in figure 3-3.

**Table 3-2:** Channel Restoration Scenarios and Feature Lengths

<b>Reach Scenarios</b>	<b>Total Reach Length (m)</b>	<b>Riffle Length (m)</b>	<b>Pool Length (m)</b>
UN	133	0	0
R	133	26.6	0
P	133	0	26.6
RP	133	20.0	20.0
M	190.5	0	0
RM	190.5	38.1	0
PM	190.5	0	38.1
RPM	190.5	28.6	28.6

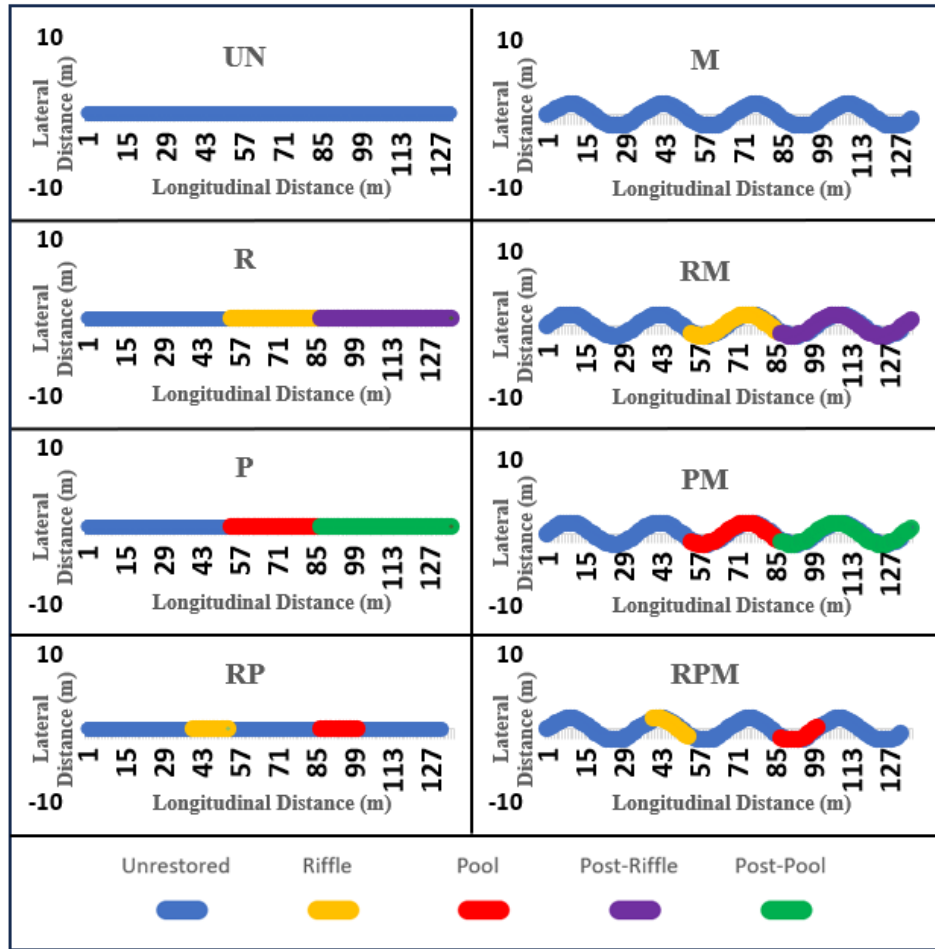


**Figure 3-3:** The eight plan-view depictions of the channel restoration scenarios that were evaluated in this study. (Graph axes are not to-scale.)

Since tree canopy was expected to have a significant impact on the uptake rates in the stream, a total of 16 scenarios were executed in this study- the 8 channel restorations detailed above with closed-canopy PAR data, plus the same 8 channel scenarios with open canopy PAR data. Though PAR data can be obtained using sensors installed in the field, sensors were not present at this study location over the simulation time period, so hourly PAR data ( $\mu\text{mol}\cdot\text{m}^2\cdot\text{s}^{-1}$ ) was simulated using the SLB RHESSys model. RHESSys was chosen because it has the capability of simulating canopy attenuation of solar radiation. The closed canopy PAR data

included RHESSys solar radiation output from the immediate surface area of the stream reach, which is covered by riparian canopy under the unrestored scenario. The open-canopy PAR data included RHESSys solar radiation results from nearby area that contained no tree canopy over the simulation period.

We simulated seasonal denitrification, algal DIN uptake, mineralization, and calculated Net DIN uptake rates between all of the simulated scenarios over the periods of January 2012 to December 2017. We compare the simulated DIN processing rates between all 16 scenarios and conduct Dunn tests for non-parametric pairwise comparisons to identify differences between all of the restoration scenarios that are the most probable in regard to annual DIN uptake rates. We consider any differences in uptake rates to be significant with a p value less than 0.05.

### **3.2 Results**

The simulated whole reach denitrification, algal DIN uptake, mineralization, and net DIN uptake rates by season is shown in figure 3-4. Unsurprisingly, open canopy increased Reach net uptake rates versus closed canopy scenarios across all channel designs. Figure 3-5 shows the PAR for the closed and open canopy scenarios as simulated using RHESSys. Open scenarios exhibit higher PAR during the summer and fall compared to the closed canopy scenarios, which was more shaded during the leaf-out periods.

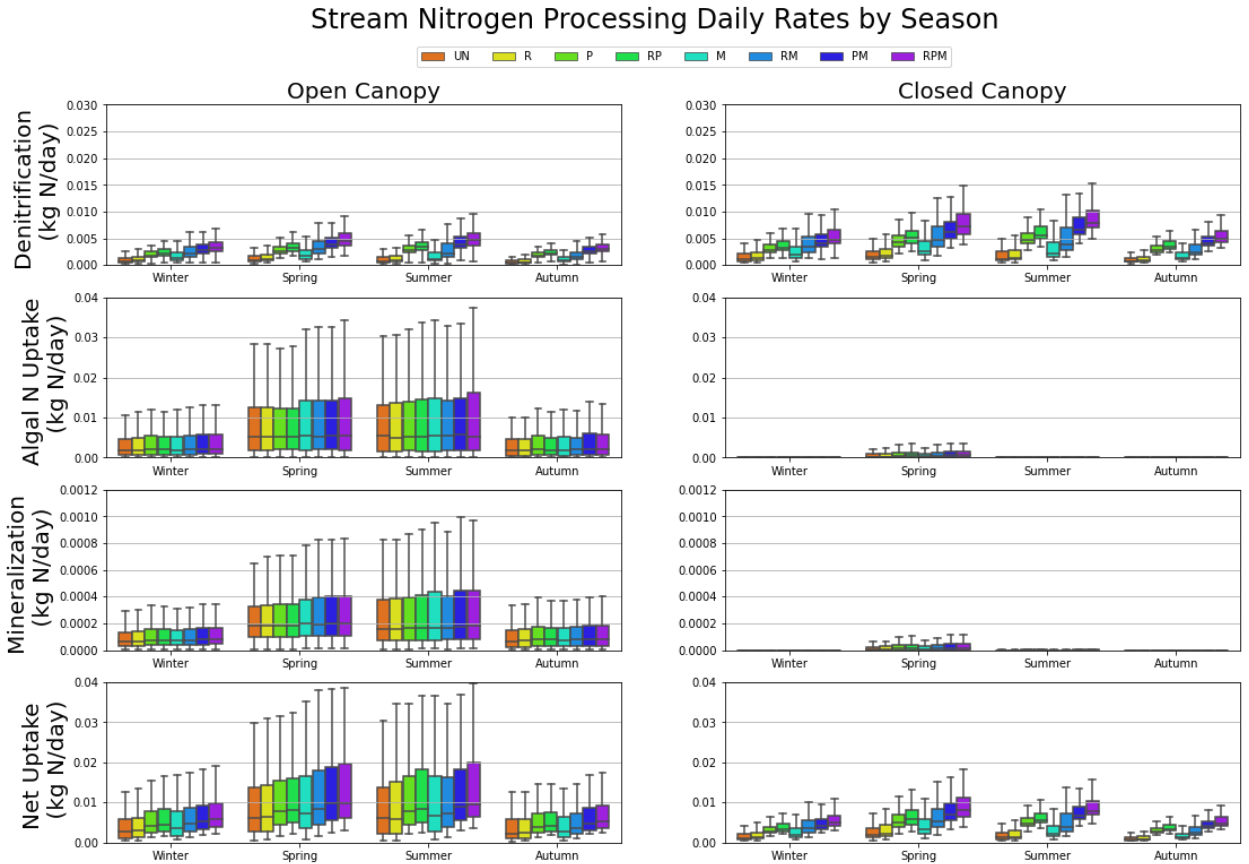


**Figure 3-4:** Simulated whole reach DIN uptake and release rates in kilograms per day by season between 2012 – 2017 at SLB.

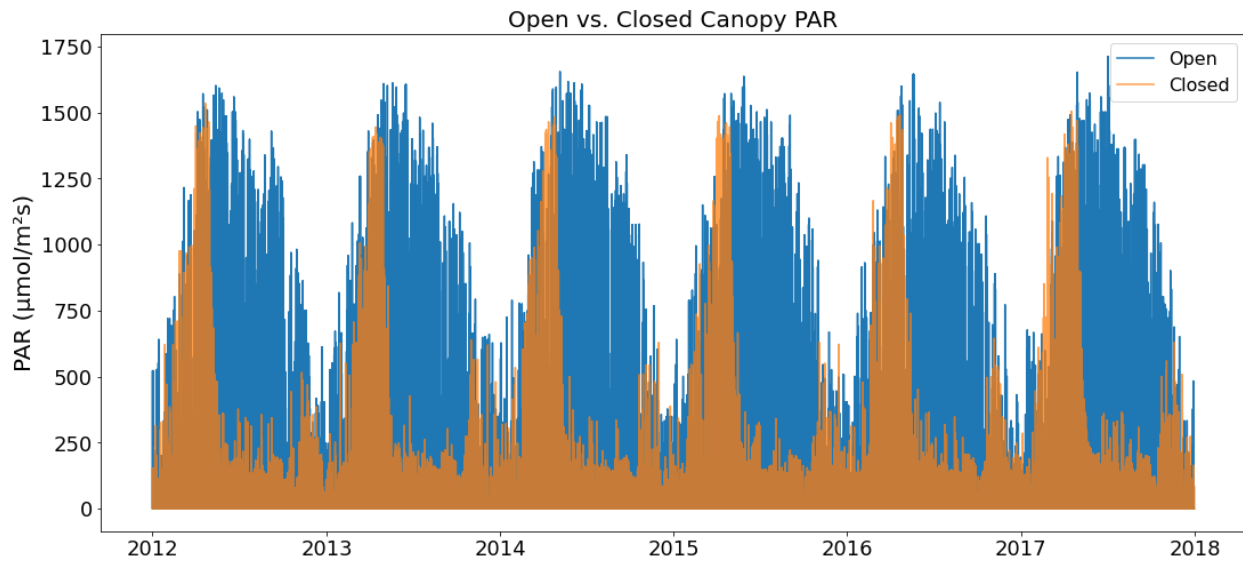


**Figure 3-5:** Simulated PAR results from the RHESSys model at the SLB whole reach under closed and open canopy conditions.

Denitrification was the greatest contributor to net annual N uptake under the closed canopy condition. Figure 3-6 shows the change in annual denitrification rates in kg per year for each scenario under both canopy conditions. Under the open canopy and closed canopy conditions, respectively, all scenarios showed significantly different denitrification rates relative to the unrestored channel scenario. Figure 3-7 are heat maps for the open and closed canopy conditions that indicate which scenario denitrification rates are significantly different from each other according to Dunn tests for non-parametric pairwise comparisons. All reach modifications showing significant differences in denitrification rates compared to each other except the pool (P) and riffle-meander (RM) scenarios under both canopy conditions. The open canopy condition resulted in remarkable reductions in the median denitrification rates in the stream, reductions that can be attributed to the increased algal DIN uptake, which slightly decreased the DIN concentration in the water column that was available for denitrification. Moreover, the denitrification rate was lower under the unrestored and riffle channels in the open canopy condition compared to the original unrestored channel under the closed canopy condition. Denitrification was lowest in the winter followed by the fall and highest in the summer followed by the spring across all 16 scenarios. Table 3-3 shows the changes in denitrification by season in kilograms per year for each reach scenario relative to the unrestored-closed-canopy scenario. The addition of a pool and the combination of a riffle and a pool had the greatest impact on the simulated daily denitrification rates compared to the other feature configurations, especially in conjunction with meandering.

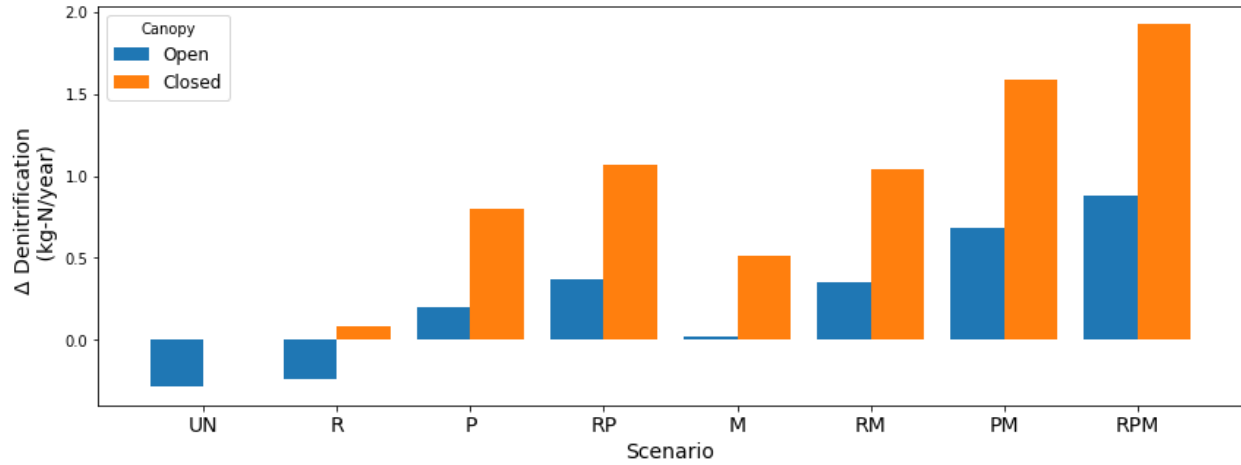


**Figure 3-6:** Changes in annual whole reach denitrification relative to the closed-canopy unrestored scenario.

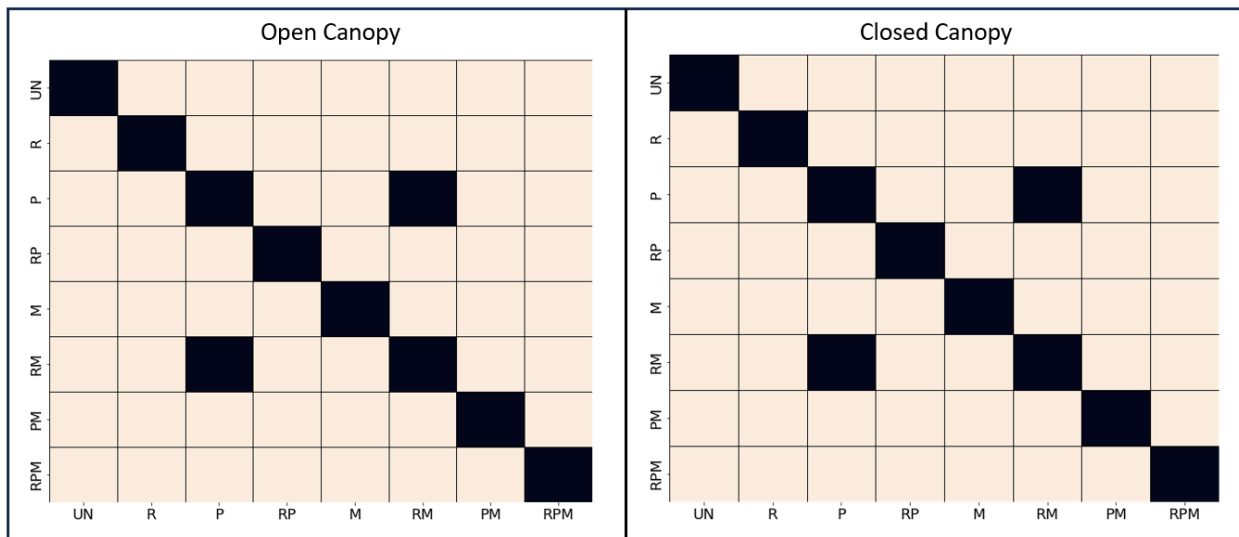


**Figure 3-7:** Dunn test for non-parametric pairwise comparison results for whole reach denitrification. Black squares indicate that there was not a significant difference between paired scenarios ( $p > 0.05$ ).

**Table 3-3:** Changes in total reach denitrification rates by season in kilograms per year for each channel scenario relative to the closed canopy unrestored scenario.

Season	Open Reach Scenarios							
	UN	R	P	RP	M	RM	PM	RPM
Winter	-5.8E-02	-4.7E-02	2.2E-02	-4.7E-02	1.3E-02	8.4E-02	1.3E-01	1.7E-01
Spring	-8.7E-02	-6.9E-02	5.0E-02	-6.9E-02	1.5E-02	1.2E-01	2.0E-01	2.6E-01
Summer	-9.4E-02	-7.9E-02	7.5E-02	-7.9E-02	-1.1E-02	8.1E-02	2.1E-01	2.7E-01
Autumn	-4.9E-02	-4.0E-02	5.2E-02	-4.0E-02	7.3E-03	6.5E-02	1.4E-01	1.9E-01
Season	Closed Reach Scenarios							
	UN	R	P	RP	M	RM	PM	RPM
Winter	-	1.71E-02	1.23E-01	1.71E-02	1.08E-01	2.16E-01	2.82E-01	3.40E-01
Spring	-	2.70E-02	2.16E-01	2.70E-02	1.63E-01	3.32E-01	4.57E-01	5.53E-01
Summer	-	2.49E-02	2.94E-01	2.49E-02	1.49E-01	3.13E-01	5.38E-01	6.49E-01
Autumn	-	1.40E-02	1.64E-01	1.40E-02	9.06E-02	1.82E-01	3.13E-01	3.81E-01

Algal DIN uptake was the greatest contributor to net uptake of DIN in the stream under the open canopy condition. Figure 3-8 shows the change in annual algal DIN uptake rates in kg per year for each scenario under both canopy conditions. Under the open canopy condition, there were no significant differences in algal uptake between all channel scenarios. Under the closed canopy condition, the riffle (R), meander (M), and riffle-meander (RM) scenarios were not significantly different from the unrestored channel scenario. Figure 3-9 are heat maps for the respective open and closed canopy conditions that indicate which channel scenario algal DIN uptake rates are significantly different from each other according to Dunn tests for non-parametric pairwise comparisons. Under an open canopy, algal DIN uptake rates were greatest in the spring and summer compared to the other seasons. Under closed canopy scenario, algal DIN uptake was greatest in the spring and was dormant for all the other seasons. Table 3-4 shows the increases in algal uptake by season in kilograms per year for each reach scenario relative to the closed-canopy unrestored scenario. Overall, open canopy was the greatest influence on algal DIN uptake compared to the channel restoration features.

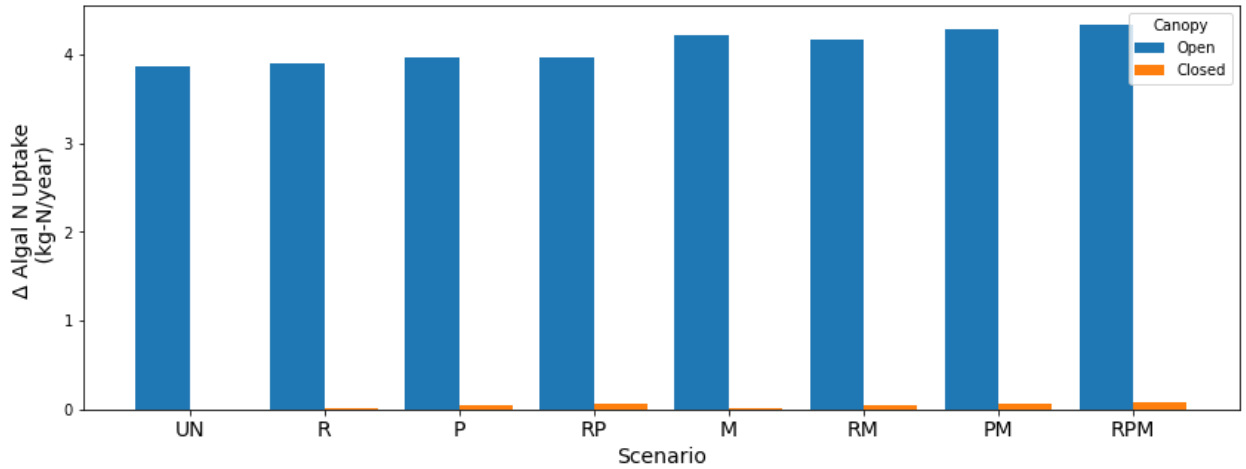


**Figure 3-8:** Changes in annual whole reach algal DIN uptake relative to the closed-canopy unrestored scenario.

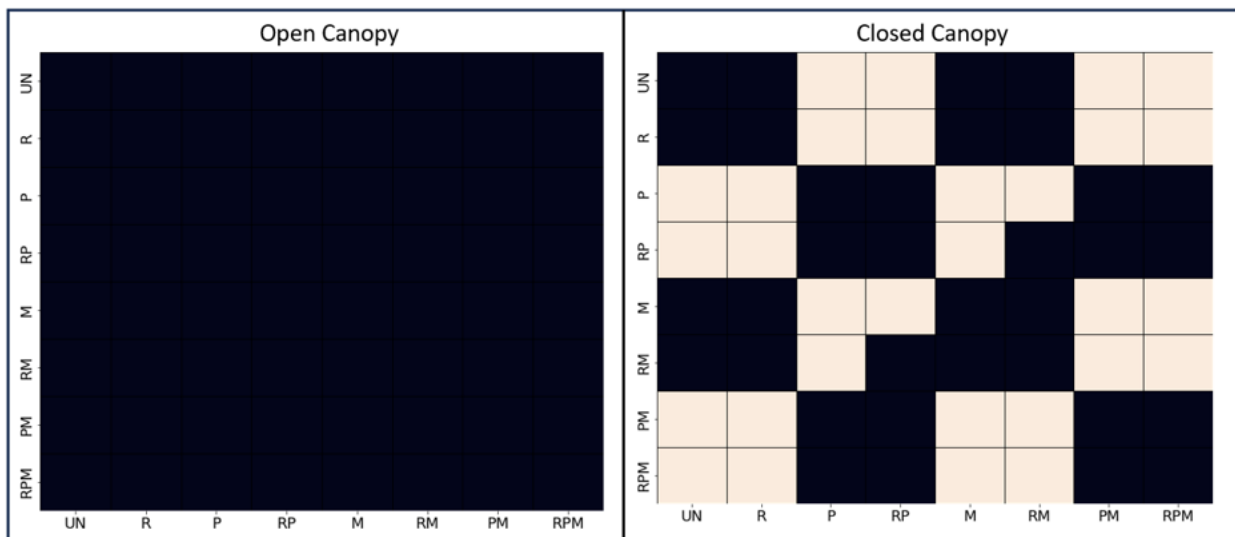


**Figure 3-9:** Dunn test for non-parametric pairwise comparison results for whole reach algal DIN uptake and mineralization. Black squares indicate that there was not a significant difference between paired scenarios ( $p > 0.05$ ).

**Table 3-4:** Changes in total reach algal DIN uptake by season in kilograms per year for each reach scenario relative to the closed canopy unrestored scenario.

Season	Open Reach Scenarios							
	UN	R	P	RP	M	RM	PM	RPM
Winter	0.5	0.5	0.5	0.5	0.5	0.5	0.5	0.5
Spring	1.2	1.1	1.1	1.1	1.3	1.3	1.3	1.3
Summer	1.5	1.6	1.6	1.6	1.7	1.6	1.7	1.7
Autumn	0.7	0.7	0.7	0.7	0.8	0.8	0.8	0.8
Season	Closed Reach Scenarios							
	UN	R	P	RP	M	RM	PM	RPM
Winter	-	1.0E-03	8.5E-03	1.0E-03	5.0E-03	1.1E-02	1.5E-02	1.7E-02
Spring	-	8.6E-03	3.7E-02	8.6E-03	1.1E-02	3.1E-02	4.8E-02	5.2E-02
Summer	-	4.4E-04	3.4E-03	4.4E-04	1.4E-03	2.6E-03	5.3E-03	6.0E-03
Autumn	-	2.3E-10	4.2E-09	2.3E-10	4.8E-10	1.9E-09	6.0E-09	6.9E-09

Mineralization was the simulated process in SSHBS that contributes to the net release of N in the stream and is highly correlated with Algal DIN uptake under all respective scenarios and seasons ( $0.95 \leq R^2 \leq 0.99$ ). Figure 3-10 shows the change in annual mineralization rates in kg per year for each scenario under both canopy conditions. Under just the open canopy condition there were no significant differences in mineralization rates between all channel scenarios. Under the closed canopy condition, the riffle (R), meander (M), and riffle-meander (RM) scenarios were not significantly different from the unrestored channel scenario. Figure 3-9 are heat maps for the open and closed canopy conditions that indicate which scenario mineralization rates are significantly different from each other according to Dunn tests for non-parametric pairwise comparisons. Under an open canopy, mineralization was greatest in the spring and summer compared to the other seasons. Under closed canopy scenario, mineralization was greatest in the spring and was nearly dormant for all the other seasons. Table 3-5 shows the increases in mineralization by season in kilograms per year for each reach scenario relative to the closed-

canopy unrestored scenario. Overall, open canopy was the greatest influence on mineralization compared to the channel restoration features.

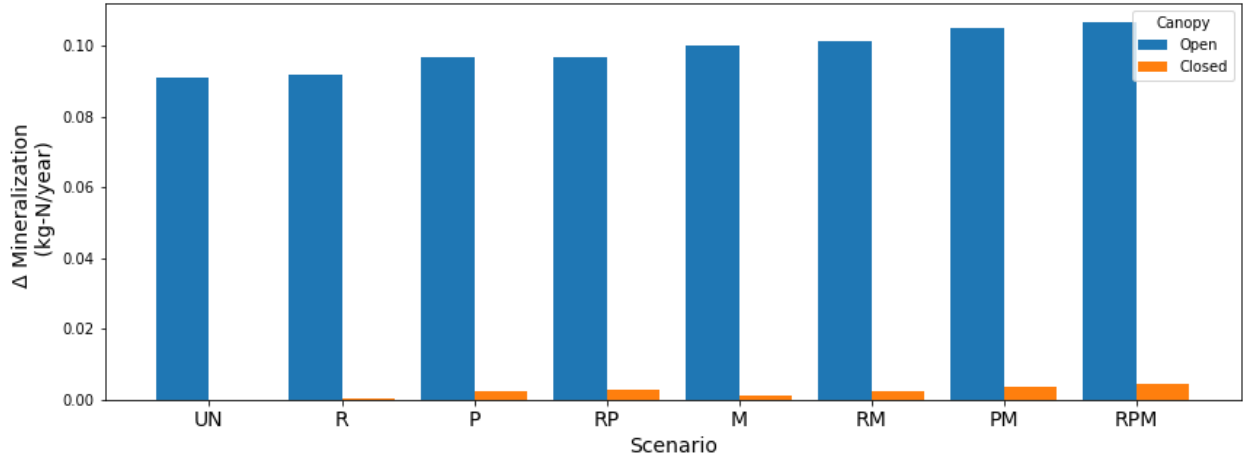


**Figure 3-10:** Changes in whole reach annual N mineralization relative to the closed-canopy unrestored scenario

**Table 3-5:** Changes in total reach mineralization rates by season in kilograms per year for each reach scenario relative to the closed canopy unrestored scenario.

Season	Open Reach Scenarios							
	UN	R	P	RP	M	RM	PM	RPM
Winter	1.2E-02	1.2E-02	1.4E-02	1.2E-02	1.3E-02	1.4E-02	1.5E-02	1.6E-02
Spring	2.7E-02	2.6E-02	2.7E-02	2.6E-02	3.0E-02	3.0E-02	3.1E-02	3.0E-02
Summer	3.7E-02	3.8E-02	3.9E-02	3.8E-02	4.0E-02	4.0E-02	4.1E-02	4.2E-02
Autumn	1.6E-02	1.6E-02	1.7E-02	1.6E-02	1.7E-02	1.7E-02	1.8E-02	1.8E-02
Season	Closed Reach Scenarios							
	UN	R	P	RP	M	RM	PM	RPM
Winter	-	1.3E-04	1.2E-03	1.3E-04	6.4E-04	1.7E-03	2.3E-03	2.7E-03
Spring	-	2.2E-04	1.0E-03	2.2E-04	2.9E-04	8.4E-04	1.3E-03	1.4E-03
Summer	-	1.2E-05	1.0E-04	1.2E-05	3.9E-05	7.5E-05	1.5E-04	1.7E-04
Autumn	-	7.3E-12	1.3E-10	7.3E-12	1.5E-11	6.1E-11	1.9E-10	2.2E-10

Net DIN uptake is the sum of denitrification and algal DIN uptake subtracted by mineralization. Figure 3-11 shows the changes in annual net uptake rates in kilograms per year relative to the unrestored scenario. Under the open canopy condition, most channel reach

scenarios showed significant differences in net DIN uptake, except for a few cases. Specifically, the pool (P), riffle-pool (RP), and riffle-meander (RM) scenarios did not significantly differ in their daily uptake rates from each other under the open canopy condition. Similarly, there were no significant differences observed between the unrestored (UN) and riffle (R) channel scenarios in their daily uptake rates under the open canopy condition. All reach scenarios were significantly different from each other under the closed-canopy condition except the pool (P) and the riffle-meander (RM) scenarios. Figure 3-12 are heat maps for the open and closed canopy conditions that indicate which scenario's net DIN uptakes rates are significantly different from each other according to Dunn tests for non-parametric pairwise comparisons. Table 3-6 shows the increases in net DIN uptake by season in kilograms per year for each reach scenario relative to the closed-canopy unrestored scenario. Overall, pool features, and open canopy were the greatest influences on net DIN uptake, which was further enhanced by the meandering pattern.

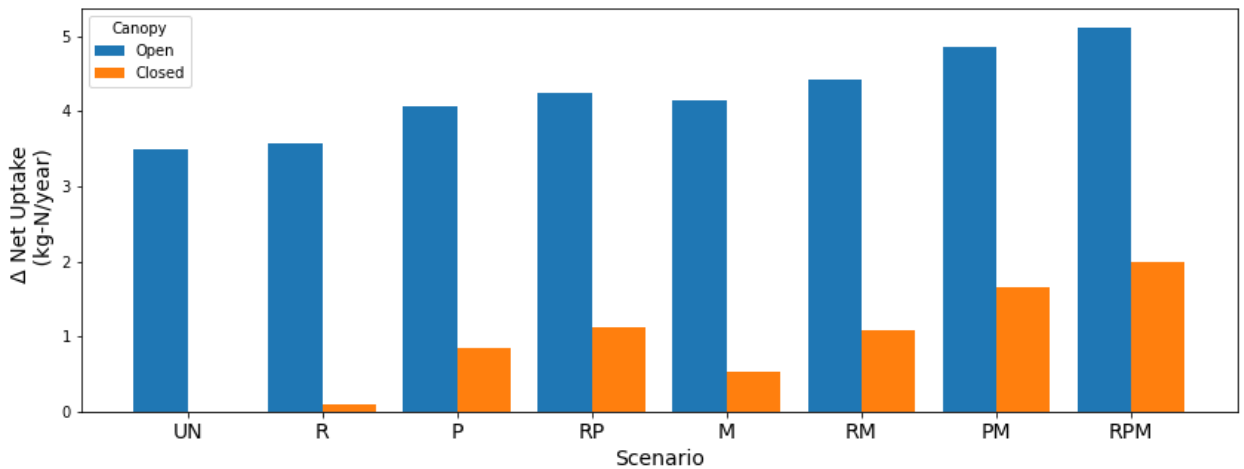


**Figure 3-11:** Changes in whole reach annual net DIN uptake relative to the closed-canopy unrestored scenario.

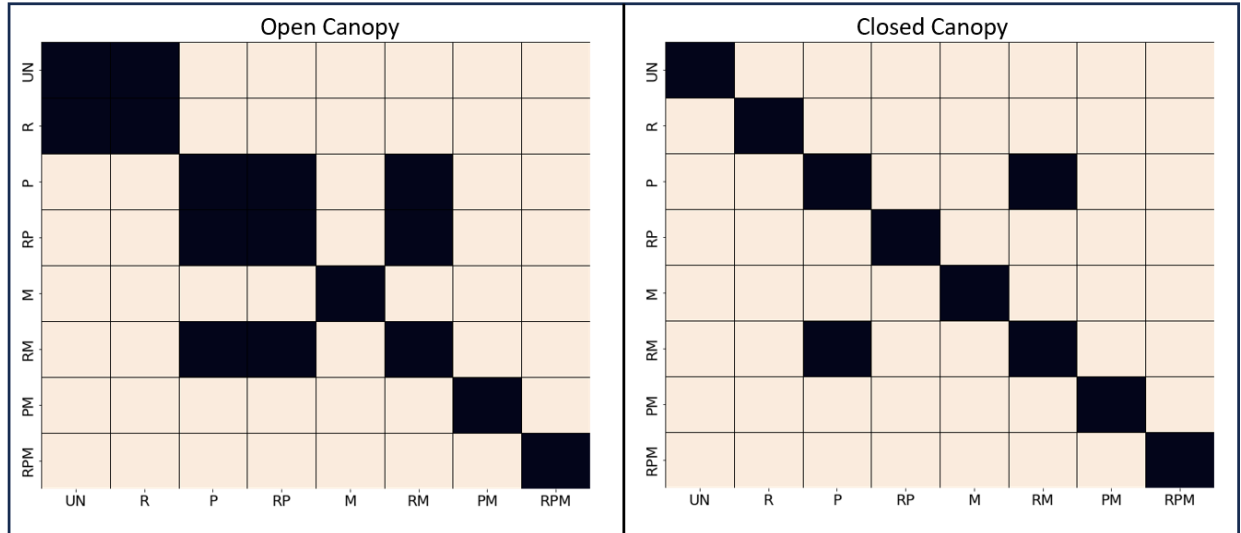


**Figure 3-12:** Dunn test for non-parametric pairwise comparison results for whole reach net DIN uptake. Black squares indicate that there was not a significant difference between paired scenarios ( $p > 0.05$ ).

**Table 3-6:** Changes in the total whole reach net DIN uptake by season in kilograms per year for each reach scenario relative to the closed canopy unrestored scenario.

Season	Open Reach Scenarios							
	UN	R	P	RP	M	RM	PM	RPM
Winter	0.1	0.1	0.1	0.1	0.1	0.1	0.1	0.1
Spring	0.2	0.2	0.2	0.2	0.2	0.2	0.2	0.3
Summer	0.2	0.2	0.3	0.2	0.3	0.3	0.3	0.3
Autumn	0.1	0.1	0.1	0.1	0.1	0.1	0.1	0.2
Season	Closed Reach Scenarios							
	UN	R	P	RP	M	RM	PM	RPM
Winter	-	0.0	0.1	0.0	0.1	0.2	0.3	0.4
Spring	-	0.0	0.3	0.0	0.2	0.4	0.5	0.6
Summer	-	0.0	0.3	0.0	0.2	0.3	0.5	0.7
Autumn	-	0.0	0.2	0.0	0.1	0.2	0.3	0.4

In general, our results show that all of the simulated channel restoration scenarios would increase whole reach DIN uptake at the SLB reach, though these increases are expected to be reduced significantly with the riparian canopy regrowth. Canopy along the flood plain and riparian areas are often removed during restoration, but it can return depending on longer term

plans. We quantified the possible impact of the regrowth of canopy situation at SLB for each of the eight channel scenarios and summarized those results in table 3-7. Our results suggest that all tested channel restorations are able to sustain whole reach DIN uptake rates more effectively compared to the unrestored channel scenario upon the return of canopy, particularly those restorations with multiple features.

**Table 3-7:** Expected percent reductions in net DIN uptake if riparian canopy regrows for the eight channel restoration scenarios.

Channel Scenario	% Reduction
UN	80
R	78
P	65
RP	61
M	72
RM	63
PM	56
RPM	52

The results indicate that the restoration scenarios generally increase the daily whole reach uptake rates (kg/day) but they do not appear to have the same effect on the daily areal uptake rates (kg/m<sup>2</sup> day). Actually, they appear to have reduced the areal uptake rates primarily by decreasing the algal DIN uptake per unit area. Figure 3-13 shows the daily DIN uptake rates per square meter by season.

### Stream Nitrogen Processing Daily Areal Rates by Season

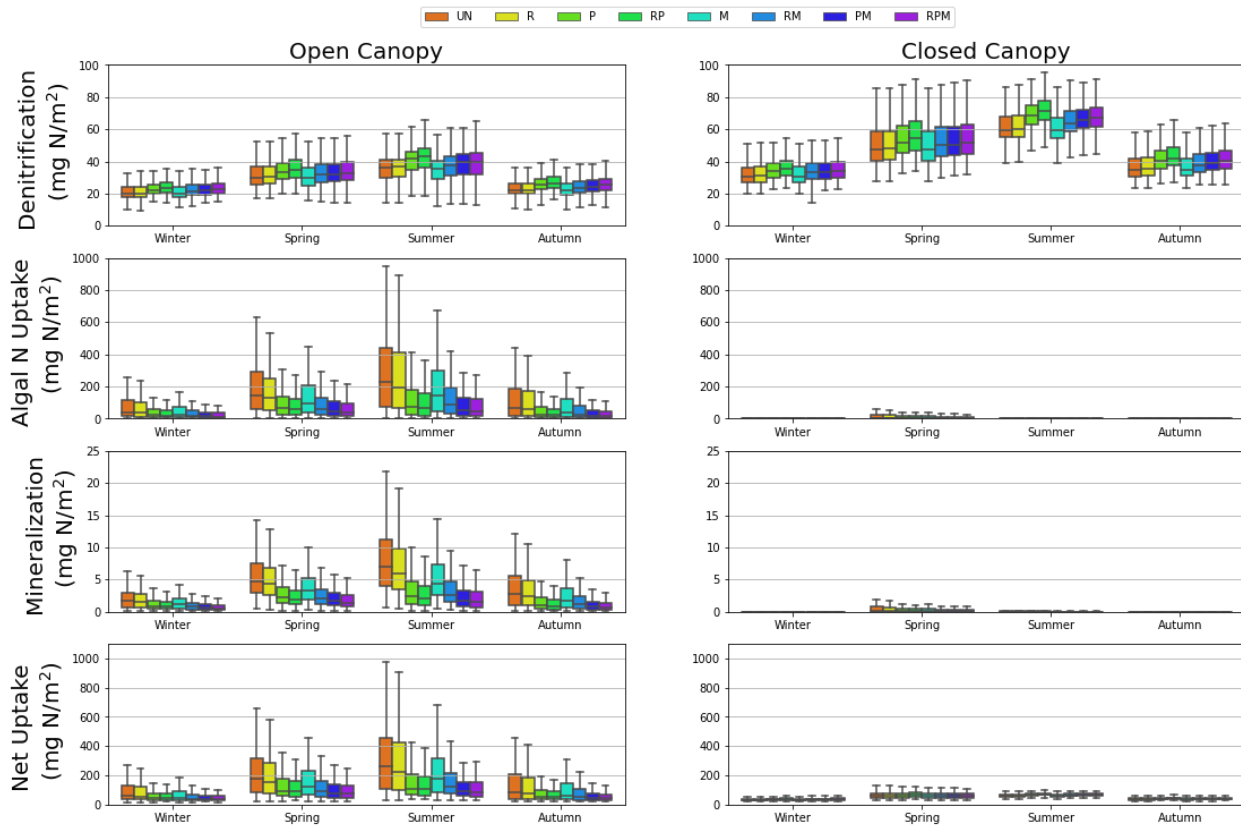


**Figure 3-13:** Simulated daily DIN uptake per square meter and release rates by season between 2012 – 2017 at SLB .

These reductions can be attributed to the decrease in simulated water column DIN concentration due to the increases in whole reach denitrification and algal DIN uptake, which are depicted in figure 3-4. The larger benthic area leads to an overall increase in DIN uptake, thereby reducing the supply of DIN in the water column and subsequently lowering the areal uptake rates. This suggests that the variations in whole reach DIN uptake rates between the different channel scenarios are primarily influenced by the augmented benthic area, particularly under the closed canopy conditions. Figure 3-14 shows the benthic area by season for each of the channel restoration scenarios.

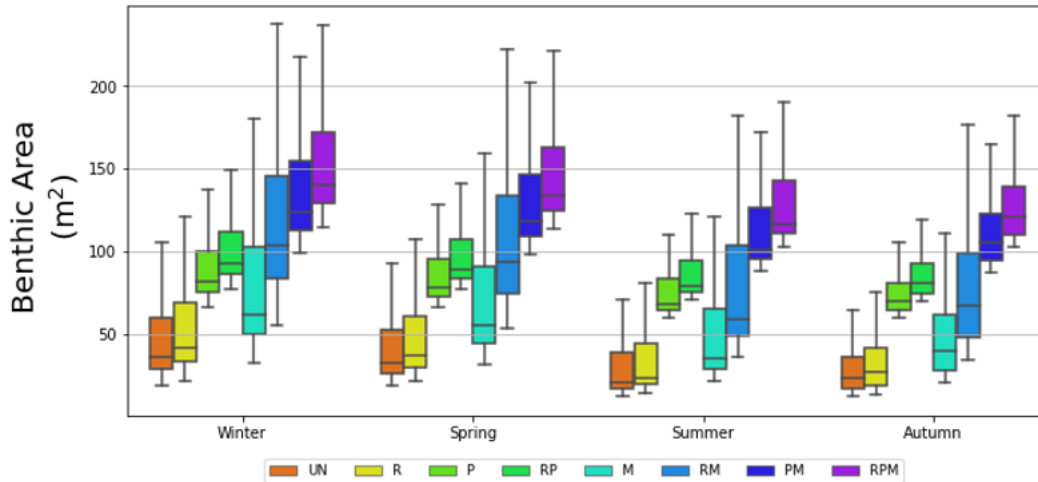


Figure 3-14: Benthic area by season for each of the channel restoration scenarios.

### 3.3 Discussion

#### 3.3.1 Case Study Outcomes

According to the original parameterization of SSHBS for SLB (UN: closed-canopy condition), denitrification was the greatest contributor to N uptake in the stream under closed-canopy conditions. Increases in denitrification rates relative to the unrestored channel scenario were most prominent with the addition of a pool and the combination of a riffle and pool, which were both further enhanced by the meandering pattern. SSHBS simulation results show significant differences in denitrification rates between all the channel scenarios with the exception of the P and the RM scenarios according to the results from the Dunn test. This implies that we cannot be as confident that these two scenarios will have different denitrification rates and managers can be more confident that the option that is less expensive between the two would be more cost-efficient if enhancing denitrification is the goal. Denitrification rates under the open canopy condition were reduced compared to the closed canopy scenarios, where algal DIN uptake removed more of a share of water column DIN that would have been more available for

denitrification. When the canopy regrows, denitrification rates are expected to increase based on our simulation results.

The canopy condition was the greatest influence on simulated algal DIN uptake, mineralization, and net DIN uptake at SLB (kg N/day), which is consistent with empirical evidence (e.g. Reisinger et al., 2019). Open canopy increased median whole reach Algal DIN uptake rates under the unrestored channel scenario by about 0.05, 1.2, 1.5, and 0.7 kilograms per year in the winter, spring, summer, and fall, respectively. The algal DIN uptake and mineralization rates were highly correlated with each other and had the same Dunn test results, which indicates that the model for mineralization for SSHBS is dependent on algal production and standing stock. All channel scenario algal DIN uptake and mineralization rates under the open canopy condition were all significantly different from each other. The Dunn test results for the closed canopy condition indicate that we cannot be confident that channel scenarios R, M, and RM would alter algal DIN uptake and mineralization compared to the unrestored channel and that scenarios P, RP, PM, and RPM scenarios may be equally effective at increasing algal DIN uptake and mineralization compared to the unrestored scenario and so the least expensive option would be desirable to managers if there are budget limitations.

Denitrification accounted for approximately 93% of the whole reach net DIN uptake under the closed canopy condition on average across all channel scenarios, and approximately 20% under the open canopy condition. In general, most of the channel scenarios resulted in significantly different whole reach DIN uptake, with only a few exceptions. Under the open-canopy setting, the simulated whole reach DIN uptake did not show significant differences between the UN and R scenarios. Similarly, there was no significant difference between the P,

RP, and RM scenarios, while the P and RM scenarios also displayed no significant differences under the closed canopy condition.

Overall, our findings suggest that all simulated channel restoration scenarios would enhance whole reach net DIN uptake at the SLB reach. However, these enhancements are anticipated to decrease notably due to the regrowth of riparian canopy. Restoration efforts typically involve removing canopy from floodplain and riparian areas, but these may recover over time based on the long-term plans for restoration. Our findings indicate that channel scenarios combining multiple features (RP, RM, PM, and RPM) are likely to exhibit lower reductions in net DIN uptake under the regrowth of canopy situation. Among the single and combination feature scenarios, pool scenarios are expected to show less reduction compared to others.

### **3.3.2 Lessons, Limitations, and Future Work**

Based on this study, SSHBS appears to have considerable potential as a tool for evaluating the potential effects of a variety of stream restoration designs. SSHBS allows for the testing of different channel and canopy cover scenarios using known cross-sectional dimensions and simple manipulations of the Manning's equation. In addition to evaluating restoration design, statistical comparison tests like the Dunn test employed in this study can be utilized on simulated outcomes. These tests help establish the level of confidence regarding the distinctions between various channel restoration scenarios.

It should be noted that using the Manning's equation as the sole method for stream hydraulic analysis is not the conventional approach for designing various stream restoration projects. The Manning equation is more applicable to low flow conditions in which the surface

water slope is equal to the bed slope and may be less reliable during stormflow when the majority of the nutrient load is transported (Shields et al., 2008). Typically, geomorphologists and engineers have the responsibility not just to estimate changes in stream velocity within engineered channels but also to delve into more complex hydraulic functions involving stream flow power, shear stress, bank resistance, and potential sediment movement (U.S. NRCS, 2007). These analyses are usually conducted at sub-daily or even sub-hourly intervals, which is necessary to fully grasp the extent of change and assess the risk of potential stream channel integrity issues. This underscores the significance of collaboration between geomorphologists, focused on precise in-stream hydraulics modeling, and stream ecologists, working on stream channel flow equations, to provide a more comprehensive understanding of restoration projects. Furthermore, the Manning's equation, while straightforward for generating various channel features, has limitations in accurately representing different channel cross-section shapes, leading to equifinality. For instance, it cannot effectively differentiate between an atypical square channel often found in unrestored streams and a more naturally shaped one. Subsequent research will employ a channel flow model that can discern between various channel shapes. Additionally, the Manning's equation assumes constant slope and hydraulic gradient of the channel under varying stream depth, which may lead to an underestimate of stream velocity at higher flows. HEC-RAS offers a more precise modeling of hydraulic gradients and customizability of different restored shapes compared to relying solely on the Manning's equation.

Many stream restorations involve reconnecting the stream channel to the floodplain, which can enhance the terrestrial denitrification of overflowing water (Kaushal et al, 2008). The findings from this study suggest open canopy stream conditions promote more in-stream uptake. However, it does not shed light on potential reductions in DIN input into the stream, which could

occur due to the presence of riparian vegetation (Dosskey et al., 2010). The SSHBS model, in this study, focuses on DIN uptake within the stream channel and hyporheic storage zones within the stream bottom. The subsequent chapter of this dissertation provides some insights into how non-riparian green infrastructure can affect in-stream DIN uptake and export from the stream. However, it is important to note that future research should consider the influence of floodplains and riparian vegetation on DIN inputs and additional uptake resulting from restoration efforts.

SSHBS is an open-source model amenable to modifications for specific stream restoration channel and riparian canopy designs. This study demonstrates that it can be modified to evaluate a variety of channel configurations and it comprehensively simulates ecosystem and nutrient flux processes using a minimum set of equations that can be adapted and calibrated in a variety of ways but there appears to be limitation to the potential for wide-spread use of SSHBS. Although cross-section geometry data can be collected using modeling or surveying techniques, SSHBS does require input and calibration data that is not readily collected at most tributaries. Under the calibration method used by Lin et. al (2021), data to simulate gross primary productivity and ecosystem respiration are required as well as several years of weekly samples of  $\text{NO}_3$ ,  $\text{NH}_4$ , and  $\text{PO}_4$  concentrations in the study stream.

The results of this model study indicate that stream restoration design analyses conducted with SSHBS may partially support the central tenet of NCD- that some engineered channels can greatly enhance net DIN uptake in streams, given large enough benthic area enhancements, though simulated whole reach DIN uptake was most augmented by open canopy, which is similar to what Reisinger et al. (2019) observed. Reisinger et al.'s (2019) assessment of real restorations did not account for variations in benthic areas between restorations, and due to the nature of empirical studies that compare different restorations at separate locations, could not

control key boundary conditions. These are the main advantages of conducting simulated studies using SSHBS since it allows for the testing of benthic area variation within a single reach while controlling important boundary conditions such as flow and DIN inputs from the watershed. Results from this simulated study suggest that benthic areas may be a key variable to consider when evaluating differences between restoration projects across separate locations. Future simulation studies should apply SSHBS to different study areas and further explore its uses and limitations.

### **3.4 Conclusions**

In this study, we explored the potential impacts of riffle, pool, and meander channel configurations on net DIN uptake processes in an urbanized stream by conducting channel scenario analyses using a novel stream ecosystem model that was previously developed and calibrated (Lin et al., 2021). Though the specific simulation results in this study were not verified with field data, we demonstrated that SSHBS can be a viable modeling option for stream restoration designers who are interested in estimating the impacts of geomorphic restoration features on net DIN uptake rates in a stream, which could enhance current methods of stream restoration design. Our results suggest that: 1) Increases in benthic area, most prominently increased by pools and meandering features, enhanced simulated whole reach net DIN uptake through increased denitrification under the closed-canopy conditions; 2) The removal of riparian canopy, that often coincides with channel restoration efforts, was the most prominent catalyst for enhancing net DIN uptake through substantially increased algal DIN uptake; 3) The pool (P) and the riffle-meander (RM) scenario enhanced simulated net DIN uptake at statistically similar rates under the both open and closed canopy conditions; 4) Channel restoration designs with a combination of riffle, pool, and meander features performed better than those with just one or

two of these features; 5) The regrowth of canopy after removal is anticipated to reduce the overall increase in net DIN uptake for all restoration designs primarily because there is less DIN uptake by algae due to decreased photosynthetically active radiation reaching the stream. Upon the return of tree canopy growth, restorations with a combination of features, particularly those including a pool, might prove more effective in maintaining net DIN uptake rates in comparison to the single feature or unrestored channel scenarios.

### 3.5 Chapter 3 Works Cited

- Baltimore County. (2013a). *Middle Gwynns Falls Small Watershed Action Plan Volume I*.
- Baltimore County. (2013b). *Middle Gwynns Falls Small Watershed Action Plan Volume II*.
- Baltimore Ecosystem Study. (2019). WATERSHED STUDIES.  
<https://baltimoreecosystemstudy.org/2019/06/18/watershed-studies-2/>
- Bennett, S. J., Simon, A., Castro, J. M., Atkinson, J. F., Bronner, C. E., Blersch, S. S., & Rabideau, A. J. (2011). The evolving science of stream restoration. *Geophysical Monograph Series, 194*, 1–8. <https://doi.org/10.1029/2011GM001099>
- Bernhardt, E. S., Palmer, M. A., Allan, J. D., Alexander, G., Barnas, K., Brooks, S., Carr, J., Clayton, S., Dahm, C., Galat, D., Gloss, S., Goodwin, P., Hart, D., Hassett, B., Jenkinson, R., Katz, S., Kondolf, G. M., Lake, P. S., Lave, R., ... Sudduth, E. (2005). Synthesizing U.S. River Restoration Efforts. *Science, 308*(April), 636–638.
- Calfe, M. L., Scott, D. T., & Hester, E. T. (2022). Nitrate removal by watershed-scale hyporheic stream restoration: Modeling approach to estimate effects and patterns at the stream network scale. *Ecological Engineering, 175*(June 2021), 106498.  
<https://doi.org/10.1016/j.ecoleng.2021.106498>
- Chesapeake Conservancy. (2019). “CBP land use/land cover data project.” Accessed May 2, 2023. <https://www.chesapeakeconservancy.org/conservation-innovation-center/high-resolution-data/lulc-data-project-2022/>.
- Crumpton, W. G., & Isenhardt, T. M. (1987). Nitrogen Mass Balance in Streams Receiving Secondary Effluent: the Role of Algal Assimilation. *Journal of the Water Pollution Control Federation, 59*(9), 821–824.
- Cunha, D. G. F., Finkler, N. R., Calijuri, M. do C., Covino, T. P., Tromboni, F., & Dodds, W. K. (2018). Nutrient uptake in a simplified stream channel: Experimental manipulation of hydraulic residence time and transient storage. *Ecohydrology, 11*(7), 1–10.  
<https://doi.org/10.1002/eco.2012>
- Dosskey, M. G., Vidon, P., Gurwick, N. P., Allan, C. J., Duval, T. P., & Lowrance, R. (2010). The role of riparian vegetation in protecting and improving chemical water quality in streams. *Journal of the American Water Resources Association, 46*(2), 261–277.  
<https://doi.org/10.1111/j.1752-1688.2010.00419.x>
- Doyle, M. W., Shields, & F., D. (2012). Compensatory Mitigation for Streams Under the Clean Water Act: Reassessing Science and Redirecting Policy. *Journal of the American Water Resources Association, 48*(3), 494–509. <https://doi.org/10.1111/j.1752-1688.2011.00631.x>
- Google Earth Pro. (2019). *Scott’s Level Branch, Baltimore County*. Accessed June 1, 2023
- Hall, R. K., Guiliano, D., Swanson, S., Philbin, M. J., Lin, J., Aron, J. L., Schafer, R. J., & Heggem, D. T. (2014). An ecological function and services approach to total maximum daily load (TMDL) prioritization. *Environmental Monitoring and Assessment, 186*(4),

2413–2433. <https://doi.org/10.1007/s10661-013-3548-x>

- Hall, R. O., & Tank, J. L. (2003). *Ecosystem metabolism controls nitrogen uptake in streams in Grand Teton National*. 48(3), 1120–1128.
- Hirsch, R. M., Moyer, D. L., & Archfield, S. A. (2010). Weighted regressions on time, discharge, and season (WRTDS), with an application to Chesapeake Bay river inputs. *Journal of the American Water Resources Association*, 46(5), 857–880. <https://doi.org/10.1111/j.1752-1688.2010.00482.x>
- Kaushal, S. S., Groffman, P. M., Mayer, P. M., Striz, E., & Gold, A. J. (2008). Effects of stream restoration on denitrification in an urbanizing watershed. *Ecological Applications*, 18(3), 789–804. <https://doi.org/10.1890/07-1159.1>
- Klocker, C. A., Kaushal, S. S., Groffman, P. M., Mayer, P. M., & Morgan, R. P. (2009). Nitrogen uptake and denitrification in restored and unrestored streams in urban Maryland, USA. *Aquatic Sciences*, 71(4), 411–424. <https://doi.org/10.1007/s00027-009-0118-y>
- Lave, R., Doyle, M., & Robertson, M. (2010). Privatizing stream restoration in the US. *Social Studies of Science*, 40(5), 677–703. <https://doi.org/10.1177/0306312710379671>
- Lawrence, J. E., Skold, M. E., Hussain, F. A., Silverman, D. R., Resh, V. H., Sedlak, D. L., Luthy, R. G., & McCray, J. E. (2013). Hyporheic zone in urban streams: A review and opportunities for enhancing water quality and improving aquatic habitat by active management. *Environmental Engineering Science*, 30(8), 480–501. <https://doi.org/10.1089/ees.2012.0235>
- Lin, L., Reisinger, A. J., Rosi, E. J., Groffman, P. M., & Band, L. E. (2021). Evaluating Instream Restoration Effectiveness in Reducing Nitrogen Export from an Urban Catchment with a Data-Model Approach. *Journal of the American Water Resources Association*, 57(3), 449–473. <https://doi.org/10.1111/1752-1688.12922>
- Mayer, P. M., Pennino, M. J., Newcomer-Johnson, T. A., & Kaushal, S. S. (2022). Long-term assessment of floodplain reconnection as a stream restoration approach for managing nitrogen in ground and surface waters. *Urban Ecosystems*, 25(3), 879–907. <https://doi.org/10.1007/s11252-021-01199-z>
- Palmer, M. A., Hondula, K. L., & Koch, B. J. (2014). Ecological restoration of streams and rivers: Shifting strategies and shifting goals. *Annual Review of Ecology, Evolution, and Systematics*, 45(1), 247–269. <https://doi.org/10.1146/annurev-ecolsys-120213-091935>
- Peters, N. E., Böhlke, J. K., Brooks, P. D., Burt, T. P., Gooseff, M. N., Hamilton, D. P., Mulholland, P. J., Roulet, N. T., & Turner, J. V. (2011). Hydrology and Biogeochemistry Linkages. In *Treatise on Water Science* (Vol. 2, Issue December). <https://doi.org/10.1016/B978-0-444-53199-5.00038-5>
- Reisinger, A. J., Doody, T. R., Groffman, P. M., Kaushal, S. S., & Rosi, E. J. (2019). Seeing the light: urban stream restoration affects stream metabolism and nitrate uptake via changes in canopy cover. *Ecological Applications*, 29(6). <https://doi.org/10.1002/eap.1941>
- Reisinger, A. J., Woytowicz, E., Majcher, E., Rosi, E. J., Belt, K. T., Duncan, J. M., Kaushal, S.

- S., & Groffman, P. M. (2019). Changes in long-term water quality of Baltimore streams are associated with both gray and green infrastructure. *Limnology and Oceanography*, *64*, S60–S76. <https://doi.org/10.1002/lno.10947>
- Roley, S. S., Tank, J. L., & Williams, M. A. (2012). Hydrologic connectivity increases denitrification in the hyporheic zone and restored floodplains of an agricultural stream. *Journal of Geophysical Research: Biogeosciences*, *117*(3), 1–16. <https://doi.org/10.1029/2012JG001950>
- Rosgen, D. (1998). The reference reach: A blueprint for natural channel design. *Engineering Approaches to Ecosystem Restoration*, 1009–1016. [https://doi.org/10.1061/40382\(1998\)166](https://doi.org/10.1061/40382(1998)166)
- Rosgen, D. L. (2011). Natural channel design: Fundamental concepts, assumptions, and methods. *Geophysical Monograph Series*, *194*, 69–93. <https://doi.org/10.1029/2010GM000990>
- Shields, F. D. (2008). Nutrient transport in the Yazoo River Basin, Mississippi. Water Quality & Ecology Research Unit, National Sedimentation Laboratory.
- Simon, A., Doyle, M., Kondolf, M., Shields, F. D., Rhoads, B., & McPhillips, M. (2007). Critical evaluation of how the Rosgen classification and associated “natural channel design” methods fail to integrate and quantify fluvial processes and channel response. *Journal of the American Water Resources Association*, *43*(5), 1117–1131. <https://doi.org/10.1111/j.1752-1688.2007.00091.x>
- United States Environmental Protection Agency (USEPA). (2022). Nonpoint Source Program Success Story. in 1995, 1–2. [https://www.epa.gov/system/files/documents/2022-08/MD\\_Scotts%20Level%20Branch\\_2049\\_508.pdf](https://www.epa.gov/system/files/documents/2022-08/MD_Scotts%20Level%20Branch_2049_508.pdf)
- United States Geological Survey (USGS). (2023). *Stream Gage at Scotts Level Branch at Rockdale, MD*. USGS Water Data for the Nation. <https://waterdata.usgs.gov/monitoring-location/01589290/#parameterCode=00065&period=P7D>
- United States Natural Resources Conservation Service (NRCS). (2007). Chapter 11 Rosgen Geomorphic Channel Design. United States Department of Agriculture Natural Resources Conservation Service, Part 654(Stream Restoration Design Part 654, National Engineering Handbook), 82
- Webster, J. R., Mulholland, P. J., Tank, J. L., Valett, H. M., Dodds, W. K., Peterson, B. J., Bowden, W. B., Dahm, C. N., Findlay, S., Gregory, S. V., Grimm, N. B., Hamilton, S. K., Johnson, S. L., Martí, E., McDowell, W. H., Meyer, J. L., Morrall, D. D., Thomas, S. A., & Wollheim, W. M. (2003). Factors affecting ammonium uptake in streams - An inter-biome perspective. *Freshwater Biology*, *48*(8), 1329–1352. <https://doi.org/10.1046/j.1365-2427.2003.01094.x>
- Williams, M. R., Bhatt, G., Filoso, S., & Yactayo, G. (2017). Stream Restoration Performance and Its Contribution to the Chesapeake Bay TMDL: Challenges Posed by Climate Change in Urban Areas. *Estuaries and Coasts*, *40*(5), 1227–1246. <https://doi.org/10.1007/s12237-017-0226-1>
- Wohl, E., Lane, S. N., & Wilcox, A. C. (2015). The science and practice of river restoration. *Water Resources Research*, *51*(8), 5974–5997. <https://doi.org/10.1002/2014WR016874>

## **Chapter 4: Estimating the Impacts of Green Infrastructure on Nitrogen Uptake in an Urban Stream through the Integration of Watershed, Channel Hydraulic, and Ecosystem models.**

This chapter is currently under preparation for publication.

### **Chapter 4 Abstract**

Urbanization has significantly deteriorated regional water quality and stream ecosystems. To combat this, stormwater green infrastructure (GI) is recommended to mitigate local stream and receiving water body conditions. Elevated nutrient non-point source loading is a major contributor to this impairment, leading to eutrophication. The core research question of this study revolves around the capacity of integrated modeling tools to intricately connect different elements including watershed runoff, nutrient sources, channel hydraulics, and aquatic ecosystems. Specifically, this study aims to assess how these linked mechanisms can effectively evaluate the impact of GI on nutrient reduction and urban stream dynamics. We developed and tested an innovative integrated watershed-channel hydraulic stream-ecosystem model, packaged into a single open-source Python notebook. Our novel model couples the Stormwater Management Model (SWMM), Hydrologic Engineering Center's River Analysis System (HEC-RAS), and stream channel metabolism modules from the Stream Model Based on Spiraling and Ecological Stoichiometry Specific Fluxes (STOICMOD) and Small Streams Hydro Biogeochemistry Simulator (SSHBS). We calibrated and validated the modeling system against two years of data from an urban stream in central Virginia. Results show how this type of integrated model could benefit urban watershed managers by answering questions about linkages between urban runoff, nutrient loading, in-stream dissolved inorganic nitrogen (DIN) uptake rates, metabolic rates, algal mass, and benthic mass. We assess the impact of intense GI implementation on these parameters at select urban stream reaches. Key findings associated with our case-study area include: 1) Only 0.86% of DIN that enters the stream from the watershed is removed under all GI scenarios; 2) Stream zones with lower riparian canopy cover and lower leaf-litter input exhibit higher algal DIN uptake and lower mineralization contributing to greater net DIN uptake; 3) Watersheds with higher groundwater DIN concentrations relative to surface runoff concentrations may yield increased DIN export with infiltration-based GI because the stream ecosystem is unable to sufficiently process increased DIN during baseflow conditions; 4) Elevated DIN concentrations during baseflow periods can enhance denitrification rates; 5) Larger upstream subbasins with greater GI implementation have the greatest potential influence on net DIN uptake and other stream processes, but the greatest impacts on a per hectare of GI implemented basis may be the smaller subbasins that are more impervious. This study underscores the model's utility in assessing GI's effects on urban streams and provides insights applicable to local watershed management.

## 4.0 Introduction

Urban streams often exhibit impaired ecological functioning as a result of increased nutrient loadings and increased stormwater runoff, a condition commonly referred to as “urban stream syndrome” (Walsh et al., 2005). Urban stream syndrome can often manifest as stream incision, benthic habitat destruction from increased erosion and sedimentation of the stream channel, diminished water quality, and increased nutrient export to downstream aquatic ecosystems (Meyer et al., 2005). Eutrophication is a particular concern in the Chesapeake Bay area where the degradation of the river-estuary continuum is unequivocally attributed to agriculture, urbanization, and climate change (Duan et al., 2012, 2021; Kemp et al., 2005; Prasad et al., 2014). The reduction of eutrophication continues to be a top priority for decision makers and interested non-governmental organizations (Chesapeake Bay Program, 2023a; USEPA, 2022a).

The high human population density and the increased importation, production, and release of nitrogen (N) and phosphorus (P) are what make urban centers major sources of nutrient pollution (Bernhardt et al., 2008; Smil, 2000). Vast amounts of N and P in urban areas can be directly sourced from leaky sanitary and sewage systems, fossil fuel byproducts, lawn fertilizer application, and pet waste and are exported from urban watersheds through different pathways (Hobbie et al., 2017). Green infrastructure (GI) has been implemented to help mitigate the impact of urbanization on receiving waterbodies by reducing stressors such as stormwater runoff and nutrient loadings (Palmer & Ruhi, 2019; Walsh et al., 2005).

Stormwater green infrastructure can retain or delay runoff and nutrient constituents from entering streams. When stormwater is delayed through infiltration, it is hypothesized that there is

more opportunity for terrestrial and aquatic nutrient cycling processes such as plant uptake and redox to transform or remove these nutrients from the watershed and therefore decrease loadings into streams and export from the watershed downstream (Gold et al., 2019; Janke et al., 2014; Payne et al., 2014). Urban landscape restoration plans are typically evaluated through model simulations of GI benefits such as stormwater runoff and pollutant reduction, and urban heat reduction (Fletcher et al., 2013; Pataki et al., 2011). A variety of modeling tools are publicly available for estimating the benefits of urban landscape green infrastructure. For example, the Stormwater Management Model (SWMM) has been most widely used throughout the US to quantify the impacts of stormwater green infrastructure design and placement on runoff (Niazi et al., 2017; USEPA, 2023b); i-Tree Hydro has been used for simulating the ecosystem services of tree canopy and green space (Coville et al., 2020; i-Tree, 2023); The Hydrologic Modeling System (HEC-HMS) can be used to simulate hydrologic impacts of ponds and reduced imperviousness (Sahu et al., 2023; USACE, 2023); The Regional Hydro-Ecologic Simulation System (RHESSys) has been used to simulate the hydrologic impacts of tree canopy and urban green infrastructure (Bell et al., 2017; Miles and Band, 2015; Tague & Band, 2004; Zhang et al., 2023). A major gap in the use of these watershed models is that they focus exclusively on the terrestrial phase of the watershed and do not mechanistically simulate in-stream ecosystem processes that also influence nutrient retention and export.

Dissolved inorganic nitrogen (DIN) and phosphorus (P) flowing from terrestrial through urban stream networks are susceptible to biogeochemical interactions. While in the stream, N and P molecules alternate between downstream travel and assimilation or removal from the water column by stream biota (Ensign & Doyle, 2006; Stream Solute Workshop, 1990), a process known as stream nutrient spiraling. Algae and heterotrophic microbes sequester N and P from the

water column to satisfy cellular nutritional requirements (Baulch et al., 2011; Pearce et al., 2022; Webster et al., 2003). Assimilation can be a major contributor to nutrient retention as it temporarily stores N and P in organic form, increasing residence time, before mineralization and release back into the water column at a later time. Denitrification removes nitrate-N entirely from the stream system (Kreiling et al., 2019), and may increase with residence time.

Grimm et al. (2003) noted that stream-reach models have rarely been coupled with watershed models and argued that management issues such as eutrophication require integrated analysis tools that incorporate terrestrial and fluvial elements. Recent development in stream biogeochemistry modeling (Alexander et al., 2009; Bouwman et al., 2013; Jan et al., 2021; Lin et al., 2021; Lin & Webster, 2014; Marcé & Armengol, 2009; Webster et al., 2016; Ye et al., 2012) may enable a more complete analysis of the connection between upland green infrastructure and instream nutrient processing than was previously possible. Over the past couple of decades, the academic community has tested a limited number of prototypical integrated terrestrial and aquatic models, which have facilitated unique perspectives on the issue of urban watershed nutrient retention. For example, Alexander et al. (2009) developed a stream network scale dynamic nitrogen transport and denitrification model and found evidence that highlights the relative importance of biogeochemical versus hydrological effects on nitrate removal. Marcé and Armengol (2009) customized a Hydrological Simulation Program- Fortran (HSPF) model to simulate streamflow, nutrient retention, and discharge, providing more evidence for the relationships between the proximity to human population centers and increased nutrient export. Webster et al. (2016) developed the Stream Model Based on Spiraling and Ecological Stoichiometry Specific Fluxes (STOICMOD), which incorporates concepts of nutrient spiraling, mass balance, and ecological stoichiometry to better explore the interrelationships between

stream biota such as algae and heterotrophic microbes and their impacts on nutrient retention. Lin et al. (2021) developed the Small Stream Hydro-Biogeochemistry Simulator (SSHBS) which is a hybrid process-data driven model that can simulate stream metabolism, algal uptake, denitrification, and mineralization in response to different restoration channel designs and landscape changes. The Chesapeake Bay Watershed model (Chesapeake Bay Program, 2023b) does include both terrestrial and aquatic phases, but at very reduced resolution and complexity. As researchers and managers seek more mechanistic ways of analyzing the impacts of urbanization, restoration, and GI on urban water quality, the next evolution in modeling whole urban nutrient retention is the development of coupled process-based terrestrial GI and aquatic biogeochemical models. Results from such an integrated model could be helpful to urban managers who are interested in estimating the impacts of GI on in-stream nutrient uptake.

The objective of this study is to couple an urban green infrastructure model to a channel hydraulic model and an instream ecosystem model and package it into a single open-source python notebook. In addition to evaluating the integrated model applied to an urban case study, we answer the following research questions. 1) What are linkages between watershed runoff and nutrient loading with the estimated N uptake rates, stream metabolic rates, algal mass, and benthic mass in an urban stream? 2) How does intense implementation of different GI types at specific locations in an urban subbasin impact simulated DIN uptake rate, stream metabolic rates, algal mass, and benthic detritus mass at different reaches of an urban stream? To answer these questions, we develop python code that utilizes a combination of models including the Stormwater management model (SWMM), the U.S. Army Corp of Engineers (USACE) Hydrologic Engineering Center's River Analysis System (HEC-RAS), and stream uptake functions from STOICMOD and SSHBS. We implement the model framework in an urban

stream in Charlottesville, VA. We then use the model to compare the simulated instream DIN uptake rates and watershed export of 26 different GI scenarios to the status-quo (no additional GI added) scenario.

#### 4.0.1 Case Study Area

This study evaluates an integrated model using data from stream sections in the Meadow Creek watershed, spanning Charlottesville and Albemarle County, VA (figure 4-1). Focusing on the upper Meadow Creek, a 1415-hectare, urbanized area (40% impervious), primarily residential (70%) with a notable commercial zone (20%). Stormwater runoff and pollution reduction are top priorities for both city and county (Albemarle County, 2023; Charlottesville, 2019).

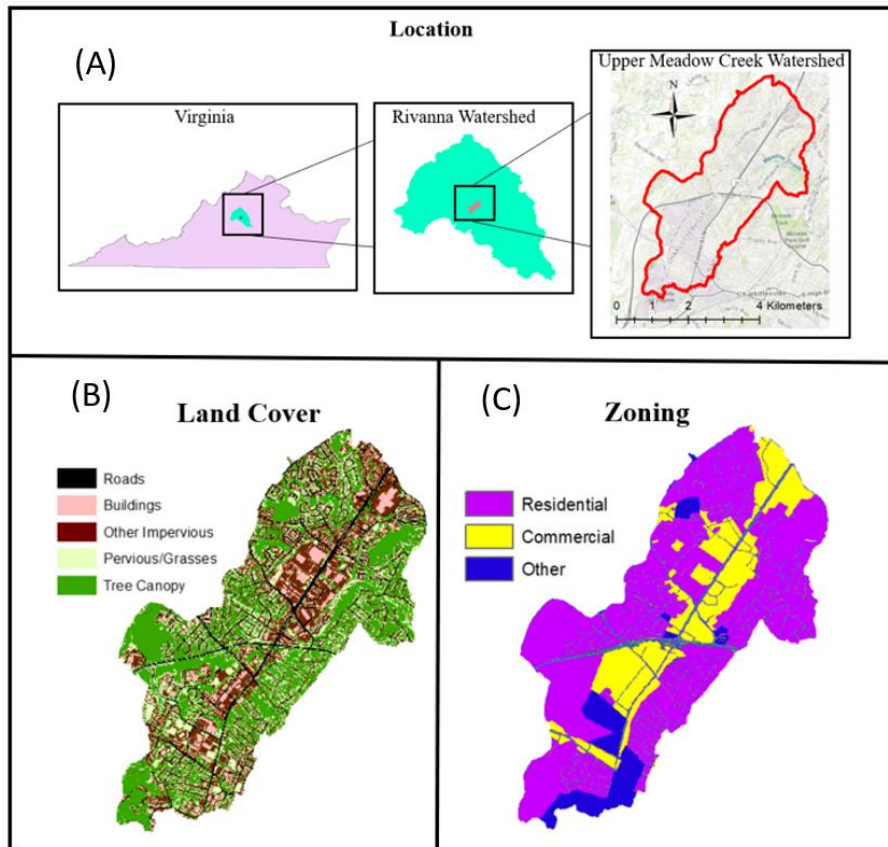


**Figure 4-1:** Upper Meadow Creek Study Area Location (A), Land Cover (B), and Zoning (C).

Urbanization has drastically changed the landscape of Charlottesville and the Meadow Creek watershed since the early 20<sup>th</sup> century. Excess impervious surface coverage has increased volumes and velocities of stormwater runoff, eroded alluvial fill derived from former agricultural land use, incising the streams, exposing steep banks of erodible sediment, and accelerated sedimentation, pollutant loading, and physical destruction of the aquatic habitat. This degradation led to the Virginia Department of Environmental Quality (VDEQ) to officially add Meadow Creek to its list of impaired waters (VDEQ, 2020). After the original impairment designation in 2006, major stream restoration activities followed (The Nature Conservancy, 2013) and were credited with nutrient reduction capabilities (Cho et al., 2014). However, stream nutrient retention processes have not been well-studied at Meadow Creek. Since late 2020, photosynthetically active radiation (PAR), dissolved oxygen, electrical conductivity, and water level sensors have been installed at multiple locations at Meadow Creek with the goal of characterizing stream ecosystem conditions that facilitate in-stream dissolved inorganic nitrogen (DIN) uptake (de Azevedo Torrellas; 2021). See the Data Availability statement for access to the ecosystem data that were collected over a two-year period (2021-2022).

## **4.1 Methods**

### **4.1.1 Developing an Integrated Ecosystem Service Model for Meadow Creek**

This section provides details about the development of a novel integrated model to study the connection between upland urban GI impacts on runoff and nutrient loading, channel hydraulics, and in-stream ecosystem processes related to DIN retention in urban streams. We couple three models that are free and publicly accessible, into a single open-source model system. Stormwater GI performance, runoff, pollutant, and baseflow inputs to our study stream

are simulated using SWMM; HEC-RAS is used to simulate in-stream steady-state flow hydraulic parameters (flow cross-sectional area, benthic area, flow velocity, and flow volume). We use STOICMOD and SSHBS uptake functions to simulate in-stream ecosystem processes associated with nutrient retention and removal from the water column including primary production, ecosystem respiration, Algal DINutrient uptake, denitrification, and mineralization. Figure 4-2 is a diagram depicting how we couple the three models.

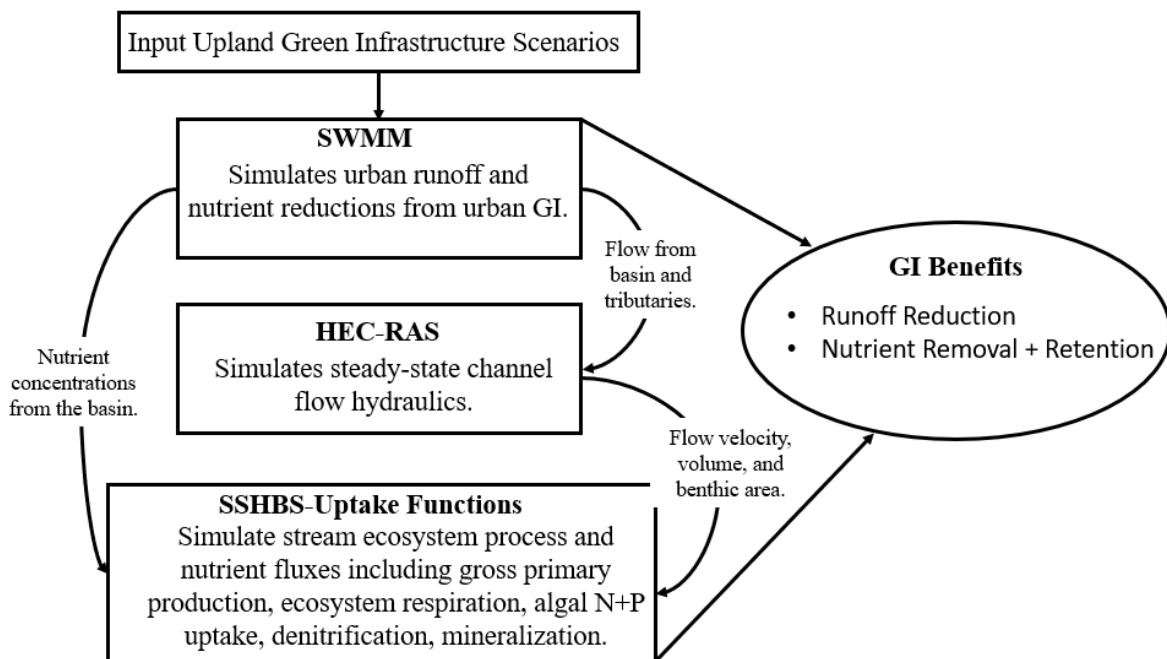


**Figure 4-2:** Integrated Watershed-Stream Ecosystem Model Diagram.

#### 4.1.2 Calibrating and Validating the Integrated Model

We calibrated our integrated model estimates of runoff, groundwater flow, and nutrient concentrations for the year 2021 and validated for the year 2022 against stream flow and daily nutrient concentrations obtained via synoptic sampling at each of the three stream reach sections (figure 4-3). We obtained depth measurements at the outlet using pressure transducer measurements recorded at a 15-minute interval and translated the depth to discharge using a

rating curve. The stream flow is manually calibrated using the Nash-Sutcliffe Efficiency (NSE) and Kling-Gupta Efficiency (KGE) metrics. The SWMM model was calibrated and validated with continuous simulations of rainfall and runoff for the years 2021 and 2022, respectively. The SWMM model was run on a 15-minute timestep, and the flow results were averaged to a daily timestep for calibration and analysis. The daily averaging of SWMM flow results simplified the calibration procedure and rendered SWMM outputs compatible with the in-stream ecosystem model inputs, which were modeled on a daily time-step. The parameters in SWMM that were adjusted during the flow calibration process were the aquifer soil porosity and conductivity and the infiltration Green and Ampt variables.

A total of 213 water samples were collected across three locations at the most downstream cross-section of three main reach zones (figure 4-3). The samples were analyzed for ammonium ( $\text{NH}_4$ ) and nitrite/nitrate ( $\text{NO}_2/\text{NO}_3$ ). Although there are other forms of N that we did not analyze, for simplification, we refer to these three N constituents collectively as dissolved inorganic nitrogen (DIN) concentrations. According to the grab sample data at the three reach zones, nitrate-N accounted for approximately 96% of the total DIN in the stream at any given time so the nitrate concentration ( $C_{\text{NO}_3\text{-N}}$ ) was assumed to be 0.96 of the total simulated DIN.

The calibration of DIN in groundwater and storm event mean concentrations in runoff was accomplished by the use of two python libraries: SWMM API (Pichler, 2022) and the Platypus nondominated-sorting genetic algorithm II (NSGA II) for multi-objective optimization. Table 4-1 shows the calibrated groundwater and event mean concentrations of N based on the land use categories with the mean absolute error (MAE) of the mean concentrations for the DIN concentrations at each of the three stream reach zones serving as the three objectives of the calibration. The solution that produced the lowest average MAE of the mean concentrations

across all three reach zones was chosen among the Pareto optimal set of solutions and was used as the calibrated parameters for this study. It's important to note that the SWMM water quality module doesn't account for seasonal trends or the impacts of varying flow conditions on N concentrations. It is also important to notice the greater concentration for groundwater relative to storm water runoff which induces a negative relationship between DIN concentrations and discharge in our modeled stream. Though not always the case in urban areas, groundwater concentrations of DIN can be higher than stormwater runoff concentrations due to excess lawn fertilizer application and/or leaky underground septic and sanitary systems (Pitt et al., 2023) compared to rainfall-runoff concentrations. Previous studies that have analyzed the nitrate-N isotopes at Meadow Creek suggest that leaky underground sanitary systems are indeed major sources of DIN at baseflow as seen in figure C-1 in appendix C (from de Azevedo Torrellas, 2021). Additionally, a concentration vs. discharge graph seen in figure C-3 also supports parameterizing our integrated model with a negative relationship between DIN concentrations and discharge at our study area. Note that it was not possible to use a calibration objective for the DIN concentrations that captured day-to-day trends such as the  $R^2$  function. This lack in the ability to obtain a good fit between the observed and the simulated DIN concentrations can be attributed to errors that were introduced due to: the relatively few samples that were collected relative to the number of days that were simulated; the fact that the samples were retrieved at only a single time during the day and assigned as the whole-day's concentration; and differences in the observed and simulated flow. Therefore, the objective of the DIN concentrations was not to obtain a good fit of the daily DIN trends, but rather to minimize the error between the average observed and the average simulated DIN concentrations.

**Table 4-1:** Calibrated groundwater and event mean dissolved inorganic nitrogen (DIN) concentrations.

N Source	Impervious			Pervious	
	Roads	Residential	Commercial	Grasses	Tree Canopy
Groundwater (mg N/L)	1.46	1.68	2.54	1.56	0.48
Stormwater Runoff (mg N/L)	1.02	1	2	0.98	0.45

Daily primary production and ecosystem respiration was modeled using the Bayesian Single-station Estimation (BASE) implemented in the R programming language (Grace, 2015) with measurements of dissolved oxygen, water temperature, electrical conductivity, PAR obtained at 15-minute intervals at the same three locations where the water grab sampling took place. BASE is a more standard stream metabolism model that uses ecosystem data and Bayesian statistics to estimate primary production and ecosystem respiration. We calibrated our primary production and ecosystem respiration process modules against the BASE stream metabolism results in the stream for the year 2021. Due to the high flashiness and sedimentation in Meadow Creek and wildlife damage, validation of the stream metabolism parameters for the year 2022 was not possible due to insufficient data collection. Once the integrated model was satisfactorily calibrated, we analyzed relationships between instream uptake processes and total N uptake in Meadow Creek. We also compared minimum, mean, and maximum rates of simulated primary production, Algal DIN uptake, immobilizer assimilation, denitrification, and mineralization as well as stocks of benthic detritus and algae mass between the three reach zones. We further evaluate the integrated model and offer insight into the implications of the stream ecosystem results in the discussion.

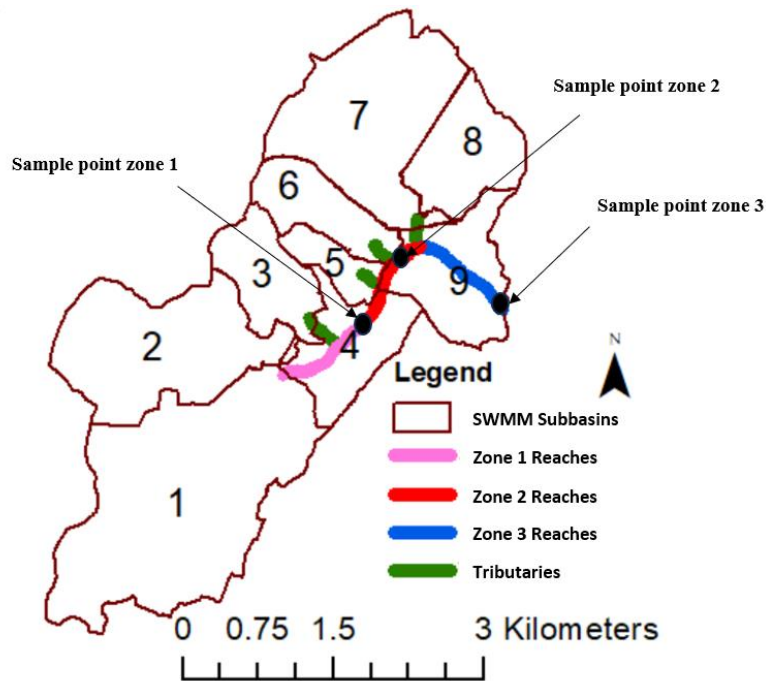


**Figure 4-3:** The upper Meadow Creek reach zones, subbasins, major tributaries, and nutrient grab sampling points at each zone.

#### 4.1.3 SWMM Model

The SWMM model used in this study is divided into 9 subbasins (Figure 4-3) ranging in size from 40 to 460 hectares according to the tributary network flowing into the main stem of the stream. SWMM is used to simulate stormwater runoff, groundwater flow, and nutrient inputs to the mainstream network reach zones numbered: 1,2, and 3 as indicated in figure 4-3. The SWMM model used in this study is a modified version of one developed by the city in partnership with URS Corporation and the U.S. Army Corp of Engineers (Charlottesville, 2008, 2010). The original model included 87 subbasins in the study area. We added a water quality model, a groundwater model, and to improve computational time we reduced the number of subbasins. The 9-subbasin model was calibrated and validated using local rain gage data and observed discharge at the outlet of the study area. Discharge was derived from water depth that was recorded using a HOBOTM pressure transducer and a rating curve that was developed over a

period of 18 months. Discharge for the rating curve was recorded at the watershed outlet using a SonTek® Flow Tracker 2 acoustic velocimeter and depth was recorded using a staff gage. Stream stage was recorded using a HOBO U20L-01 transducer. SWMM is used to simulate storm runoff, nutrient inputs to the stream network, and baseflow. SWMM simulates the performance of stormwater GI with respect to reducing runoff and dissolved nutrient input to the stream during stormflow periods. SWMM GI modifies nutrient inputs to the stream by either treating the runoff entering specific GI or by increasing runoff infiltration, converting it into groundwater. The GI types that we consider in this study include rain gardens, green roofs, and impervious conversion to grasses and tree canopy. The only considered Green Infrastructure (GI) options that modify the EMC values of subbasins in SWMM are those involving the conversion of impervious surfaces to grasses or green space since they necessitate a land use change.

We parameterized a DIN water quality model in SWMM by calibrating the concentrations of groundwater and stormwater according to different land uses in the area. We categorized the study area into five categories: impervious roads, impervious residential, impervious commercial/industrial, grasses, or tree canopy using land cover and zoning data from regional (Chesapeake Conservancy, 2019) and local geographic information system databases. Table 4-2 shows the land use composition of each of the 9 subbasins in the study area.

**Table 4-2:** Land use composition for each subbasin.

Subbasin	Impervious			Pervious	
	Roads	Residential	Commercial	Grasses	Tree Canopy
S-1	5%	13%	18%	22%	42%
S-2	4%	16%	7%	18%	55%
S-3	5%	26%	17%	17%	35%
S-4	2%	16%	18%	19%	45%
S-5	2%	29%	46%	17%	6%
S-6	4%	29%	26%	14%	28%
S-7	6%	19%	22%	17%	36%
S-8	11%	28%	20%	9%	32%
S-9	1%	14%	2%	22%	61%

#### 4.1.4 HEC-RAS as the stream flow hydraulics module

The Meadow Creek cross-sectional geometry was extracted using a 1m digital elevation model (DEM). Once flow from the SWMM model enters the stream network via tributaries or from upstream subbasins, our integrated model computes flow cross-sectional area, velocity, volume, and benthic area in the channel using a steady state HEC-RAS model. We divide the main stem into three reach zones, each containing a certain number of 30-meter-long cross-sections. Figure 4-4 shows the 1m DEM used in our HEC-RAS model along with stream reach sections at every 30m interval. Stream flow and nutrient concentrations from SWMM along with the stream reach parameters computed using HEC-RAS become input parameters to modules derived from the STOICMOD-SSHBS nutrient uptake models.

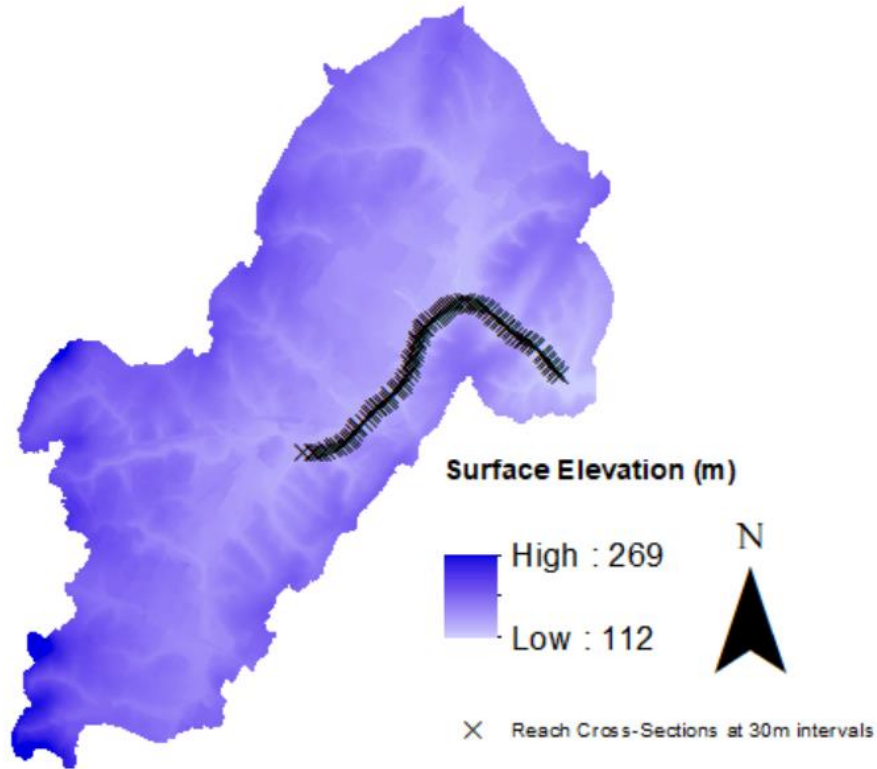


**Figure 4-4:** The 1m DEM used in the HEC-RAS model for Meadow Creek with cross-sections at 30m intervals.

#### 4.1.5 STOICMOD-SSHBS as the stream nutrient processing module

We use STOICMOD-SSHBS uptake equations for algal DIN uptake, denitrification, heterotrophic DIN uptake, mineralization, and respiration. These processes all influence watershed nutrient export and retention. We detail the STOICMOD and SSHBS uptake functions that our integrated model calculates at every 30-meter cross-section area. The mass balance of N at each cross-section and through the integrated model is computed as:

$$\Delta N_{i,t} = C_{i-1,t}Q_{i-1,t} + C_{tributary,t}Q_{tributary,t} - Uptake_{i,t} - C_{i,t}Q_{i,t} \quad (1)$$

$\Delta N$  is the change in mass of DIN in the water column,  $i$  is the cross-section,  $t$  is time,  $C_{i-1,t}$  and  $Q_{i-1,t}$  are the concentration of DIN and the stream discharge, respectively, at the section directly

upstream of section  $i$ .  $C_{\text{tributary},t}$  and  $Q_{\text{tributary},t}$  are the concentration of N and the discharge, respectively, at a tributary feeding into the cross-section  $i$  (if applicable).  $U_{\text{take},i,t}$  is the N removed from the water column via in-stream uptake processes.  $C_{i,t}$  and  $Q_{i,t}$  are the concentration of N and outflow at section  $i$ . Figure 4-5 is a diagram that summarizes all of the processes simulated using the STOICMOD-SSHBS functions with numbers in parenthesis next to the process labels corresponding to the functions outlined below.

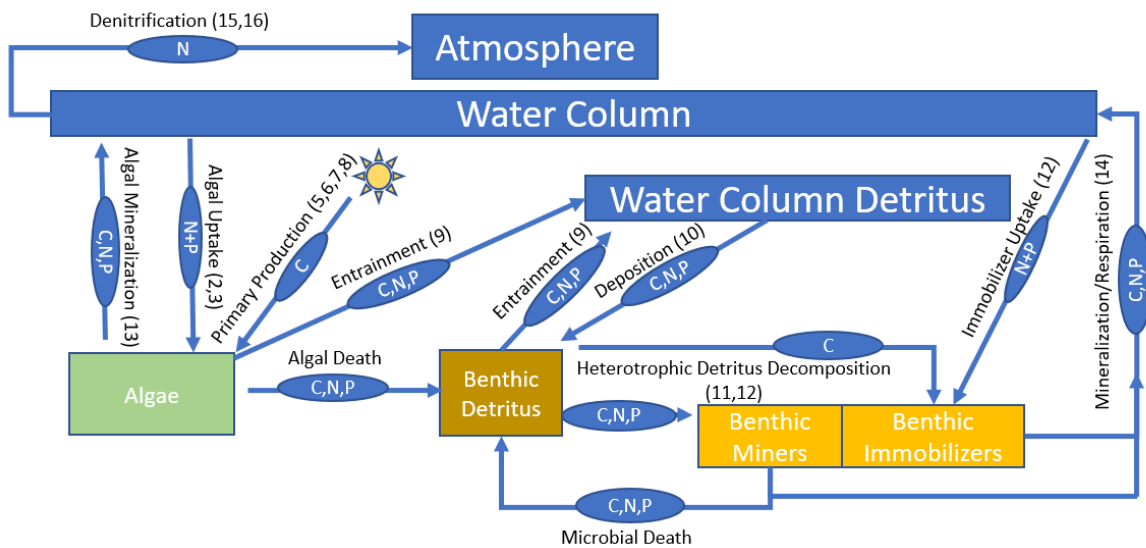


**Figure 4-5:** Carbon, nitrogen, and phosphorus processing pathways as modeled with STOICMOD-SSHBS equations.

The following uptake functions use measured input data including photosynthetically active radiation (PAR) at an hourly timestep, water temperature at a daily timestep, and an estimation of leaf litter (detritus) C, N, and P inputs to the stream. We measure PAR at one location using a HOBO® PAR Smart Sensor. PAR measurements were taken at all three zone sections, yet significant gaps exist in the data collected from the sensors at sections 1 and 2. These gaps were caused by animal tampering, resulting in sensor damage for long time periods over the simulation period. We also measured water temperature at each of the mainstream

reaches using a HOBO® Dissolved Oxygen Data Logger logging at a 15-minute interval. We do not have field measurements of daily stream detritus input, so we calibrated the daily C mass inputs into the stream at each reach zone to benthic respiration, assuming the daily watershed deposition patterns and C/N/P ratios were similar to Webster et al. (2016). See figure C-4 in appendix C for the leaf-litter C inputs per square meter at each reach zone. Note that zone 2 was parameterized to have 50% less leaf-litter input due to its lack of riparian canopy.

STOICMOD-SSHBS models algal uptake using a modified Michaelis-Menten equation:

$$AlgU_{X,i,t} = \frac{U_{max-X} \times C_{X,i,t}}{\kappa_{half,X} + C_{X,i,t}} \times AlgC_{i,t} \times g_s \times Q_{10f} \quad (2)$$

$U_{max-X}$  is the maximum daily uptake of nutrient X (X = N or P) per carbon algal biomass (mgX/mgC/d),  $C_{X,i,t}$  is the water column concentration of N or P (mgX/m<sup>3</sup>) at reach cross-section i at time t,  $\kappa_{half-X}$  is the nutrient specific half-saturation constant for uptake (mgX/m<sup>3</sup>),  $AlgC_{i,t}$  (mgC/m<sup>2</sup>) is the standing crop of algal carbon biomass per benthic area at reach cross-section i at time t. The biomass limitation of Algal DINet primary production is computed as

$$g_s = \frac{1}{1 + (\kappa_s \times AlgC_{i,t})} \quad (3)$$

$Q_{10f}$  is a function for the ecosystem process sensitivity to temperature (T) as modulated by a scaling parameter  $\phi$  which was calibrated to be 1.1 for autotrophs and 1.3 for heterotrophs, indicating a relatively low sensitivity to temperature for all uptake processes at Upper Meadow Creek.

$$Q_{10f} = \phi \frac{T_{i,t}^{-1.2}}{10} \quad (4)$$

$K_s$  (mg/mgC) is the self-limitation coefficient. The magnitude of algal uptake is dependent on algal standing biomass (mgC/m<sup>2</sup>). The potential algae carbon biomass growth ( $G_L$ , d<sup>-1</sup>) is a linear hyperbolic light-photosynthesis response function (Boston,1991):

$$G_L = G_{max} * \tanh \left( \frac{\alpha * PAR_{i,t}}{G_{max}} \right) \quad (5)$$

where  $G_{max}$  (d<sup>-1</sup>) is the maximum algae growth rate, average daily PAR is the photosynthetically active radiation (μmol/m<sup>2</sup> s), and  $\alpha$  is an initial slope parameter (m<sup>2</sup>s/μmol). Note that PAR data that was obtained at zone 7 was used at all three reach zones since it was not available over the entire two-year period at the zones 1 and 2 so  $G_{max}$  was used as a calibration parameter that distinguished photosynthetic activity at each zone due to these data gaps. In the future, we plan to employ regression or other modeling methods to complete or estimate the missing PAR data in zones 1 and 2. This future approach will ensure that  $G_{max}$  remains consistent with values referenced in the literature. Zones 1 and 3 are largely covered by canopy where zone 2 is largely devoid of overhead canopy so  $G_{max}$  was parameterized to be higher in zone 2. Gross primary production (GPP, mgC/d) is modeled using equation 6.

$$GPP_{i,t} = AlgC_{i,t} \times G_L \times g_s \times g_l \times Q_{10f} \quad (6)$$

Nutrient uptake is stoichiometrically related to C/N and C/P ratios. The internal nutrient stores limit on primary production is computed as:

$$g_l = \min \left[ 1 - \frac{N/C_{min}}{N/C_{i,t}}, 1 - \frac{P/C_{min}}{P/C_{i,t}} \right] \quad (7)$$

Where  $N/C_{min}$  and  $P/C_{min}$  are the N/C and P/C ratios that are necessary for algae subsistence and  $N/C_{i,t}$  and  $P/C_{i,t}$  are the N/C and P/C ratios at section i. Algal respiration proceeds as equation 8.

$$R_{i,t} = r_i \times B_{i,t} \times Q_{10f} \quad (8)$$

where  $r_i$  ( $d^{-1}$ ) is the respiration rate of algae and  $B_{i,t}$  ( $mgC/m^2$ ) is the standing stock of the algae carbon (equation 8 is used for other benthic organisms other than algae with different respiration rates). The sum of GPP and respiration (equation 9) is net primary production ( $NPP_{i,t}$ ) which supplements standing stocks of algal C as shown in equation 10:

$$NPP_{i,t} = GPP_{i,t} - R_{i,t} \quad (9)$$

$$AlgC_{i,t} = AlgC_{i,t-1} + NPP_{i,t} \quad (10)$$

Entrainment and deposition processes occur in relation to stream velocity ( $v$ ) and the adapted equations from Lin et al. (2021), based on Doyle (2005):

$$EF_{i,t} = \left( 0.85 / \left( 1 + e^{-\left( \frac{v_{i,t} - \sigma}{0.06} \right)} \right) \right) \quad (11)$$

$$DF_{i,t} = 1 - e^{\left( \frac{-L * BA_{i,t} * 0.05}{v_{i,t} * V_{i,t}} \right)} \quad (12)$$

Where  $EF_{i,t}$  is the fraction of benthic detritus that is entrained at section  $i$  at time  $t$ ,  $DF_{i,t}$  is the fraction of water column detritus that is deposited on the benthic area of cross-section  $i$  at time  $t$ . Detritus and microorganisms were parameterized to be more mobile and were parameterized to entrain at lower velocities compared to algal mass, so  $\sigma$  was parameterized with a value of 0.5 for algae and 0.4 for detritus. Detritus and entrained algae within the water column are deposited as it moves downstream according to equation 12. Daily water column detritus is regulated by a daily deposition rate of detritus from the watershed along with entrainment and transport from upstream of each 30m cross-section. When detritus is deposited on the stream bottom, the constituent C, N, and P are subjected to microbial assimilation, respiration, and mineralization back into the water column in dissolved form. Algae and microbe mortality also supplements benthic detritus C, N, and P.

Microbial nutrient uptake processes are conducted by one of two groups. The first microbial groups are “miners” which obtain all of their C, N, and P from benthic detritus ( $Detritus_{benthic}$ , mg/m<sup>2</sup>) at a maximum decay rate ( $k_{miners}$ , d<sup>-1</sup>) modulated by the  $Q_{10f}$ :

$$G_{miner,i,t} = Detritus_{benthic,i,t} \times k_{miner,i,t} \times Q_{10f} \quad (13)$$

The second microbial group are the immobilizers which obtain C from benthic detritus according to a Michaelis-Menten type equation:

$$G_{immobilizer,i,t} = Detritus_{benthic,i,t} \times k_{immobilizer,i,t} \times Q_{10f} \times \min\left(\frac{C_{x,i,t}}{k_{half} + C_{x,i,t}}\right) \quad (14)$$

where  $G_{immobilizer,i,t}$  is the uptake of benthic detritus C by immobilizers (mgC/m<sup>2</sup>),  $k_{immobilizer}$  is the maximum detritus decay rate (d<sup>-1</sup>), and  $k_{half}$  is the half saturation constant for immobilizers (mgX/m<sup>3</sup>). Immobilizers sequester N and P from the water column to maintain constant C/N and C/P ratios in accordance with their benthic detritus C uptake.

Miners and immobilizers maintain a constant C, N, and P ratio and so mineralize according to their intake of those nutrients. For example, miners consume detritus which have a different C, N, and P ratio compared to the miners, so the miners will release the excess C, N, or P to match their constant ratio into the water column. Organic carbon on the benthic bottom respire along with miners and immobilizers, releasing dissolved C back into the water column, according to equation 8 above where  $B_i$  and  $r_i$  are the standing crop of carbon biomass (mgC/m<sup>2</sup>) and the respiration rates (d<sup>-1</sup>) for either detritus, miners, or immobilizers., along with N and P according to respective C, N, P ratios.

Algal, miner, and immobilizer mortality are linearly proportional to standing crop.

Denitrification from the water column is simulated using the following equations:

$$v_f = 10^{(-2.975 - 0.493 \times \log_{10}(C_{NO_3-N}))} \times 0.01 \quad (15)$$

$$DeN = v_f \times C_{NO_3-N} \quad (16)$$

$v_f$  is the uptake velocity for denitrification as described by Mulholland et. al (2008) and DeN is found by multiplying the uptake velocity by the  $C_{NO_3-N}$ , which is the concentration of nitrate-N in the water column, according to in-stream nutrient spiraling principles (Stream Solute Workshop, 1990). Note that this equation for areal denitrification uptake velocity does not account for varying stream conditions (e.g. hyporheic zone depth and structure, or temperature). Note that  $C_{NO_3-N}$ , was assumed to be 0.96 times DIN according to the grab sample data. Table C-1 in appendix C summarizes the parameter variables, descriptions, and values in the appendix of this paper.

Following nutrient spiraling principles, nutrient uptake by algae or benthic microbes depends on the nutrient mass available in the water column within a given day at every cross-section. Greater nutrient amounts in the water column, coupled with reduced velocities, result in shorter nutrient spiraling lengths downstream. Nutrient molecules change form as they travel downstream as they are consumed by benthic organisms and are then subsequently subject to mineralization at a later time. Stream cross sections with larger benthic areas exhibit more enhanced overall nutrient uptake from the water column.

#### **4.1.6 GI Scenario Analysis**

A scenario analysis is used to assess the impacts of different GI types and their location within the Meadow Creek subbasin network, implemented in SWMM, on in-stream N uptake processes. These scenarios are not meant to reproduce the most likely GI implementations, or the

range of potential designs. A total of twenty-six locally extensive GI scenarios were developed in the study area – nine rain garden scenarios, eight green roof scenarios, and nine impervious conversions to tree canopy scenarios. Rain garden scenarios include implementing 10m by 10m rain gardens at every residential parcel within each subbasin. For each subbasin, the rain garden scenarios were assumed to treat 25% of the pervious and 25% of the impervious surfaces. Green roof scenarios involved the implementation of green roofs on all commercial building areas in each subbasin. Commercial building areas were determined from local structure and zoning GIS data. There are only eight green roof scenarios since subbasin 9 has a negligible amount of commercial building space. The nine impervious to greenspace scenarios are implemented by converting 25% of the commercial and residential impervious area to pervious grass and tree canopy, split evenly, in SWMM. Table 4-3 summarizes the number of residential parcels as well as the commercial roof and impervious areas that are utilized for each of the 26 GI scenarios explored in this study. To determine the impacts of urban GI on in-stream DIN retention processes, we calculated the percent change in gross primary production, Algal DIN uptake, immobilizer assimilation, denitrification, mineralization, benthic detritus, and algal mass at each downstream reach for each of the above-described GI scenarios. Note that the rain gardens have the most implementation potential and the availability of green roof space is significantly lower than the other two GI types.

**Table 4-3:** Number of rain garden parcels, commercial green roof area, and impervious conversions areas for each of the 26 GI scenarios.

<b>Subbasin</b>	<b>Residential Parcel Rain Gardens</b>	<b>Commercial Roof Area (ha)</b>	<b>Impervious to Tree Canopy (ha)</b>
1	809 (80.9 ha)	6.3	41.3
2	484 (48.4 ha)	0.8	15.2
3	428 (42.8 ha)	0.8	10.4
4	121 (12.1 ha)	0.8	5.6
5	86 (8.6 ha)	1.1	7.5
6	200 (20 ha)	7.6	11.7
7	1311 (131.1 ha)	2.5	28.4
8	219 (21.9 ha)	1.1	16.6
9	528 (52.8 ha)	-	4.9

## 4.2 Results

### 4.2.1 Integrated Model Calibration and Validation

We calibrated our integrated model to daily flow, nutrient concentrations, and primary productivity, for the year 2021 and validated nutrient concentrations for the year 2022. The calibrated Nash-Sutcliffe Efficiency (NSE) and the Kling-Gupta Efficiency (KGE) for daily flow is 0.69 and 0.70 respectively and the validated NSE and KGE is 0.57 and 0.54 respectively.

Figure 4-6 shows the time series graph for our daily flow calibration and validation.

### Flow Calibration and Validation

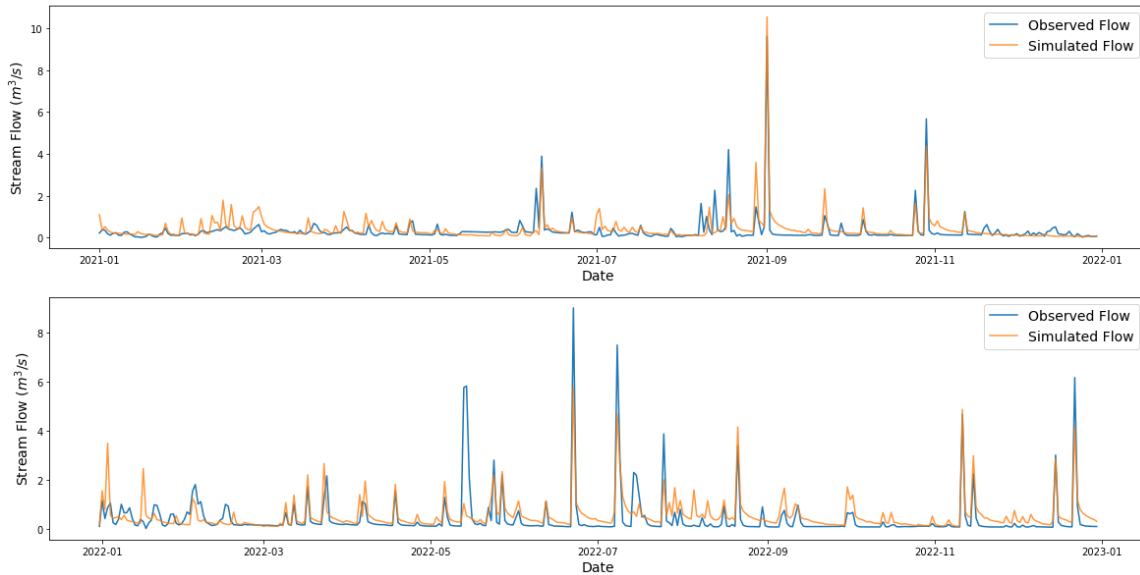


**Figure 4-6:** Time series graphs for daily flow calibration (upper graph) and validation (lower graph).

DIN concentrations were calibrated and validated at each of the three stream reach zones using the mean absolute error (MAE). Table 4-4 summarizes the number of days that were sampled at each zone for the calibration and validation periods along with the respective MAE's. Figure 4-7 is a time series showing observed and modeled DIN concentrations for each reach zone during the calibration and validation periods.

**Table 4-4:** Mean absolute error values for daily DIN concentrations for the calibration and validation periods.

Zone	Calibration (2021)		Validation (2022)	
	# of days sampled	MAE (mg N/L)	# of days sampled	MAE (mg N/L)
1	31	0.26	36	0.23
2	31	0.31	37	0.3
3	37	0.27	41	0.23

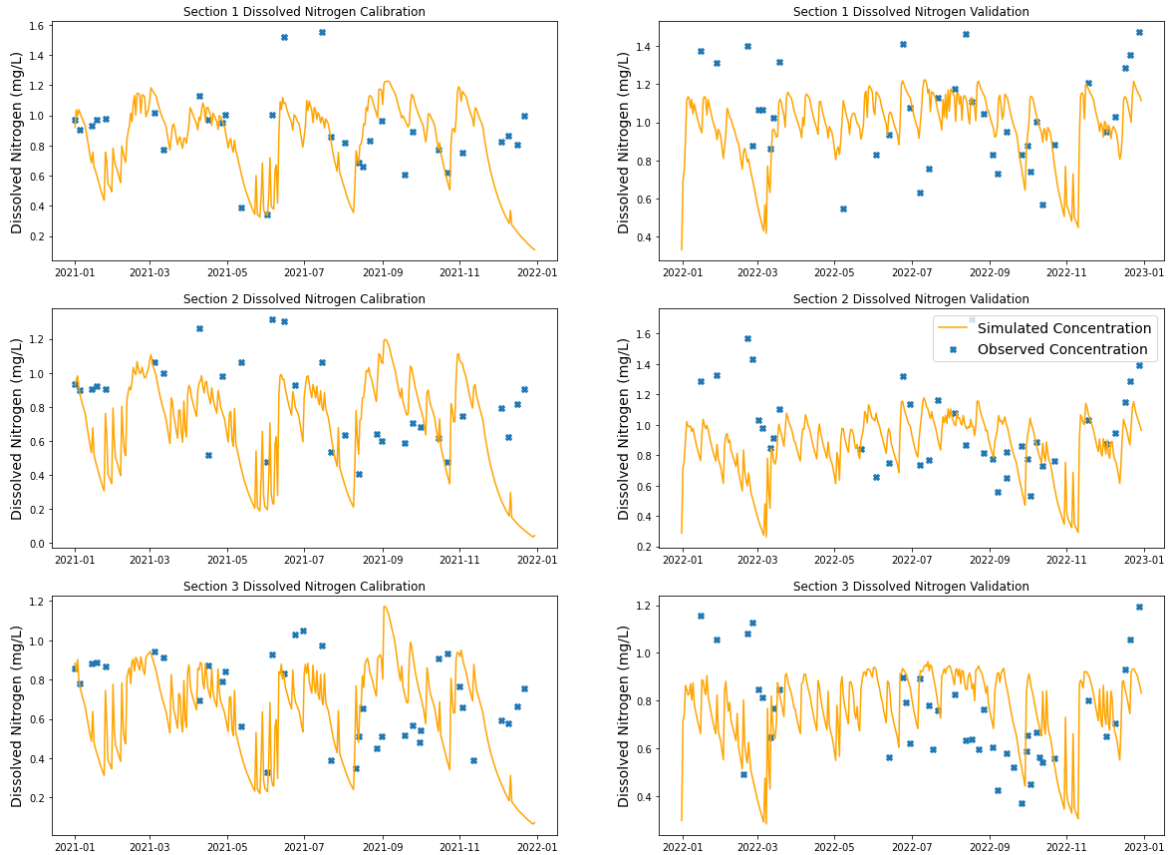


**Figure 4-7:** Time series showing observed and modeled DIN concentrations for each reach zone during the calibration and validation periods.

While the model was not specifically calibrated to DIN loads, we compared the measured loads with the model loads at the stream outlet (zone 3) throughout the simulation period (figure 4-8). The loads were not calibrated mainly because of the absence of flow data at the other two sections. This comparison demonstrates a closer correspondence between the measured and modeled data, yielding an  $R^2$  value of 0.24 over the simulation period. Although not exact, this load comparison boosts our confidence that the simulated loads, particularly at baseflow, are within in the expected range.

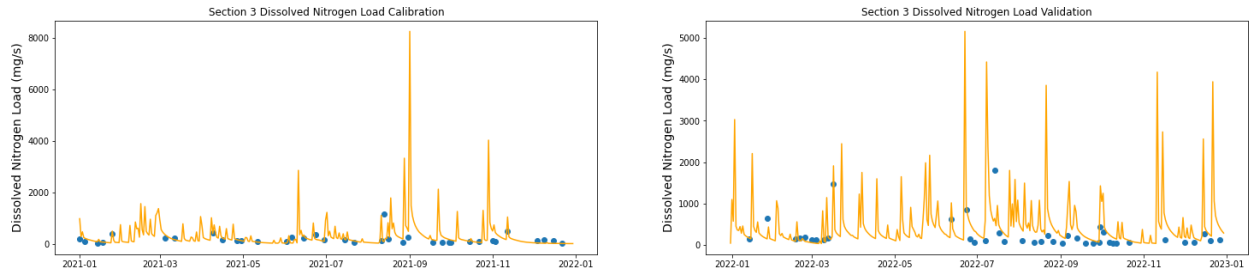


**Figure 4-8:** Measured (blue) and simulated (orange) DIN loads from zone 3 over the simulation period.

Gross primary production and ecosystem respiration were calibrated for the year 2021 at each of the three stream reach zones also using the MAE metric. Table 4-5 summarizes the number of days that stream metabolism was modeled with BASE and the MAE values corresponding to the simulated stream metabolism results from our integrated model for the year 2021. Figure 4-9 shows the monthly primary production and ecosystem respiration averages for both models in each zone.

**Table 4-5:** Primary Production and Ecosystem Respiration MAE values between BASE and our integrated model.

# of days modeled	Primary Production	Ecosystem Respiration
	MAE (g/m <sup>2</sup> )	MAE (g/m <sup>2</sup> )
158	0.22	0.38
152	0.22	0.30
222	0.23	0.28

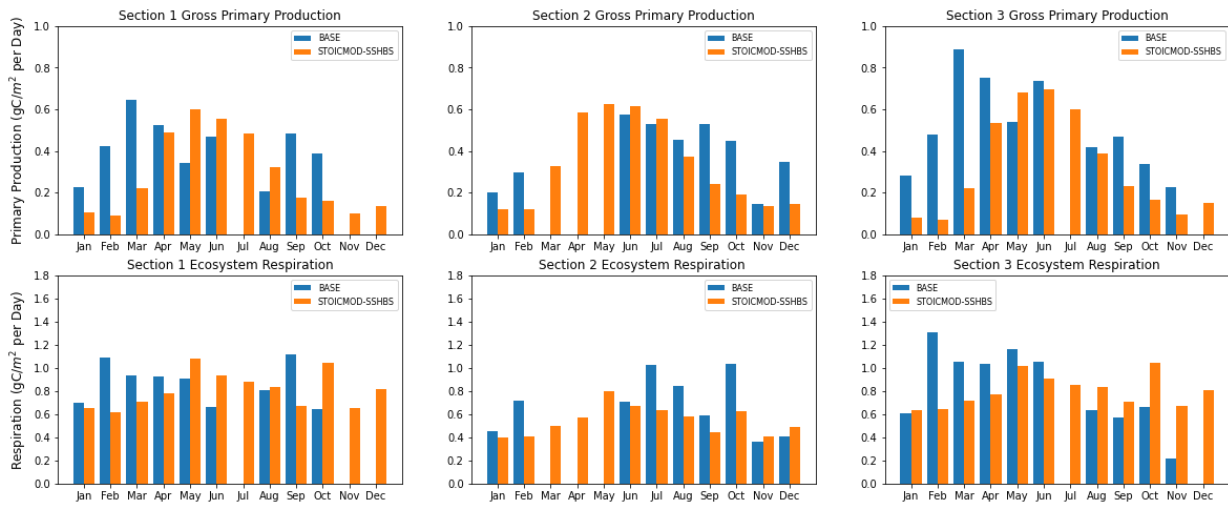


**Figure 4-9:** Monthly primary production and ecosystem respiration at each section as modeled with BASE and our integrated model.

#### 4.2.2 Simulated Stream Ecosystem DIN Processing Rates

DIN from the watershed enters the stream through the various tributaries in our integrated model and is subject to uptake processes as it travels longitudinally downstream. Figure 4-10 is a time series of simulated average daily uptake rates.

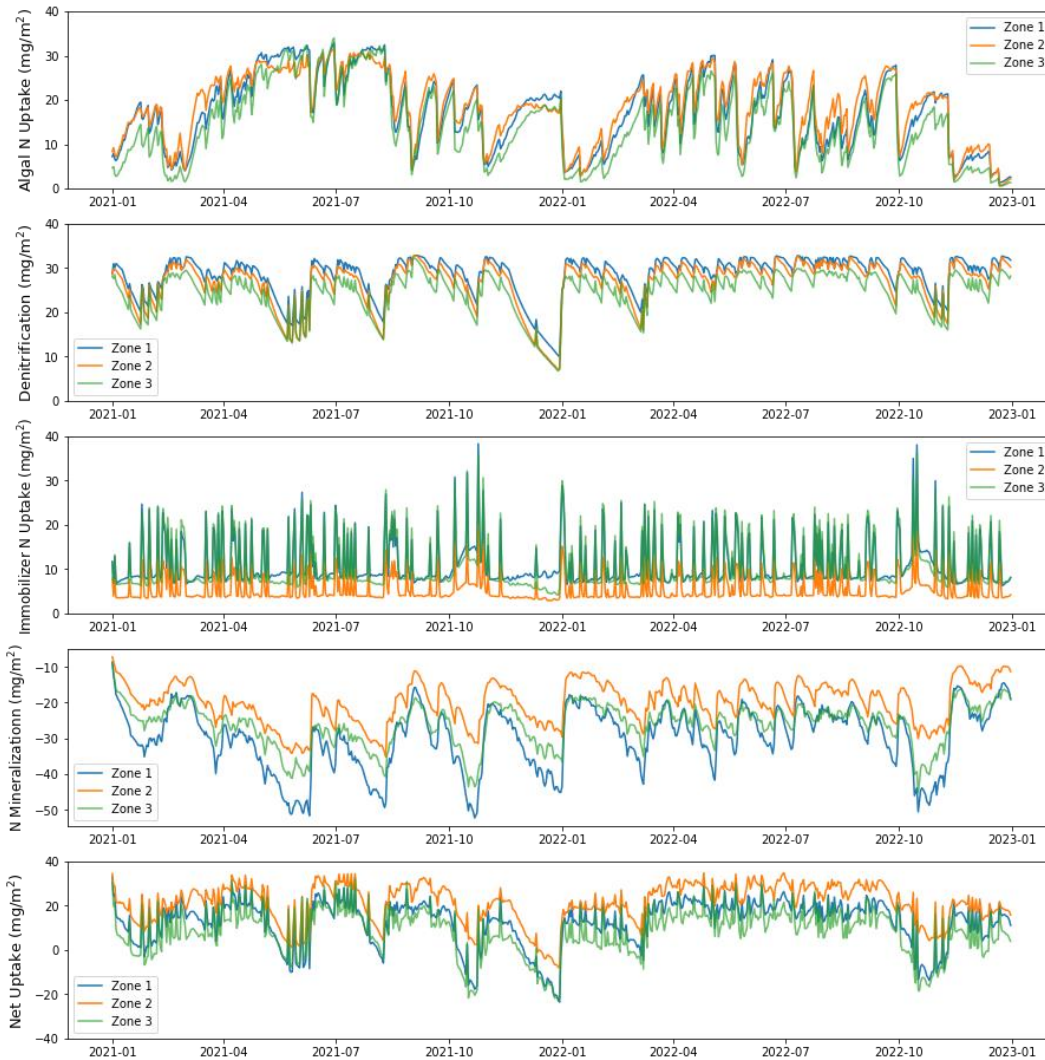


**Figure 4-10:** Modeled Algal DIN uptake, denitrification, immobilizer N assimilation, and N mineralization daily rates for reach zones 1, 2, and 3. Net mineralization is graphed and tabulated as a negative value since it adds N back into the water column, counter to the other simulated processes.

Denitrification exhibited the greatest DIN uptake rates in the stream at all three zones compared to the other processes. Denitrification was similar at all three zones but was slightly higher at zone 1 on average, where the DIN concentrations were highest. Denitrification rates are largely dependent on the DIN concentration in the stream according to our model and the concentration drops from upstream to downstream and that is reflected in the reach zone simulated denitrification rates. Algal DIN uptake was the second greatest contributor to DIN uptake and

was highest in zone 2. More algal DIN uptake at zone 2 makes sense due to the lower amount of canopy coverage at that zone which leads to more light energy being converted to algal mass. Immobilizers were estimated to have the lowest DIN uptake rates on average from the water column from each zone and were greatest in zones 1 and 3. Mineralization was greatest in zone 1. The differences in mineralization may be explained by the lower leaf litter input parameterization at zone 2 compared to the other two zones, which led to lower benthic detritus standing stocks on average and therefore less mineralization. The differences observed in the mineralization rates between zones 1 and 3 may be explained by the higher deposition rate of detritus on the stream bottom and the greater algal mass at zone 1 compared to zone 3. Net DIN uptake per square meter was the sum of simulated algal uptake, denitrification, immobilization, and mineralization and was greatest at zone 2 on average, largely due to the lower mineralization and higher algal uptake rates at that zone.

Standing stocks of algal and heterotrophic benthic biomass are also relevant parameters to the uptake of DIN within Meadow Creek. Figure 4-11 shows the standing stocks of benthic algal and detritus mass per square meter at each zone over the two-year simulation period. Across all three zones, simulated algae biomass was greatest in the late spring and lowest during the winter months while detritus showed a spike during the autumn leaf fall period but maintained relatively consistent stocks over the course of the rest of the year compared to the algae mass.

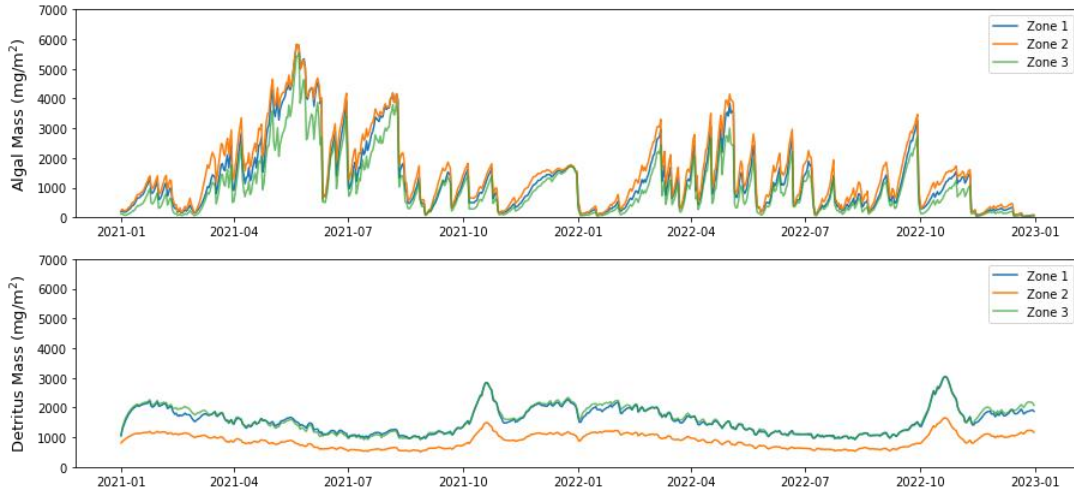


**Figure 4-11:** Daily standing stocks of algal and detritus biomass per square meters of benthic area at each zone over the two-year simulation period

The majority of the DIN cycling in upper Meadow Creek occurred at zone 2, where approximately 124 kg were removed from the water column over the two-year simulation period followed by zone 3 with 55 kg removed and zone 1 with 23 kg removed. Of the estimated 23,620 kg of DIN input in to stream from all nine subbasins combined over the two-year simulation period, approximately 202 kgs were estimated to be retained in the stream system through algal uptake, immobilizer assimilation, or removed through denitrification, which equals approximately 0.86%. This relatively low percentage suggests that upper Meadow Creek is nearly a flow-through system in terms of DIN as the stream itself plays a relatively small role in terms of N export from the watershed.

#### 4.2.3 Simulated Impacts of GI scenarios on in-stream N uptake

To evaluate the potential of each subbasin to impact DIN processing in the upper Meadow creek watershed, we tested 26 different single GI type scenarios. Our findings suggest that average ecosystem processing rates and standing stocks of benthic algae and detritus were not changed by more than 5% under all of the tested scenarios. The raingarden and impervious

conversion scenarios generally increased N uptake at all three stream reach zones with few exceptions at zone 3, while the green roof scenarios either slightly decreased average N uptake or did not impact it. The GI scenarios that were implemented at subbasin 1 yielded the greatest impacts to N uptake in the stream for all 3 GI types. Generally, the most downstream reach zone ecosystem was the most impacted by GI implementation versus the most upstream reaches. Figures 4-12, 4-13, and 4-14 are heat maps that show the impacts on the average daily DIN spiraling variables as a result of each GI scenario on each of the three zone reaches.

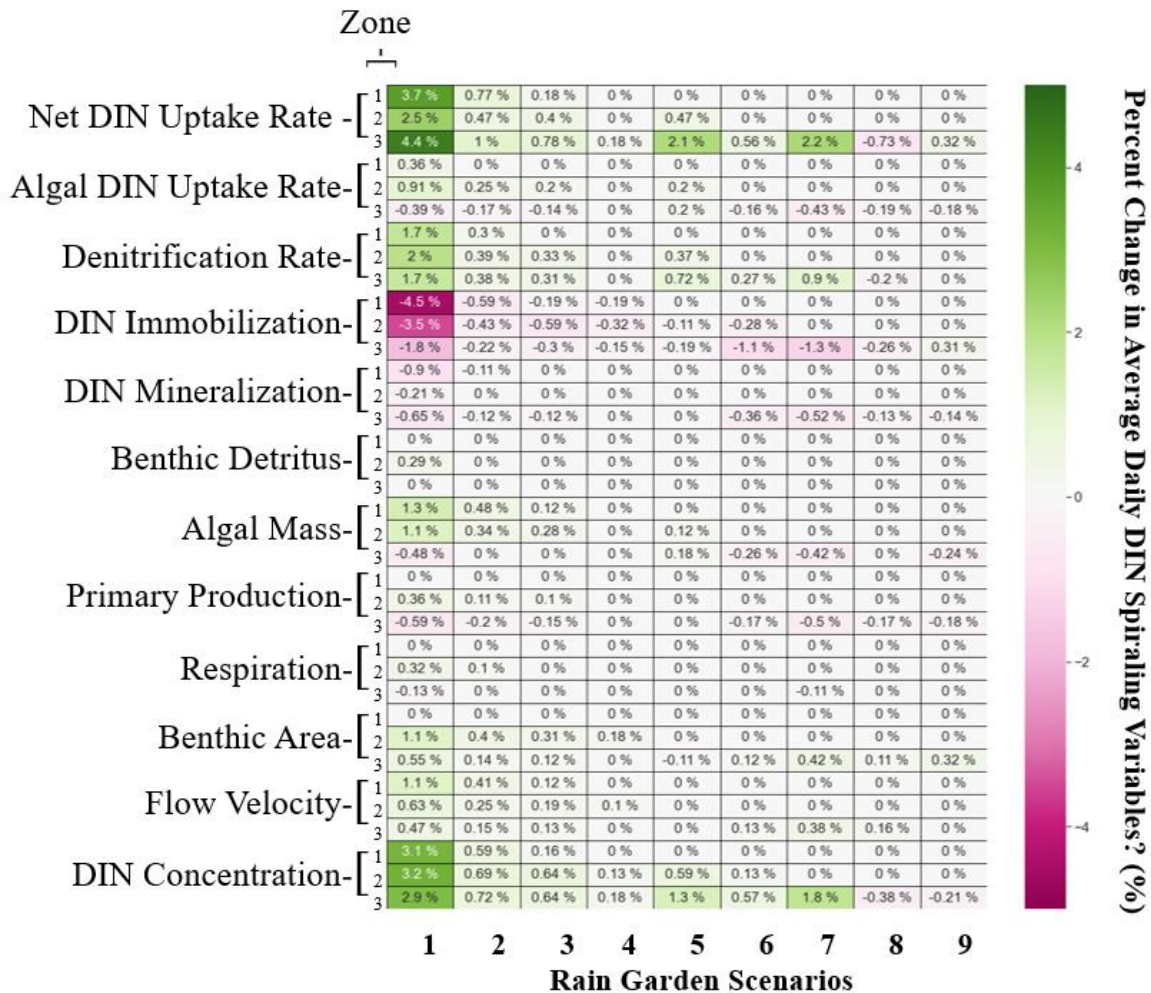


**Figure 4-12:** Simulated percent changes in daily DIN spiraling variables at the three zones under the nine rain garden scenarios. Raingarden scenarios are numbered at the bottom according to the subbasin where single 10 x 10-meter raingardens were implemented at all residential parcels. The numbers in brackets on the left indicate the zone.

As the darker shades indicate in figure 10, raingardens implemented at all residential parcels at subbasin 1 show the most change to the stream ecosystem in regard to DIN uptake. Under this scenario, the average DIN uptake rate increased in zones 1, 2, and 3 by 3.7%, 2.5%, and 4.4% ,respectively, relative to the status quo scenario. This increase coincided with increased average DIN concentrations, which elevated areal denitrification rates. Likewise, average mineralization and immobilizer uptake were reduced at all three zones while average stream flow velocities increased. The other notable changes observed in figure 4-12 occurred with raingarden implementations at subbasins 5 and 7 which yielded increases of average N uptake only at zone 3 by 2.1% and 2.2%, respectively, while implementation at subbasin 8 reduced average N uptake slightly by 0.73%.

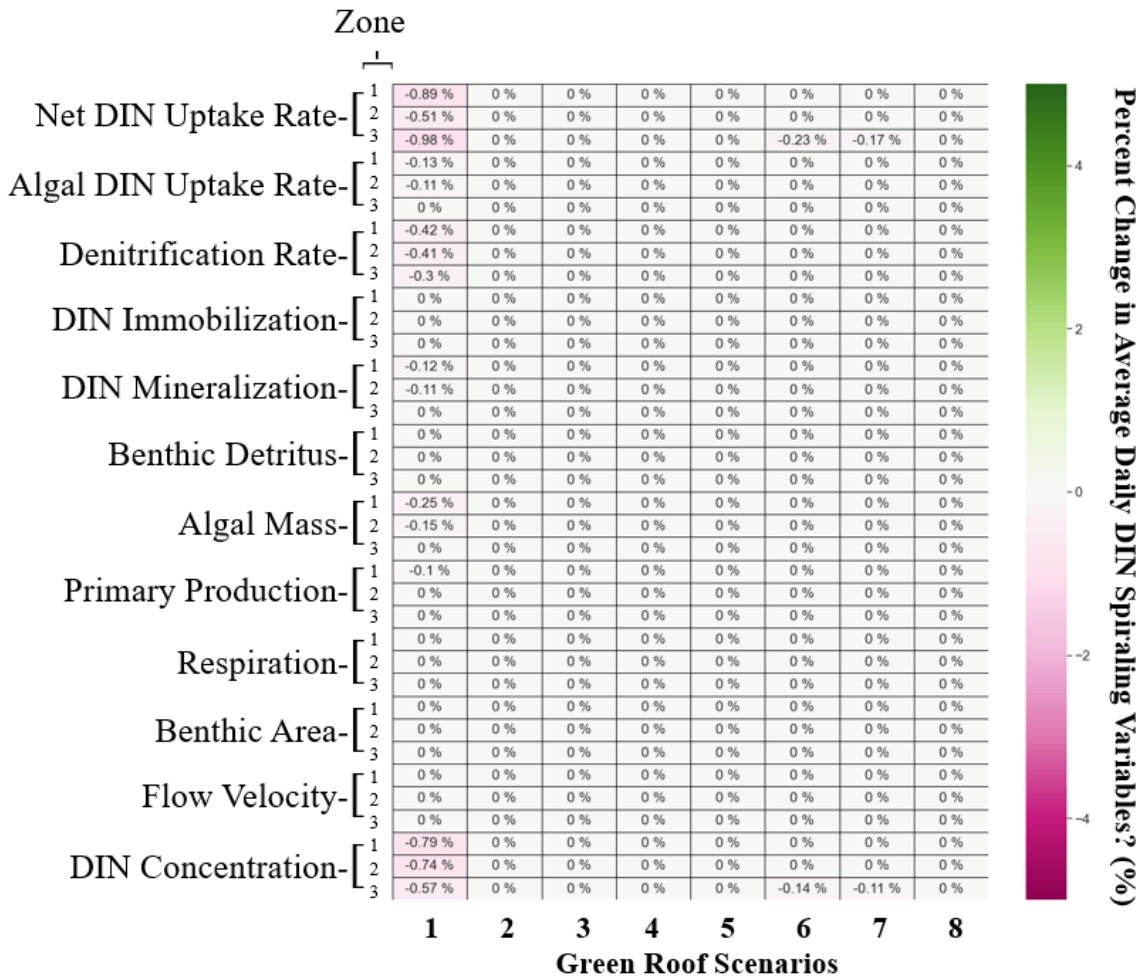


**Figure 4-13:** Simulated percent changes in daily DIN spiraling variables at the three zones under the eight green roof scenarios. Green roof scenarios are numbered at the bottom according to the subbasin where commercial roof areas were converted to green roofs in SWMM. The numbers in brackets on the left indicate the zone.

Green roofs were not as impactful to the stream ecosystem as the other two GI type scenarios, which was not surprising considering the smaller available area. The darker shades in figure 4-13 indicate that commercial roof conversions to green roofs at subbasin 1 are the most impactful compared to the other subbasin scenarios. Under this scenario, the average N uptake rate decreased in zones 1, 2, and 3 by 0.89%, 0.51%, and 0.98% respectively. This increase coincides with a decrease in average DIN concentrations and denitrification rates. The green roof scenarios at subbasins 6 and 7 show slightly reduced average N uptake rates only at zone 3 which also coincide with decreased average DIN concentrations at that zone.

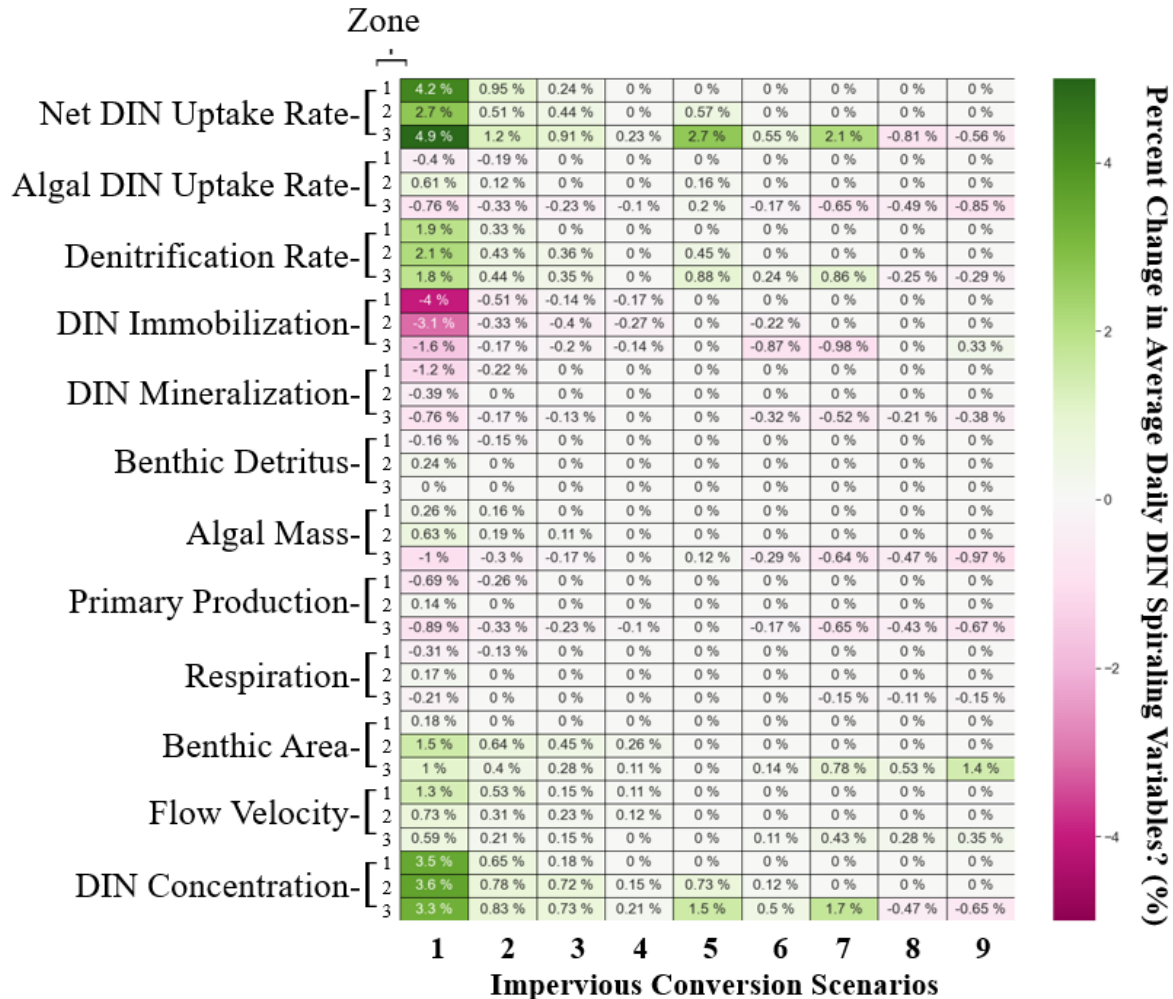


**Figure 4-14:** Simulated percent changes in daily DIN spiraling variables at the three zones under the nine impervious conversions to green space scenarios. Impervious conversion scenarios are numbered at the bottom according to the subbasin where 25% of the impervious surfaces were converted to tree canopy and grasses. The numbers in brackets on the left indicate the zone.

Like the other GI scenarios, impervious conversion to green space at subbasin 1 was the most impactful to the stream ecosystem in regard to DIN uptake. Under this scenario, the average N uptake rate increased in zones 1, 2, and 3 by 4.2%, 2.7%, and 4.9% respectively. This increase coincided with increased average DIN concentrations which elevated average denitrification rates. Likewise, mineralization and immobilizer uptake were reduced at all three zones while average stream velocities increased. The other notable changes observed in figure 4-14 occurred with at subbasins 5 and 7 which yielded increases of average N uptake only at zone

3 by 2.7% and 2.1%, respectively, while implementation at zones 8 and 9 reduced average DIN uptake by 0.81% and 0.56% respectively.

To identify the most effective GI type and subbasin for implementation, it may be important to assess in-stream impacts on a per-hectare basis. Rain gardens had the highest impact on in-stream nutrient uptake per hectare, followed by impervious conversion to green space. For visual representations, refer to Figures C-5 and C-6 in appendix C, illustrating the percent change in DIN spiraling variables on a per GI hectare basis. Notably, both GI types, particularly in subbasin 5, exhibited significant changes in net DIN uptake per hectare of GI implementation. This evidence suggests that subbasin 5, being the smallest and most impervious, might be the most influential for GI implementation on a per-hectare basis, especially at lower levels of GI implementation.

The subbasin with the most potential to influence change to the stream ecosystem and DIN uptake with GI implementation was found to be subbasin 1, mostly because of its size and potential for GI implementation. The most impactful changes were related to flow velocity and DIN concentrations. Table 4-6 shows the average flow velocities and concentrations under each of the four flow quantiles for the GI scenarios at subbasin 1.

**Table 4-6:** Simulated average daily velocity and DIN concentrations for the status-quo and the GI scenarios at subbasin 1 at the four flow quantiles.

Flow Quantile	Flow Velocity (m/s)			
	Status-Quo	Rain Garden	Green Roof	Impervious Conversion
1	0.353	0.358	0.353	0.358
2	0.437	0.444	0.436	0.444
3	0.494	0.5	0.494	0.501
4	0.639	0.636	0.640	0.637
Flow Quantile	DIN Concentration (mg/L)			
	Status-Quo	Rain Garden	Green Roof	Impervious Conversion
1	0.478	0.524	0.475	0.528
2	0.857	0.88	0.853	0.883
3	0.990	1.003	0.983	1.004
4	0.994	1.014	0.985	1.019

Flow velocities at the lower quantiles (at or below the 75<sup>th</sup> percentile of flow values) were elevated under the rain garden and impervious conversion scenarios at subbasin 1 compared to the status-quo scenario while the green roof scenario was more similar to the status-quo. Average flow velocities were reduced at the highest quantile of flow (above the 75<sup>th</sup> percentile of flow values) under the rain garden and impervious conversion scenarios compared to the status-quo scenario while the green roof scenario was more similar to the status-quo. The reduced velocities at stormflow contributed to less algal mass entrainment but the increased velocities at baseflow reduced the benthic immobilizer population and led to a decrease in the average immobilization of DIN from the water column under these scenarios.

The rain garden and impervious conversion scenarios increased infiltration into the aquifer, which increased the groundwater flow into the stream. Under these scenarios, DIN concentration was elevated under all flow quantiles because groundwater was parameterized to have a higher DIN concentration than stormwater runoff. These observations appear to be the reason why denitrification was elevated under the rain garden and impervious conversion

scenarios, which are infiltration-based GI, while it was reduced under the green roof scenario. This change in denitrification was the major driver in the change in average net DIN uptake.

Due to the higher DIN concentration parameterization for groundwater relative to runoff, the vast majority of the infiltration-based GI scenarios (rain gardens and impervious surface conversion) resulted in a net increase in DIN concentrations and export from the watershed. For example, the GI scenarios from subbasin 1 resulted in an additional 331 kgs and 452 kgs of DIN being input into the stream from the subbasins for the rain garden and impervious surface conversion scenarios, respectively, relative to the status quo scenario, with 0.86% of that being removed from the water column for all three scenarios. Although there are slight increases in DIN uptake with the rain garden and impervious conversion GI-types implemented at subbasin 1, the increased infiltration and higher concentrated groundwater flow resulting from these scenarios led to more DIN entering the stream and exported from the watershed. This was not the case for green roofs, where increased infiltration was not as much of a factor. See tables C-3 to C-6 in appendix C for a more details on the DIN inputs and zonal processing rates for each GI scenario.

## **4.3 Discussion**

### **4.3.1 Utility of the Integrated Model**

The integrated model developed in this study is intended for use by urban hydrologic modelers who are familiar with the three coupled models: SWMM, HEC-RAS (which both are widely used in the fields of hydrology, environmental science, and engineering), and STOICMOD-SSHBS ecosystem functions. The integrated model also requires familiarity with python programming especially knowledge on how to execute GI scenarios using python SWMM API (Pichler, 2022). The model for the upper Meadow Creek watershed, which is

contained within a python notebook, is posted to an open-source website (see data availability statement) for users to access freely. The python notebook contains tutorial instructions on how to set-up and execute the upper Meadow Creek model and how the notebook can be adapted for use at another study watershed. The open-source nature of the integrated model in python notebook form allows for customization of the code to fit specific conditions within a given watershed and allows for the model to be improved by any user.

The integrated model requires a minimum of daily precipitation, flow, temperature, and hourly PAR. To calibrate with stream metabolism parameters, at least hourly PAR, dissolved oxygen concentrations, and electrical conductivity measurements would be required. Field sensors for all of these parameters are obtainable at a low cost. More years of data collection are recommended for the integrated model to capture seasonal patterns more effectively, which was not necessarily possible under this two-year case-study period. If these data are not available, it is possible to parameterize the integrated model with seasonal DIN groundwater and stormwater concentrations if necessary. The integrated model also requires nutrient sampling at the highest possible frequency, and stream geomorphology in the form of channel cross-sections and roughness. Our integrated model was calibrated and validated using measured streamflow and a limited number of DIN concentration data from water samples that were collected largely under baseflow conditions over a period of two calendar years.

Coupling models for urban hydrology, stream channel hydraulics, and stream ecosystem processing enables the opportunity to examine whole watershed N retention processes, and the potential of watershed GI to improve N retention. The coupling of a watershed model to a more mechanistic aquatic ecosystem model allowed for a detailed investigation of stream ecosystem processes that are related to N uptake in the stream. Coupling SWMM and HEC-RAS to

STOICMOD-SSHBS enabled the estimation of the impacts of urban green infrastructure on nitrogen processing in a local urban stream. The modeling framework and code is adaptable to local modeling goals and data availability. This includes the analysis of increased imperviousness and urbanization and the impacts on stream ecosystems. If the modeling efforts are less focused on urban green infrastructure development or a more mechanistic terrestrial and/or groundwater model is desired, SWMM can be replaced by other terrestrial models such as RHESSys as long as they can be implemented in a compatible programming language.

We used our integrated model to help estimate how in-stream ecosystem processes influence nitrogen uptake within Meadow Creek. Algal DIN uptake was more variable than the other simulated uptake rates which can be attributed to more variable stream velocities and entrainment patterns between the three reach zones. Denitrification was the greatest factor involved in N retention in Meadow Creek among the simulated processes. Combined algal DIN uptake and denitrification were greater than mineralization rates which contributed to an average net positive uptake of DIN from the water column at each zone. When mineralization was greater than algal uptake and denitrification during the winter months or during periods of low DIN concentration, there was a net release of N into the water column from the benthic biota, indicating that Meadow Creek can be a net source of DIN at certain times of the year, which is consistent with the spiraling paradigm.

#### **4.3.2 Integrated Model Uncertainty**

This study harbors notable sources of uncertainty, stemming from limited data collection and imprecise measurements of DIN concentrations and stream metabolism variables, alongside spatial and temporal aggregations of model data. The integrated model's component structure, especially concerning the groundwater flow and denitrification submodules, also contributes to

these uncertainties. A comprehensive uncertainty analysis for the integrated model falls beyond the present study's scope and is reserved for future research.

In essence, our inability to capture day-to-day variations in DIN and stream metabolism data during calibration and validation restricts our confidence in the integrated model's results, which are primarily reported at an annual scale. Practical constraints prevented us from obtaining sub-hourly DIN concentration measurements on a daily basis, which could have enhanced our daily DIN results and potentially reduced equifinality in DIN calibration. Furthermore, the ecosystem model outcomes were derived from data (PAR, DIN concentrations, and flow) averaged on a daily basis, potentially overlooking the complete dynamics of sub-daily processes. Additionally, when simulating watershed processes, including the effects of green infrastructure, we employed a semi-distributed, largely lumped method over extensive subbasin areas, which might not accurately represent all specific locations within the modeled landscape. Flow predictions, particularly in post-storm baseflow, tend to be overestimated, likely due to SWMM's incapacity to model complex aquifer structures that may exist in urban regions. Moreover, the denitrification model relied on regression analysis from a different watershed, warranting improvement through a similar regression specific to our research area. Additionally, the inclusion of temperature and hyporheic exchange parameters within the channel denitrification functions would refine the model's accuracy. These issues are elaborated upon, where necessary, in the following paragraphs. Given these limitations, the integrated model has been sufficiently calibrated and validated for purposes of this study.

Since only about 10% of the days were sampled for nutrient concentrations in the stream, calibration metrics that focused more on trends of the observed versus modeled data such as the  $R^2$  value were not possible to use for calibrating our integrated model to stream DIN

concentrations. The goodness-of-fit of between the observed and simulated DIN concentrations would be improved with greater sampling frequency and/or with the use of in-situ sensors that can capture DIN concentration data at continuous intervals. We obtained water samples every 1 to 2 weeks but the DIN calibration would be much improved with a continuous in-situ optical sensor that could record concentrations at a sub hourly rate, which are now becoming more widely available to researchers.

The calibration of primary production and ecosystem respiration was also conducted using results from the stream metabolism model where possible. Over the modeling period, the sensors that were deployed to collect input data for stream metabolism were subject to flashy stream conditions and wildlife tampering that significantly impaired stream metabolism data collection efforts particularly during the 2022 validation year. Additionally, most of the error observed in the stream metabolism calibration was observed in the colder months, which may be due to differences in temperature sensitivity between the two models as STOICMOD-SSHBS appears to be much more sensitive to temperature than BASE.

Over the calibration and validation period, our simulated model overestimated the flow rate on average by  $0.1 \text{ m}^3/\text{s}$ , overestimating low-to-moderate flows in quantiles 1,2, and 3 by  $0.16 \text{ m}^3/\text{s}$  and underestimating high flows within the fourth quantile of flow rates by  $0.08 \text{ m}^3/\text{s}$ . The simulated total flow volume is approximately 30% greater compared to what was observed, mostly occurring at low flows. This is largely due to the difficulty and lack of success with calibrating the recession limbs of the hydrographs using SWMM during post-storm periods. Ultimately, this suggests that upper Meadow Creek is flashier and contains less groundwater input to the stream at baseflow than what was simulated. One possible explanation for the integrated model's inability to accurately simulate the flashiness of Meadow Creek is SWMM's

incapability of representing 'urban karst' conditions within the aquifer. Urban karst conditions pertain to human constructed subsurface pathways, such as stormwater and sanitary sewer pipes, which have the potential to modify groundwater flow patterns and expedite the drainage of aquifers compared to natural conditions (Bonneau et al., 2017). Another factor influencing the integrated model's capability to represent Meadow Creek's flashiness could be the potential for increased infiltration and groundwater inflow into stormwater pipes (Bhaskar et al. 2015), which cannot be directly modeled using SWMM. Additionally, the lack of evapotranspiration in the model may also contribute to elevated baseflow. The opens-source nature of the integrated model could potentially allow for a manual correction of the simulated groundwater flow inputs to the stream which could improve the flow calibration, but the specifics of how to accomplish that is left to future users and developers of the model.

#### **4.3.3 Reducing DIN Export: Terrestrial and Fluvial Environment Contributions**

The study's findings reveal that Meadow Creek, an urban stream, plays a relatively minor role in reducing DIN export from the watershed, even in restored sections. Across all scenarios evaluated, less than 1% of the DIN transported by the stream was removed from the water column through various nutrient spiraling processes. This aligns with prior research (Claessens & Tague, 2009; Jansson et al., 1994; Pind et al., 1997), which indicates that streams typically remove or retain between 1% and 5% of the total N entering the stream from the watershed. Notably, urban streams tend to remove less than their forested counterparts. Consequently, the study underscores the urban terrestrial landscape as the primary avenue for mitigating DIN export from the watershed. Implementing strategies that curtail DIN inputs into the stream from the outset holds the key to more substantial reductions.

#### **4.3.4 Simulated Impacts of Green Infrastructure on DIN Processing in the Stream**

The aim of the GI analysis conducted in this study using our integrated model was to examine the potential for intense, localized, single GI-type scenarios to influence DIN uptake in Meadow Creek. In general, the GI scenarios that were implemented at subbasin 1 were the most effective at increasing nitrogen uptake rates in the stream. This can be largely attributed to subbasin 1 being the most upstream and largest subbasin while having one of the greatest potentials for GI implementation. Other GI scenarios that induced notable changes to the simulated stream ecosystem processes include raingardens and impervious surface conversion at subbasins 5 and 7, which increased Net DIN uptake most significantly at zone 3. All increases in net uptake were due to increased denitrification stemming from increased DIN concentrations from infiltration-based GI types.

The vast majority of raingarden and impervious conversion scenarios led to an increase in DIN concentrations and export from our watershed. This is due to the calibration of our SWMM water quality model, which set groundwater concentrations to be significantly greater than runoff concentrations which is in line with observations at Meadow Creek (see figures C1 and C2 in appendix C). Our parameterization of the SWMM water quality model resulted in higher DIN concentrations and input of N into the stream when infiltration-based GI scenarios were implemented. The increases in baseflow flow and average benthic area as a result of the infiltration-based GI-types increased DIN uptake in upper Meadow Creek, but this increase in uptake was not enough to offset the estimated increase in N input into the stream as a result of increased, higher concentrated, groundwater flow. These simulation results would likely be observed at other locations that are observed to have a negative concentration vs. discharge relationship and suggests that watershed export of N may be increased as a result of GI

implementation in areas where there are appreciable DIN sources within the aquifer. In these cases, our results suggest that commercial green roofs are a better option for reducing DIN, in the stream compared to rain gardens and impervious surface conversion because they do not increase groundwater flow into the stream, although they are not known for treating pollution as well as the other GI types.

Results from this study indicate that implementing infiltration-based GI can unintentionally lead to increased DIN concentrations and stream export, contrary to typical expectations in watershed management practices if subsurface sources of DIN are not controlled. For instance, the runoff reduction method employed in Virginia emphasizes using infiltration-based GI for water quality improvement (Virginia, 2011). However, this study highlights that intensive GI implementation should proceed cautiously, as it may not yield positive outcomes for urban water quality. To enhance confidence in this conclusion, it's imperative to refine the water quality modules of the integrated model. SWMM is the standard model for modeling urban GI impacts on runoff in the U.S. but the current binary SWMM water quality module (event mean concentration vs. groundwater concentrations calibrated to land uses) may oversimplify N concentration simulations in the stream. In addition to its inability to model karst conditions within the aquifer, SWMM lacks the capacity to consider varying concentrations resulting from different flow conditions and antecedent dry periods. Additionally, SWMM does not incorporate denitrification and uptake processes occurring within GI, which can impact N concentrations in infiltrated runoff. As noted in the previous chapter of this dissertation, riparian canopy, and the floodplain function as significant sinks for urban DIN, factors not currently integrated into the model. Addressing these aspects would bolster the model's accuracy and reliability in assessing water quality impacts.

Even though the infiltration-based GI-type scenarios were estimated to increase DIN export, which may very well be an accurate estimation if there are appreciable DIN sources within the aquifer, our case-study results do not necessarily suggest that GI implementation is a bad idea if other benefits of GI are considered. For example, the infiltration-based GI did significantly reduce peak flows in the stream and may reduce erosion and sedimentation. Figure 4-15 shows an example of how each of the GI scenarios implemented at subbasin 1 could reduce peak flow during storms at zone 1, with impervious conversion showing the most reduction. Additionally, there may be social benefits to GI implementation which are not considered in this case-study.

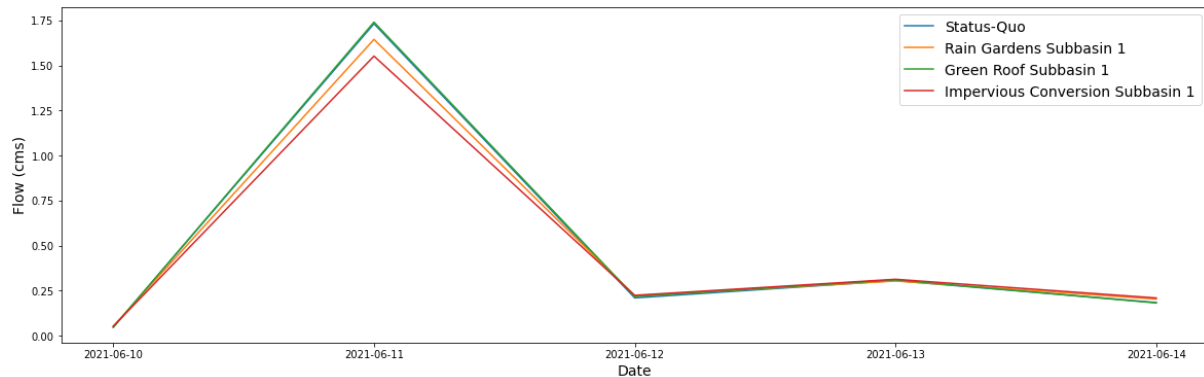


**Figure 4-15:** Hydrograph for stormflow and post-stormflow illustrating the impact of GI scenarios at subbasin 1 on peak flow within zone reach 1. Note that green roofs do not appear to be the best option for peak flow reduction but may be best for reducing DIN input into the stream.

## 4.4 Conclusions

In this study, we developed and tested an integrated watershed-channel hydraulic stream-ecosystem model and packaged it into a single open-source python notebook. The integrated model is a novel coupling of a local Stormwater Management Model (SWMM), a Hydrologic Engineering Center’s River Analysis System (HEC-RAS) model, as well as modules from the Stream Model Based on Spiraling and Ecological Stoichiometry Specific Fluxes (STOICMOD) and Small Streams Hydro Biogeochemistry Simulator (SSHBS) as the stream ecosystem model.

Although the calibration and validation of the integrated model could be improved given a longer study period and increased frequency of in-stream nutrient concentration sampling, simulation results suggest that the model could be valuable to those studying the potential relationship between benthic ecosystem processes, GI implementation, and DIN uptake in an urban stream. Using the integrated model, we simulated denitrification, algal uptake, immobilization, and mineralization as well as standing stocks of benthic detritus and algae mass at various locations along an urban stream. Simulation results show for our case-study area that: 1) Roughly 0.86% of the DIN that entered the stream from the watershed was removed from the water column under the status-quo and all GI-type scenarios, indicating no significant changes in DIN retention as a result of GI implementation; 2) That stream reach zones with lower leaf-litter and benthic detritus input resulted in lower mineralization rates and higher Net DIN uptake rates. 3) Watersheds with higher groundwater N concentrations relative to surface runoff will yield a net increase in the export of DIN with the implementation of infiltration-based GI. 4) The major stream ecosystem changes that impacted net DIN uptake was increased N concentrations during baseflow periods, which increased simulated denitrification rates in the stream. 5) More upstream, larger subbasins, with greater feasible areas for GI implementation have the greatest potential to influence DIN uptake and other stream ecosystem processes while smaller more impervious subbasins may have more influence at lower levels of implementation.

#### **4.5 Data Availability Statement**

The data that support the findings of this study are openly available in GITHUB at URL: <https://github.com/rsh6pb/Integrated-Model-Data>. The integrated model code and input data as well as a user's manual are available on GITHUB also at URL: <https://github.com/rsh6pb/SHRSE-Integrated-Model>.

## 4.6 Chapter 4 Works Cited

- Albemarle County. (2023). *Albemarle County Local TMDL Action Plan : 22902(434)*.
- Alexander, R. B., Böhlke, J. K., Boyer, E. W., David, M. B., Harvey, J. W., Mulholland, P. J., Seitzinger, S. P., Tobias, C. R., Tonitto, C., & Wollheim, W. M. (2009). Dynamic modeling of nitrogen losses in river networks unravels the coupled effects of hydrological and biogeochemical processes. *Biogeochemistry*, 93(1–2), 91–116. <https://doi.org/10.1007/s10533-008-9274-8>
- Anim, D. O., & Banahene, P. (2021). Urbanization and stream ecosystems: The role of flow hydraulics towards an improved understanding in addressing urban stream degradation. *Environmental Reviews*, 29(3), 401–414. <https://doi.org/10.1139/er-2020-0063>
- Baulch, H. M., Stanley, E. H., & Bernhardt, E. S. (2011). Can algal uptake stop NO<sub>3</sub>- pollution? *Nature*, 477(7366), 9–10. <https://doi.org/10.1038/nature10418>
- Bell, C. D., Tague, C. L., & McMillan, S. K. (2017). A model of hydrology and water quality for stormwater control measures. *Environmental Modelling and Software*, 95, 29–47. <https://doi.org/10.1016/j.envsoft.2017.05.007>
- Bernhardt, E. S., Band, L. E., Walsh, C. J., & Berke, P. E. (2008). Understanding, managing, and minimizing urban impacts on surface water nitrogen loading. In *Annals of the New York Academy of Sciences* (Vol. 1134, pp. 61–96). Blackwell Publishing Inc. <https://doi.org/10.1196/annals.1439.014>
- Bhaskar, A. S., Welty, C., Maxwell, R. M., & Miller, A. J. (2015). Untangling the effects of urban development on subsurface storage in Baltimore. *Water Resources Research*, 51(2), 1158–1181. <https://doi.org/10.1002/2014WR016039>.Received
- Bonneau, J., Fletcher, T. D., Costelloe, J. F., & Burns, M. J. (2017). Stormwater infiltration and the ‘urban karst’ – A review. *Journal of Hydrology*, 552, 141–150. <https://doi.org/10.1016/j.jhydrol.2017.06.043>
- Boston, H. L., & Hill, W. R. (1991). *Photosynthesis-light relations of stream periphyton communities*. 36(4), 644–656.
- Bouwman, A. F., Bierkens, M. F. P., Griffioen, J., Hefting, M. M., Middelburg, J. J., Middelkoop, H., & Slomp, C. P. (2013). Nutrient dynamics, transfer and retention along the aquatic continuum from land to ocean: Towards integration of ecological and biogeochemical models. *Biogeosciences*, 10(1), 1–23. <https://doi.org/10.5194/bg-10-1-2013>
- Brumley Jessica, Marks Christopher, Lowrance Richard, Huang Junqi, Ross Randall, Acree Steven, Beak Douglas, Chau Alexis, & Richardson Cassie. (2018). *The Influence of Green Infrastructure Practices on Groundwater Quality: The State of the Science*. August. [www.epa.gov/research](http://www.epa.gov/research)
- Charlottesville. (2019). *Chesapeake Bay TMDL Phase II Action Plan*.
- Chesapeake Bay Program. (2023a). *Chesapeake Bay Watershed Agreement*. Chesapeake Bay. <https://www.chesapeakebay.net/what/what-guides-us/watershed-agreement>

- Chesapeake Bay Program. (2023b). *Modeling*. Chesapeake Bay.  
<https://www.chesapeakebay.net/what/what-guides-us/watershed-agreement>
- Cho, L., Graham, M., Frisbee, D., & Frisbee, D. (2014). *Meadow Creek Stream Restoration - Methodology for Landscape Performance Benefits*.  
<https://www.landscapeperformance.org/case-study-briefs/meadow-creek-stream-restoration>
- Claessens, L., & Tague, C. L. (2009). Transport-based method for estimating in-stream nitrogen uptake at ambient concentration from nutrient addition experiments. *Limnology and Oceanography: Methods*, 7(DEC), 811–822. <https://doi.org/10.4319/lom.2009.7.811>
- Coville, Robert; Endreny, Ted; Nowak, David J. 2020. Modeling the impact of urban trees on hydrology. In: Levia, D.; Carlyle-Moses, D.; Iida, S.; Michalzik, B.; Nanko, K.; Tischer, A., eds. *Forest-water interactions*. Cham, Switzerland: Springer: 459-487. Chapter 19.
- de Azevedo Torrellas, E. (2021). *Spatial and Temporal Patterns of Nutrient Loading, Nutrient Sourcing, and Stream Metabolism in Restored and Unrestored Urban Stream Reaches of Charlottesville, Virginia* (thesis). University of Virginia, Charlottesville .
- Doyle, M. W. (2005). Incorporating hydrologic variability into nutrient spiraling. *Journal of Geophysical Research*, 110(G1), 1–11. <https://doi.org/10.1029/2005jg000015>
- Duan, S., Kaushal, S. S., Groffman, P. M., Band, L. E., & Belt, K. T. (2012). *Phosphorus export across an urban to rural gradient in the Chesapeake Bay watershed*. 117, 1–12.  
<https://doi.org/10.1029/2011JG001782>
- Duan, S., Kaushal, S. S., Rosenfeldt, E. J., Huang, J., & Murthy, S. (2021). Changes in concentrations and source of nitrogen along the Potomac River with watershed land use. *Applied Geochemistry*, 131(2021), 105006-.
- Ensign, S. H., & Doyle, M. W. (2006). Nutrient spiraling in streams and river networks. *Journal of Geophysical Research: Biogeosciences*, 111(4), 1–13.  
<https://doi.org/10.1029/2005JG000114>
- Fletcher, T. D., Andrieu, H., & Hamel, P. (2013). Understanding, management and modelling of urban hydrology and its consequences for receiving waters: A state of the art. *Advances in Water Resources*, 51, 261–279. <https://doi.org/10.1016/j.advwatres.2012.09.001>
- Gold, A. C., Thompson, S. P., & Piehler, M. F. (2019). Nitrogen cycling processes within stormwater control measures: A review and call for research. In *Water Research* (Vol. 149, pp. 578–587). Elsevier Ltd. <https://doi.org/10.1016/j.watres.2018.10.036>
- Grimm, N. B., Gergel, S. E., McDowell, W. H., Boyer, E. W., Dent, C. L., Groffman, P., Hart, S. C., Harvey, J., Johnston, C., Mayorga, E., McClain, M. E., & Pinay, G. (2003). Merging aquatic and terrestrial perspectives of nutrient biogeochemistry. *Oecologia*, 137(4), 485–501. <https://doi.org/10.1007/s00442-003-1382-5>
- Hobbie, S. E., Finlay, J. C., Janke, B. D., Nidzgorski, D. A., Millet, D. B., & Baker, L. A.

(2017). Contrasting nitrogen and phosphorus budgets in urban watersheds and implications for managing urban water pollution. *Proceedings of the National Academy of Sciences of the United States of America*, 114(16), 4177–4182.  
<https://doi.org/10.1073/pnas.1618536114>

i-Tree. (2020). *i-Tree Hydro*. <https://www.itreetools.org/tools/hydro>

Jan, A., Coon, E. T., & Painter, S. L. (2021). Toward more mechanistic representations of biogeochemical processes in river networks: Implementation and demonstration of a multiscale model. *Environmental Modelling and Software*, 145(August), 105166.  
<https://doi.org/10.1016/j.envsoft.2021.105166>

Janke, B. D., Finlay, J. C., Hobbie, S. E., Baker, L. A., Sterner, R. W., Nidzgorski, D., & Wilson, B. N. (2014). Contrasting influences of stormflow and baseflow pathways on nitrogen and phosphorus export from an urban watershed. *Biogeochemistry*, 121(1), 209–228.  
<https://doi.org/10.1007/s10533-013-9926-1>

Jansson, M., Leonardson, L., & Fejes, J. (1994). Denitrification and nitrogen retention in a farmland stream in southern Sweden. *Ambio*, 23(6), 326–331.

Kaushal, S. S., Groffman, P. M., Band, L. E., Shields, C. A., Morgan, R. P., Palmer, M. A., Belt, K. T., Swan, C. M., Findlay, S. E. G., & Fisher, G. T. (2008). Interaction between urbanization and climate variability amplifies watershed nitrate export in Maryland. *Environmental Science and Technology*, 42(16), 5872–5878.  
<https://doi.org/10.1021/es800264f>

Kemp, W. M., Boynton, W. R., Adolf, J. E., Boesch, D. F., Boicourt, W. C., Brush, G., Cornwell, J. C., Fisher, T. R., Glibert, P. M., Hagy, J. D., Harding, L. W., Houde, E. D., Kimmel, D. G., Miller, W. D., Newell, R. I. E., Roman, M. R., Smith, E. M., & Stevenson, J. C. (2005). Eutrophication of Chesapeake Bay: Historical trends and ecological interactions. *Marine Ecology Progress Series*, 303, 1–29.  
<https://doi.org/10.3354/meps303001>

Kreiling, R. M., Richardson, W. B., Bartsch, L. A., Thoms, M. C., & Christensen, V. G. (2019). Denitrification in the river network of a mixed land use watershed: unpacking the complexities. *Biogeochemistry*, 143(3), 327–346. <https://doi.org/10.1007/s10533-019-00565-6>

Lin, L., Reisinger, A. J., Rosi, E. J., Groffman, P. M., & Band, L. E. (2021). Evaluating Instream Restoration Effectiveness in Reducing Nitrogen Export from an Urban Catchment with a Data-Model Approach. *Journal of the American Water Resources Association*, 57(3), 449–473. <https://doi.org/10.1111/1752-1688.12922>

Lin, L., & Webster, J. R. (2014). Detritus decomposition and nutrient dynamics in a forested headwater stream. *Ecological Modelling*, 293, 58–68.

<https://doi.org/10.1016/j.ecolmodel.2013.12.013>

Marcé, R., & Armengol, J. (2009). Modeling nutrient in-stream processes at the watershed scale using Nutrient Spiralling metrics. *Hydrology and Earth System Sciences*, 13(7), 953–967. <https://doi.org/10.5194/hess-13-953-2009>

Meyer, J. L., Paul, M. J., & Taulbee, W. K. (2005). Stream ecosystem function in urbanizing landscapes. *Journal of the North American Benthological Society*, 24(3), 602–612. <https://doi.org/10.1899/04-021.1>

Miles, B., & Band, L. E. (2015). Green infrastructure stormwater management at the watershed scale: Urban variable source area and watershed capacitance. *Hydrological Processes*, 29(9), 2268–2274. <https://doi.org/10.1002/hyp.10448>

Mulholland, P. J., Helton, A. M., Poole, G. C., Hall, R. O., Hamilton, S. K., Peterson, B. J., Tank, J. L., Ashkenas, L. R., Cooper, L. W., Dahm, C. N., Dodds, W. K., Findlay, S. E. G., Gregory, S. V., Grimm, N. B., Johnson, S. L., McDowell, W. H., Meyer, J. L., Valett, H. M., Webster, J. R., ... Thomas, S. M. (2008). Stream denitrification across biomes and its response to anthropogenic nitrate loading. *Nature*, 452(7184), 202–205. <https://doi.org/10.1038/nature06686>

Niazi, M., Nietch, C., Maghrebi, M., Jackson, N., Bennett, B. R., Tryby, M., & Massoudieh, A. (2017). Storm Water Management Model: Performance Review and Gap Analysis. In *Journal of Sustainable Water in the Built Environment* (Vol. 3, Issue 2). <https://doi.org/10.1061/jswbay.0000817>

Palmer, M., & Ruhi, A. (2019). Linkages between flow regime, biota, and ecosystem processes: Implications for river restoration. *Science*, 365(6459). <https://doi.org/10.1126/science.aaw2087>

Pataki, D. E., Carreiro, M. M., Cherrier, J., Grulke, N. E., Jennings, V., Pincetl, S., Pouyat, R. V., & Whitlow, T. H. (2011). Coupling biogeochemical cycles in urban environments: ecosystem services, green solutions. In *Ecology and the Environment* (Vol. 9, Issue 1).

Payne, E. G. I., Fletcher, T. D., Russell, D. G., Grace, M. R., Cavagnaro, T. R., Evrard, V., Deletic, A., Hatt, B. E., & Cook, P. L. M. (2014). Temporary storage or permanent removal? The division of nitrogen between biotic assimilation and denitrification in stormwater biofiltration systems. *PLoS ONE*, 9(3). <https://doi.org/10.1371/journal.pone.0090890>

Pearce, N. J. T., Parsons, C. T., Pomfret, S. M., & Yates, A. G. (2022). Periphyton Phosphorus Uptake in Response to Dynamic Concentrations in Streams: Assimilation and Changes to Intracellular Speciation. *Environmental Science and Technology*. <https://doi.org/10.1021/acs.est.2c06285>

Pind, A., Risgaard-Petersen, N., & Revsbech, N. P. (1997). Denitrification and microphytobenthic NO<sub>3</sub> consumption in a Danish lowland stream: Diurnal and seasonal variation. *Aquatic Microbial Ecology*, 12(3), 275–284. <https://doi.org/10.3354/ame012275>

- Pitt, R., Clark, S. E., Parmer, K., & Field, R. (2023). *Groundwater contamination from stormwater infiltration*. Routledge.
- Prasad, M. B. K., Maddox, M. C., Sood, A., Kaushal, S., & Murtugudde, R. (2014). Nutrients, chlorophyll and biotic metrics in the Rappahannock River estuary: Implications of urbanisation in the Chesapeake Bay watershed, USA. *Marine and Freshwater Research*, 65(6), 475–485. <https://doi.org/10.1071/MF12351>
- Sahu, Mukul, K., Shwetha, H. R., & Dwarakasih, G. . (2023). State-of-the-art hydrological models and application of the HEC-HMS model: a review. *Modeling Earth Systems and Environment*. <https://doi.org/https://doi.org/10.1007/s40808-023-01704-7>
- Smil, V. (2000). Phosphorus in the Environment : Natural Flows and Human Interferences. *Annu. Rev. Energy Environ.*, 53–88.
- Tague, C. L., & Band, L. E. (2004). RHESSys: Regional Hydro-Ecologic Simulation System-An Object-Oriented Approach to Spatially Distributed Modeling of Carbon, Water, and Nutrient Cycling. In *Earth Interactions* (Vol. 8, Issue 19). Paper No. <http://earthinteractions.org>
- U.S. Army Corp of Engineers (USACE) (2023). *HEC-HMS*. <https://www.hec.usace.army.mil/software/hec-hms/>
- USEPA. (2023a). *Restoration of the Chesapeake Bay*. EPA. <https://www.epa.gov/restoration-chesapeake-bay>
- USEPA. (2023b). *Storm Water Management Model (SWMM)*. EPA. <https://www.epa.gov/water-research/storm-water-management-model-swmm>
- Walsh, C. J., Fletcher, T. D., & Ladson, A. R. (2005). Stream restoration in urban catchments through redesigning stormwater systems: Looking to the catchment to save the stream. *Journal of the North American Benthological Society*, 24(3), 690–705. <https://doi.org/10.1899/04-020.1>
- Walsh, C. J., Roy, A. H., Feminella, J. W., Cottingham, P. D., Groffman, P. M., & Morgan, R. P. (2005). The urban stream syndrome: Current knowledge and the search for a cure. *Journal of the North American Benthological Society*, 24(3), 706–723. <https://doi.org/10.1899/04-028.1>
- Webster, J. R., Mulholland, P. J., Tank, J. L., Valett, H. M., Dodds, W. K., Peterson, B. J., Bowden, W. B., Dahm, C. N., Findlay, S., Gregory, S. V., Grimm, N. B., Hamilton, S. K., Johnson, S. L., Martí, E., McDowell, W. H., Meyer, J. L., Morrall, D. D., Thomas, S. A., & Wollheim, W. M. (2003). Factors affecting ammonium uptake in streams - An inter-biome perspective. *Freshwater Biology*, 48(8), 1329–1352. <https://doi.org/10.1046/j.1365-2427.2003.01094.x>
- Webster, J. R., Newbold, J. D., & Lin, L. (2016). Nutrient Spiraling and Transport in Streams: The Importance of In-Stream Biological Processes to Nutrient Dynamics in Streams. *The*

Importance of In-Stream Biological Processes to Nutrient Dynamics in Streams. In *Stream Ecosystems in a Changing Environment*. <https://doi.org/10.1016/B978-0-12-405890-3.00005-1>

Ye, S., Covino, T. P., Sivapalan, M., Basu, N. B., Li, H. Y., & Wang, S. W. (2012). Dissolved nutrient retention dynamics in river networks: A modeling investigation of transient flows and scale effects. *Water Resources Research*, *48*(6), 1–18. <https://doi.org/10.1029/2011WR010508>

Zhang, R., Band, L. E., Groffman, P. M., Suchy, A. K., Duncan, J. M., & Gold, A. J. (2023). Simulation of spatially distributed sources , transport , and transformation of nitrogen from fertilization and septic system in an exurban watershed. *Hydrology and Earth System Sciences*, November, 1–28.

## **Chapter 5: Concluding Remarks**

### **5.0 Dissertation Conclusions and Future Research Opportunities**

The expansion of impermeable urban development has amplified issues such as increased stormwater runoff, heightened flow velocities, and elevated nutrient levels in local and regional streams. These factors have led to the deterioration of natural channels and receiving water bodies, marked by processes like erosion, scouring, sediment buildup, eutrophication, and impaired water quality. To address these challenges, engineering measures like stormwater green infrastructure (GI) and stream restoration are recommended. These interventions have the potential to mitigate the degradation of local streams and downstream water bodies. From a practical and cost efficiency perspective, it is often advantageous to assess the potential impacts of various GI plans and stream restoration designs before their actual implementation. The central challenge tackled in this dissertation pertains to the fragmented and predominantly technocratic approaches adopted in watershed restoration modeling endeavors.

Typically, different groups of experts, such as urban managers, geomorphologists, and stream ecologists, employ modeling tools within their specific areas of expertise, resulting in limited assessments of the benefits. This siloed approach restricts the ability of modern GI and stream restoration modeling to fully estimate the social and ecological advantages and risks comprehensively. As shown in the preceding chapters, contemporary modeling solutions necessitate the integration of various models to achieve a holistic analysis of the overall watershed benefits that can arise from engineered landscape and in-stream interventions. The results of this dissertation indicate that the use of more comprehensive models could offer valuable and specific insights into the potential consequences of urban green infrastructure (GI)

and stream restoration projects. These findings also highlight the possibility of improving integrated GI and stream restoration models in the future.

The second chapter and first project of this dissertation emphasizes the importance of defining "optimal" GI plans in a way that incorporates more social objectives that are aligned with public sentiment and preferences in combination with hydrologic and hydraulic goals. Without this expansion of consideration, GI plans deemed optimal, strictly from hydrologic and economic perspectives, may not necessarily equitably benefit communities. The first study of this dissertation shows that GI optimization algorithms are highly adaptable, as seen in the integration of the LID/GI-Social Vulnerability Index (SVI) correlation objective. This integration demonstrates the potential to simultaneously achieve runoff management goals, increase GI implementation in marginalized areas, and explore the interplay between hydrologic and equity objectives. Overall, the analysis in chapter two underscores that GI planning is inherently a social process, and the most effective and acceptable plans should incorporate social goals. Future research that utilizes similar metrics as the LID/GI-SVI correlation objective should engage the community in an iterative process to determine the most acceptable and quantifiable social equity indicators for their specific area, as suggested by Fletcher et al. (2022).

While GI is frequently hailed as a crucial management strategy for enhancing in-stream ecosystem conditions, the focus is often disproportionately on the physical engineering of stream channels towards more of natural channel design (NCD) or other designs that assume that geomorphic modification will necessarily result in ecosystem improvement. However, many stream restoration models that follow the NCD or other geomorphic design methods lack an analysis of potential impacts on in-stream nutrient reductions resulting from ecosystem processes. These benefits are often assumed without support from modeling results. The third

chapter of this dissertation introduces an adaptation of the Small Streams Hydro-Biogeochemistry Simulator (SSHBS). This model is used to assess changes in in-stream nitrogen uptake dynamics resulting from various configurations of riffles, pools, and meanders in an unrestored urban stream segment in Baltimore County. The study demonstrates the utility of this process-based model in replacing assumptions about how modified stream hydraulics affect in-stream ecosystem processes and nitrogen retention. Chapter three also underscores the importance of collaboration between geomorphologists and engineers, who study hydraulic changes in streams, and stream ecologists, who analyze stream metabolism and nutrient retention processes. To make process-based ecosystem models like SSHBS more accessible to stream restoration managers and integrated into restoration practices, comprehensive data collection efforts are essential for all potentially restorable urban streams. Where sufficient data exists, SSHBS can serve as a valuable tool for modelers to understand how enhanced benthic area, improved stream hydraulics, and various tree canopy conditions influence nitrogen uptake in restored streams. Furthermore, restoration evaluations using SSHBS offer distinct advantages over field-based studies that include testing a variety of restoration features and benthic area changes under the same boundary conditions at a single reach.

Chapter four serves as a bridge between urban green infrastructure (GI) and in-stream ecosystem process modeling, showcasing the practical utility of integrated watershed-hydraulic-stream ecosystem models for watershed managers. However, it also highlights the challenges and limitations inherent in developing and using such models using modern techniques. Building and utilizing integrated models currently necessitate the coupling of separate models, which may not fully capture the complex biophysical and biogeochemical dynamics within urban watersheds. Future studies adopting integrated models, like the one discussed in chapter four, should

incorporate more detailed water quality modules for terrestrial environments. These modules should account for nutrient uptake and removal processes within GI and the aquifer. Calibrating an integrated model requires extensive, high-frequency data collection that is not typical of most urban locations. Despite these challenges, Chapter four illustrates the capabilities and novel analyses enabled by integrated models. They can estimate the relative contributions of terrestrial and stream environments to nutrient export from urban watersheds. While substantial investments are made in stream restorations, this research, along with other studies, reveals that much of the nutrient export from a watershed is influenced by terrestrial factors beyond the control of in-stream ecosystem processes. Moreover, Chapter four suggests that intensive use of infiltration-based GI may inadvertently increase nitrogen export from a watershed, an unintended consequence of GI implementation. Integrated models can also illuminate the dominant in-stream processes influenced by GI and other landscape decisions, as well as pinpoint the most influential locations for GI implementation and the necessary extent to achieve meaningful impacts on in-stream processes.

This dissertation explores advanced methods for modeling Green Infrastructure (GI) and stream restoration, integrating urban social vulnerability and stream ecosystem dynamics into urban watershed management. These approaches aim to improve existing standards in urban GI and stream restoration, offering more holistic strategies adaptable to diverse study areas. The goal is to transcend limitations of current practices and achieve a comprehensive understanding and enhanced management of urban water environments.

## Appendix A

This document is a summary of the calibration and validation results for upper Meadow Creek watershed. Observed (Obs) and simulated (Sim) rainfall, peak streamflow, and total runoff export are tabulated in table A1 along with the coefficient of determination ( $R^2$ ) and the Nash-Sutcliffe Efficiency (NSE) for each event. Figures A1 to A6 are the rainfall-streamflow hydrographs for each of the tabulated events.

**Table A-1:** Summary of individual storm event calibration and validation results for chapter 2.

	Rainfall		Peak Streamflow		Total Runoff Export		$R^2$	NSE
	Event	Depth	Obs	Sim	Obs	Sim		
Calibration	1	27.2	12.1	16.1	110718.9	140055.1	0.96	0.84
Validation	1	11.7	8.3	5.4	52641.02	58814.09	0.79	0.74
	2	35.6	26.0	27.2	206571.4	195131.4	0.92	0.92
	3	19.1	7.8	11.5	64732.31	96673.72	0.93	0.61
	4	41.7	17.9	16.0	169929.4	210450.8	0.81	0.78
	5	66.0	55.4	58.8	555859.7	342350.7	0.79	0.75

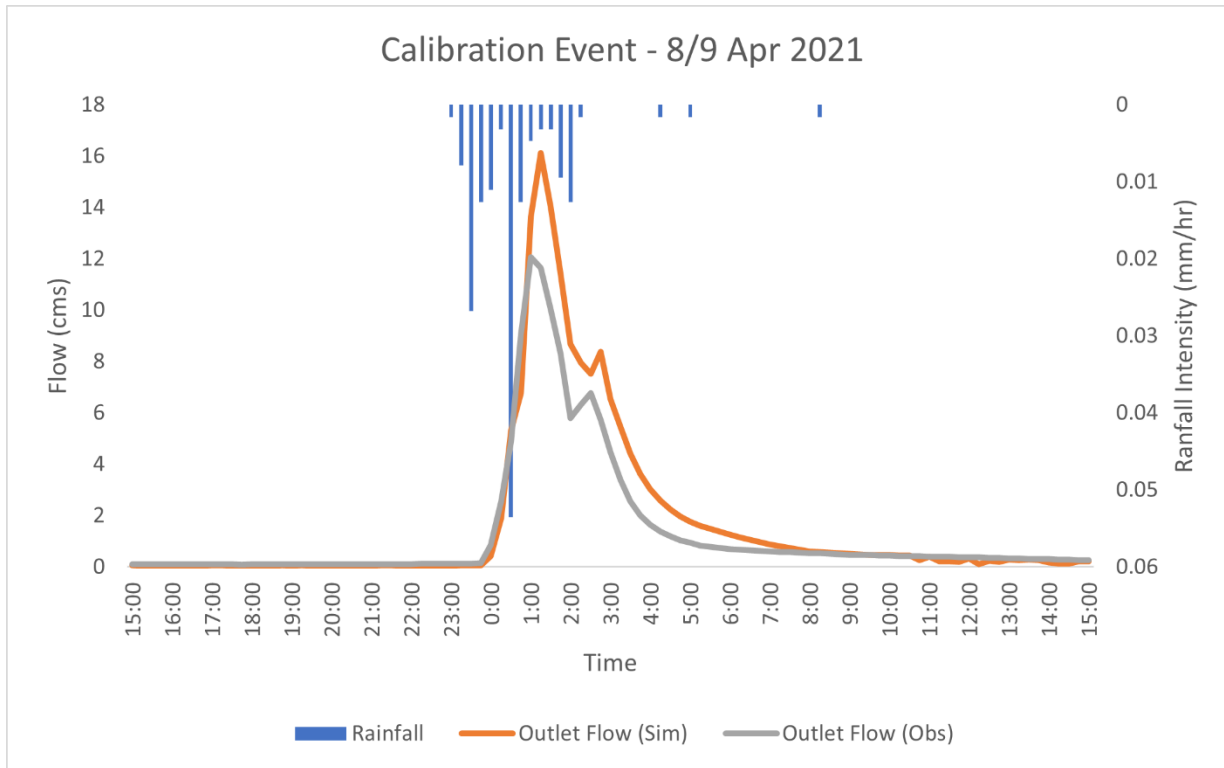


**Figure A-1:** Hydrograph and hyetograph for 8/9 April 2021 calibration storm event.

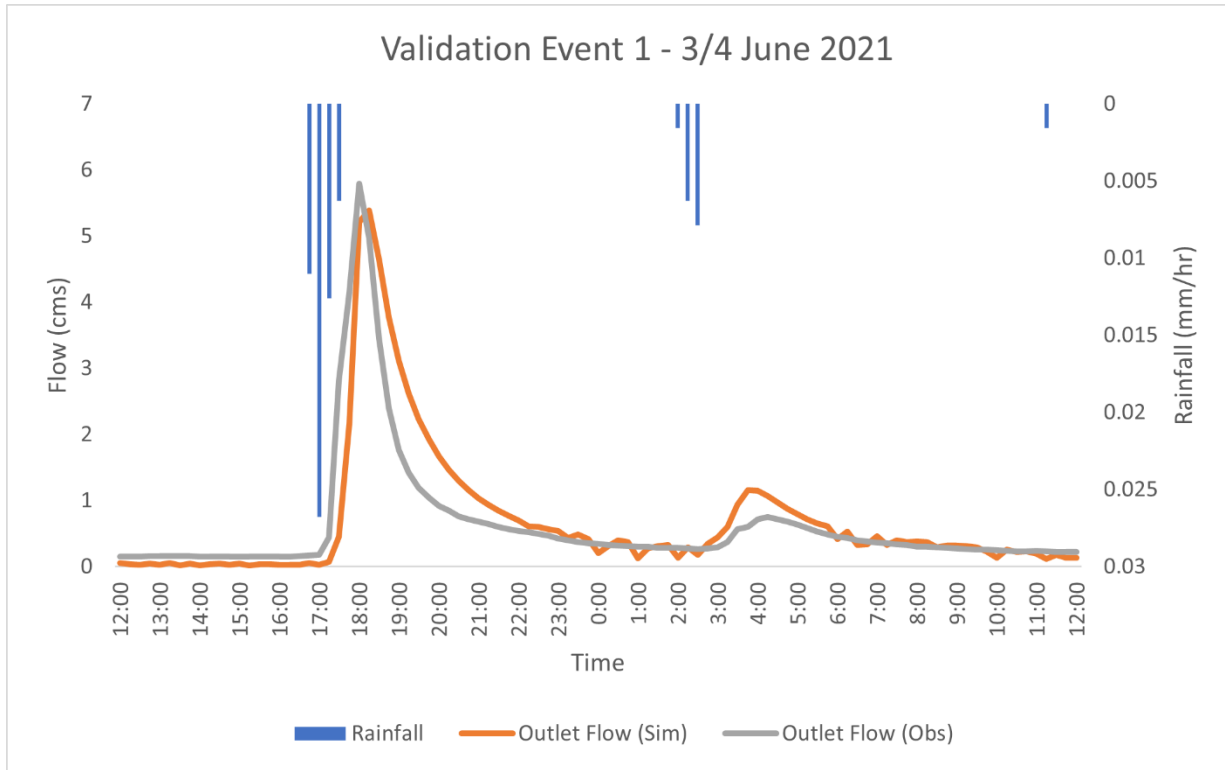


**Figure A-2:** Hydrograph and hyetograph for 3/4 June 2021 validation storm event 1.

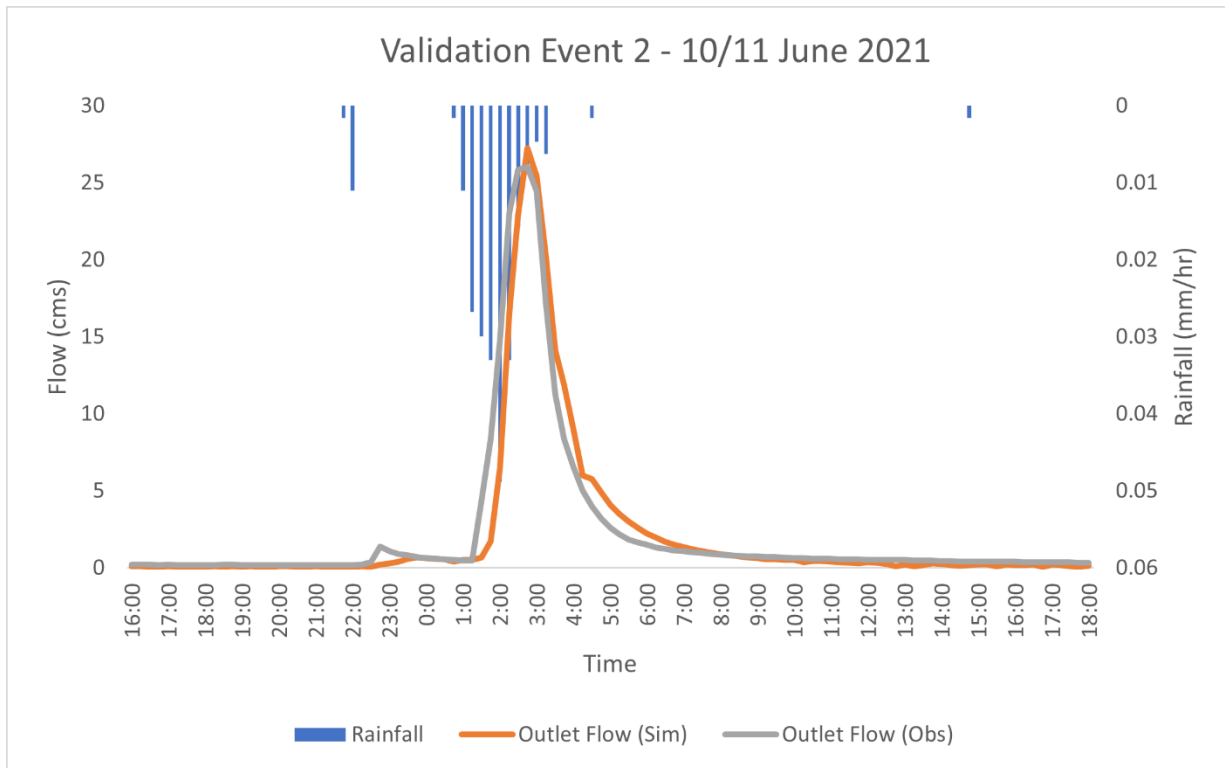


**Figure A-3:** Hydrograph and hyetograph for 10/11 June 2021 validation storm event 2.

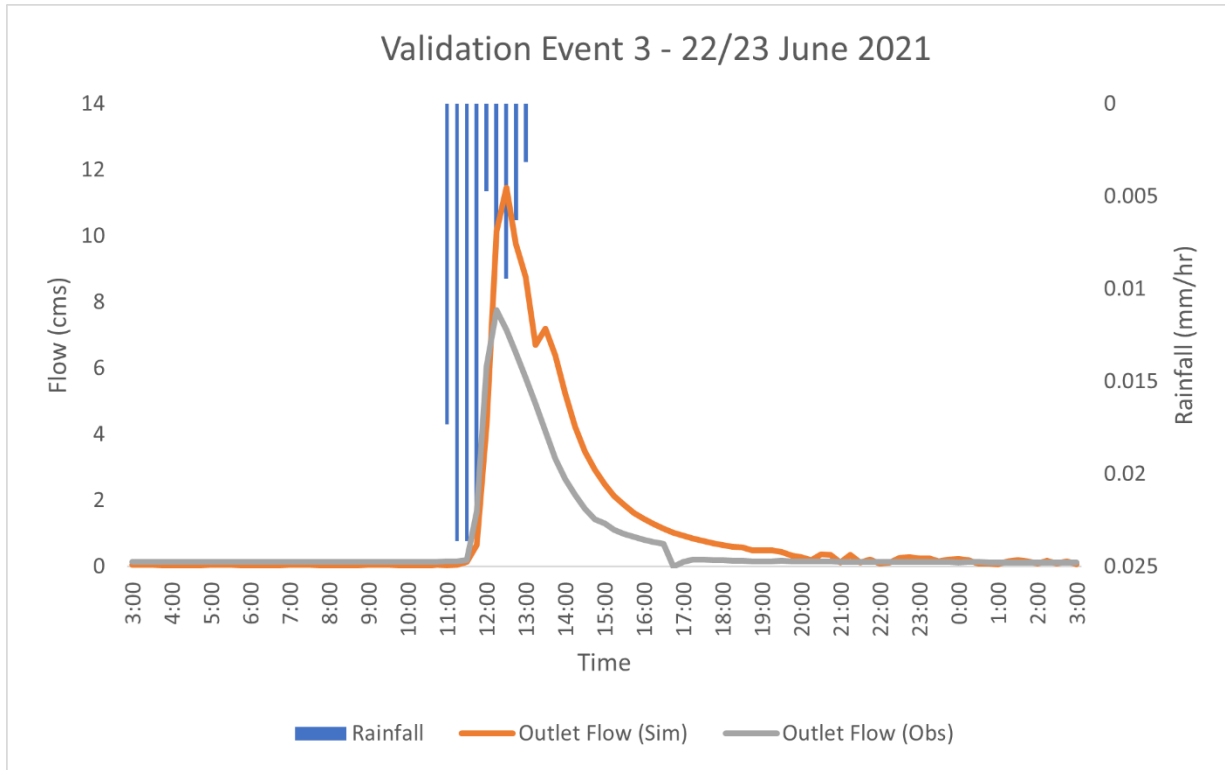


**Figure A-4:** Hydrograph and hyetograph for 22/23 June 2021 validation storm event 3.

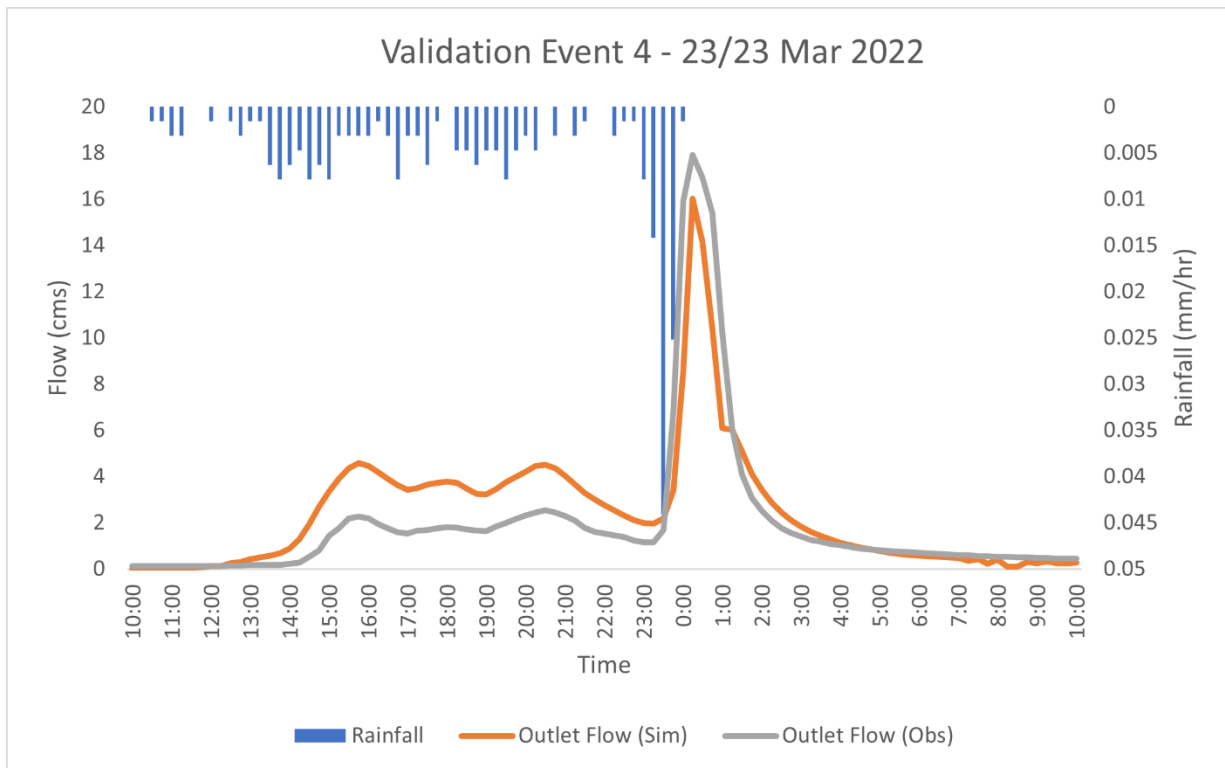


**Figure A-5:** Hydrograph and hyetograph for 22/23 Mar 2022 validation storm event 4.

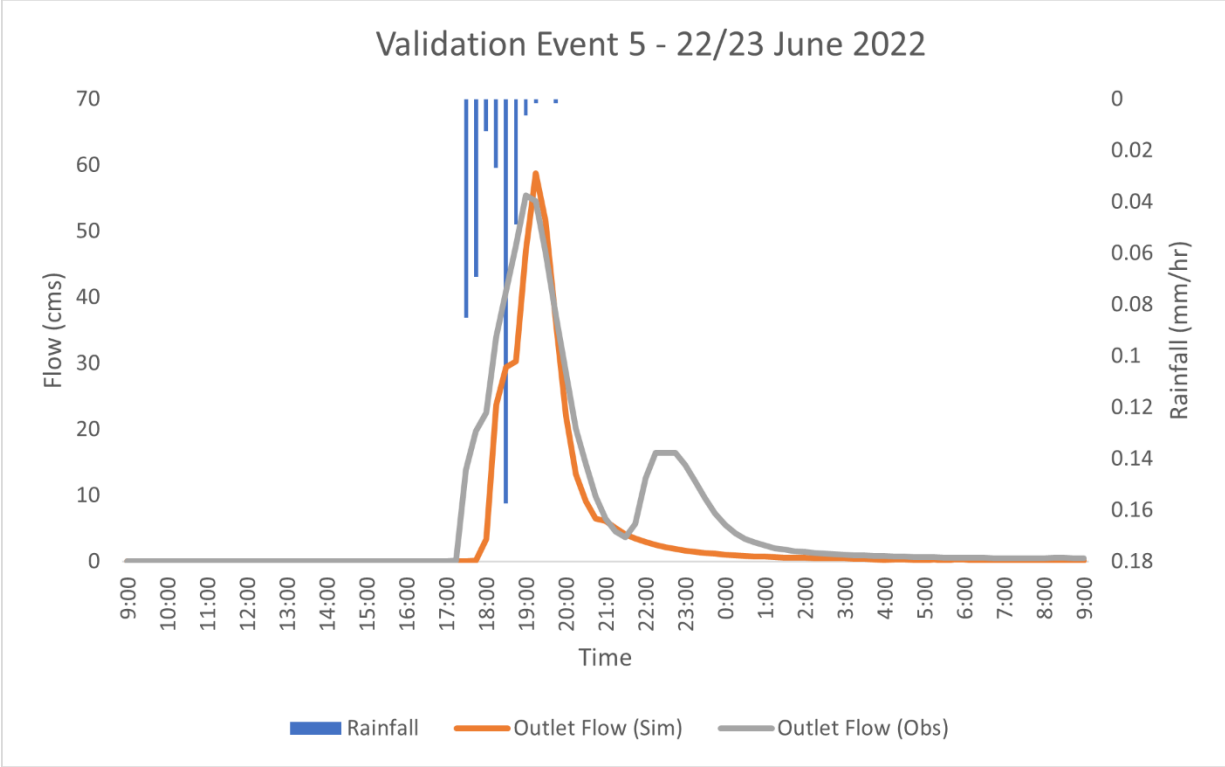


**Figure A-6:** Hydrograph and hyetograph for 22/23 June 2022 validation storm event 5.

## Appendix B

### Summary of Small Streams Hydro-Biogeochemistry Functions

Discharges and nutrient mass lateral inputs at any zone along the study stream are drainage area-weighted based on the observed downstream flow. Flow at each zone at a given time is calculated using the Manning's equation below:

$$Q_{i,t} = \frac{A_{i,t} \times R_{i,t}^{\frac{2}{3}} \times \sqrt{S_i}}{n_i} \quad (\text{B1})$$

where  $Q_{i,t}$  ( $\text{m}^3/\text{s}$ ) is drainage area-weighted discharge at zone  $i$  at time  $t$ .  $A_{i,t}$  ( $\text{m}^2$ ) and  $R_{i,t}$  ( $\text{m}$ ) are the cross-sectional area of the water column and the hydraulic radius in discharge zone  $i$  at time  $t$ ,  $S_i$  is the zone reach longitudinal slope, and  $n$  is the zone Manning's  $n$  roughness coefficient.

Zone volume ( $\text{m}^3$ ) is given by:

$$V_{i,t} = A_{i,t} \times L_i \quad (\text{B2})$$

where  $L_i$  ( $\text{m}$ ) is the length of each zone reach. The mass ( $M_{i,t}$ ) of nitrogen or phosphorus ( $\text{mg}$ ), concentrations ( $\text{mg}/\text{m}^3$ ) within the transient storage zone ( $C_{stor,i,t}$ ), and the zonal flux ( $F_{i,t}$ ) is computed, respectively as:

$$M_{col,i,t} = C_{col,i,t} \times V_{i,t} \quad (\text{B3})$$

$$C_{stor,i,t} = \frac{M_{stor,i,t}}{\tau_{i,t}} \quad (\text{B4})$$

$$F_{i,t} = \frac{Q_{i,t}}{V_{i,t}} \times M_{col,i,t} \quad (\text{B5})$$

where  $C_{col,i,t}$  and is zone concentrations in the water column.  $\tau_{it}$  is the zonal transient storage volume ( $\text{m}^3$ ) and is described in the supplemental information provided by Lin et. al (2021). The

changes in nutrient mass in the water column and transient storage zone over time are computed using equations B6 and B7.

$$\frac{\Delta S_{col,i,t}}{\Delta t} = F_{i-1,t} - F_{i,t} + S_{i,t} + \alpha \times V_{i,t} \times (C_{stor,i,t} - C_{col,i,t}) - \tau_{i,t} \times U_{col,i,t} \quad (B6)$$

$$\frac{\Delta S_{stor,i,t}}{\Delta t} = \alpha \times V_{i,t} \times \frac{A_{i,t}}{\tau_{i,t}} \times (C_{col,i,t} - C_{stor,i,t}) - \tau_{i,t} \times U_{stor,i,t} \quad (B7)$$

$\alpha$  is the channel storage exchange rate and  $U_{col,i,t}$  and  $U_{stor,i,t}$  are the water column and transient storage zone uptake functions which are further explained in the next subsection.

The zonal nutrient cycling functions represent the sum of algal uptake, denitrification, and mineralization. Algal uptake is modeled in SSHBS using a modified Michaelis-Menten equation: STOICMOD-SSHBS models algal uptake using a modified Michaelis-Menten equation:

$$AlgU_{X,i,t} = \frac{U_{max,X} \times C_{X,i,t}}{\kappa_{half,X} + C_{X,i,t}} \times AlgC_{i,t} \times g_s \times Q_{10f} \quad (B8)$$

$U_{max-X}$  is the maximum daily uptake of nutrient X (X = N or P) per carbon algal biomass (mgX/mgC/d),  $C_{X,i,t}$  is the water column concentration of N or P (mgX/m<sup>3</sup>) at reach cross-section i at time t,  $\kappa_{half-X}$  is the nutrient specific half-saturation constant for uptake (mgX/m<sup>3</sup>),  $AlgC_{i,t}$  (mgC/m<sup>2</sup>) is the standing crop of algal carbon biomass per benthic area at reach cross-section i at time t. The biomass limitation of Algal DINet primary production is computed as

$$g_s = \frac{1}{1 + (\kappa_s \times AlgC_{i,t})} \quad (B9)$$

$Q_{10f}$  is a function for the ecosystem process sensitivity to temperature (T):

$$Q_{10f} = 2^{\frac{T_{i,t} - 10}{10}} \quad (B10)$$

$K_s$  (mg/mgC) is the self-limitation coefficient. The magnitude of algal uptake is dependent on algal standing biomass (mgC/m<sup>2</sup>).

The potential algae biomass growth is a function of the maximum algae growth rate ( $G_{max}$ ) (d<sup>-1</sup>), the Light Response Function (LRF) developed by Webster et al. (2016) and available PAR ( $\mu\text{mol/m}^2 \text{ s}$ ) reaching the stream ecosystem.

$$G_L = G_{max} * LRF * PAR_{i,t} \quad (\text{B11})$$

Net primary production GPP adds to the standing crop of algal carbon as:

$$GPP_{i,t} = AlgC_{i,t} \times G_L \times g_s \times g_l \times Q_{10} \quad (\text{B12})$$

$$AlgC_{i,t} = AlgC_{i,t-1} + GPP_{i,t}$$

Nutrient uptake is stoichiometrically related to C:N and C:P ratios. The internal nutrient stores limit on net primary production (GPP) is:

$$g_l = \min \left[ 1 - \frac{Algal \text{ Cell } N:C \text{ Quota}}{Algal \text{ Cell } N:C}, 1 - \frac{Algal \text{ Cell } P:C \text{ Quota}}{Algal \text{ Cell } P:C} \right] \quad (\text{B13})$$

Where the algal Cell N:C Quota (molN/molC) and Algal Cell P:C Quota (molP/molC) are the N/C and P/C ratios that are necessary for algae subsistence which have been parameterized to be 0.0606 and 0.00377 section i.

Denitrification is modeled in SSHBS using equations 13- 17. If the column nitrate concentration is greater than the transient storage zone nitrate concentration, then:

$$\chi = C_{NO3,i,t}^b \times C_{NO3,i,t} \quad (\text{B14})$$

$$DenU_{stor,i,t} = 0.6 \times 10^a \chi_{stor} \quad (\text{B15})$$

$$DenU_{col,i,t} = 0.6 \times 10^a \chi_{col} \quad (B16)$$

The variables a and b are obtained from a log transformed relationship between nitrate concentration and uptake velocity and methods first described by Mulholland et. al (2008). When the column nitrate concentration is less than the transient storage zone nitrate concentration, the following relationships apply:

$$DenU_{stor,i,t} = \frac{10^a}{100} \times \chi_{stor} \quad (B17)$$

$$DenU_{col,i,t} = 0 \quad (B18)$$

Changes in zonal detritus mass ( $D_{benthic}$ ) that is available for benthic microbe decomposition are modeled from input detritus data as the difference between entrainment and deposition, which depend on zonal water velocity  $\vartheta$ , the benthic area BA, and a mass transfer coefficient  $V_f$ .

$$\frac{\Delta D_{benthic,i,t}}{\Delta t} = \frac{EF \times D_{benthic,i,t} + DF \times D_{col,i,t}}{BA_{i,t}} \quad (B19)$$

$$EF = \left( \frac{0.85}{\left( 1 + e^{-\left( \frac{\vartheta_{i,t} - 0.4}{0.06} \right)} \right)} \right)^{\frac{\Delta t}{24}} \quad (B20)$$

$$DF = 1 - e^{\left( \frac{-L_i \times BA_{i,t} \times V_f}{\vartheta_{i,t} \times V_{i,t}} \right)} \quad (B21)$$

In the SSHBS conceptual model, immobilizers are the group of microbial organisms that decompose benthic detritus for carbon C and sequester N and P from the water column in accordance with their subsistent C/N and C/P ratios, which are set to be 5 and 100 respectively.

The other group of benthic microbial organisms are miners, which obtain all their nutrients C, N, and P from benthic detritus. Decay of detritus C, N, and P are stoichiometrically related to microbial miner C/N and C/P ratios, which are set to be 15 and 1000, respectively, and excess N and P are mineralized by microbial miners and released into the water column. The death and mineralization of microbes and algae are modeled as linear functions of their respective standing crops and also result in nutrients being released back into the water column primarily in the form of  $\text{NH}_4$ . Other processes that change the N composition of the water column include nitrification and respiration which are described more fully by Lin et. al (2021) and Webster et. al (2016).

## Appendix C

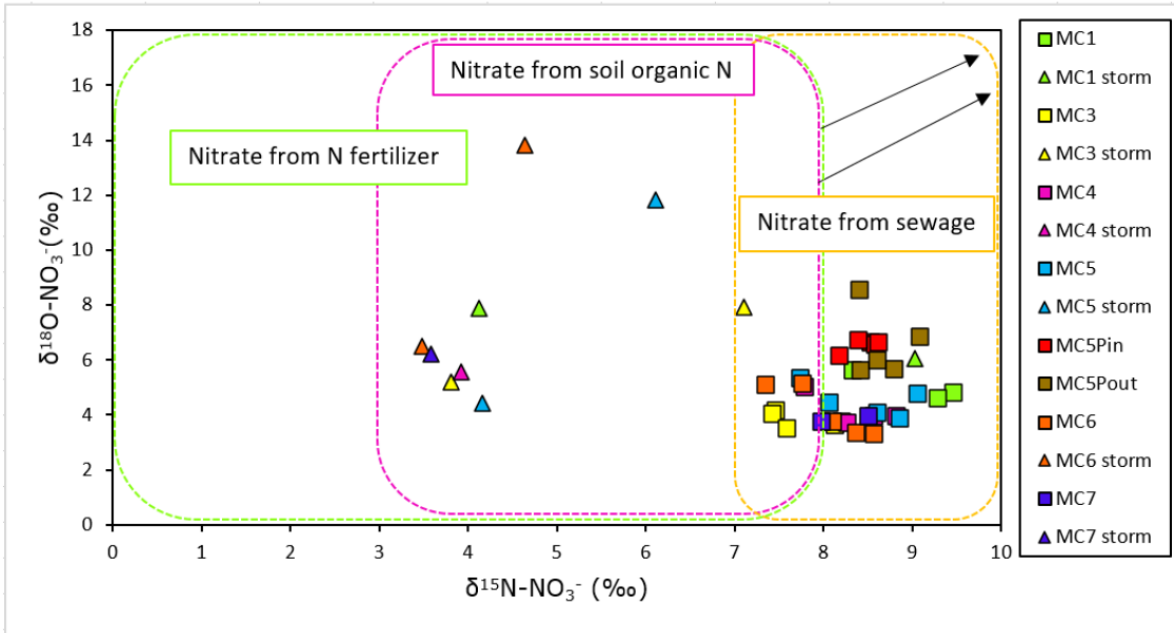


**Figure C-1:** Distribution of  $\delta^{15}\text{N}$  and  $\delta^{18}\text{O}$  from different nitrate sources. Figure created by de Azevedo Torrellas (2021). The isotope ranges and denitrification lines were taken from Zhang et al., 2019. This figure shows that the most significant source of nitrate in the upper Meadow Creek watershed is likely leaky sewage and sanitary systems. MC1 -7 (seen on the right) are the 7 different sampling points along upper Meadow Creek from upstream to downstream. Point MC4 corresponds to the sampling point at zone reach 1 at this paper and MC7 corresponds to the sampling point at zone 3.

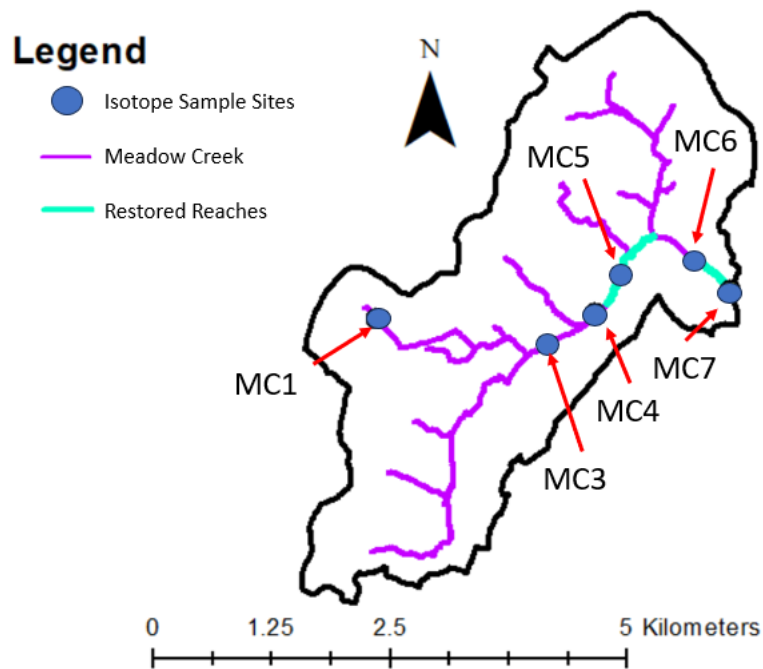


**Figure C-2:** Sampling points for isotope analysis. These points are more numerous than the number of sampling points used in chapter 4.

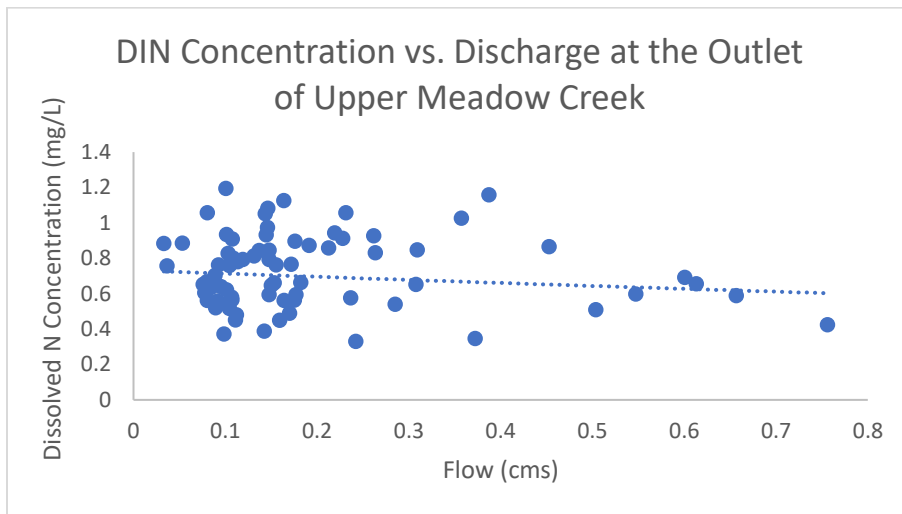


**Figure C-3:** Dissolved inorganic nitrogen (DIN) Concentration vs. Discharge at Zone 3 of Upper Meadow Creek at baseflow. This graph suggests a slightly negative relationship between DIN concentrations and discharge at Meadow Creek.

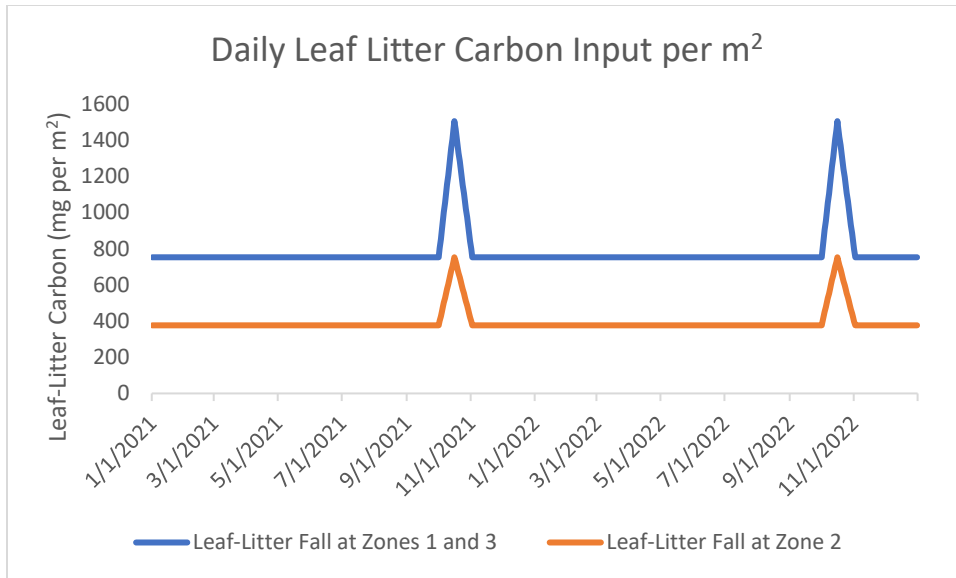


**Figure C-4:** Leaf-litter C inputs per square meter at each reach zone. Webster et. al (2016) leaf-litter inputs include a spike in leaf-litter fall during the October leaf-out period each year. Zone 2 leaf-litter fall is 50% of the other zone reaches due to its relatively lack in tree-canopy.

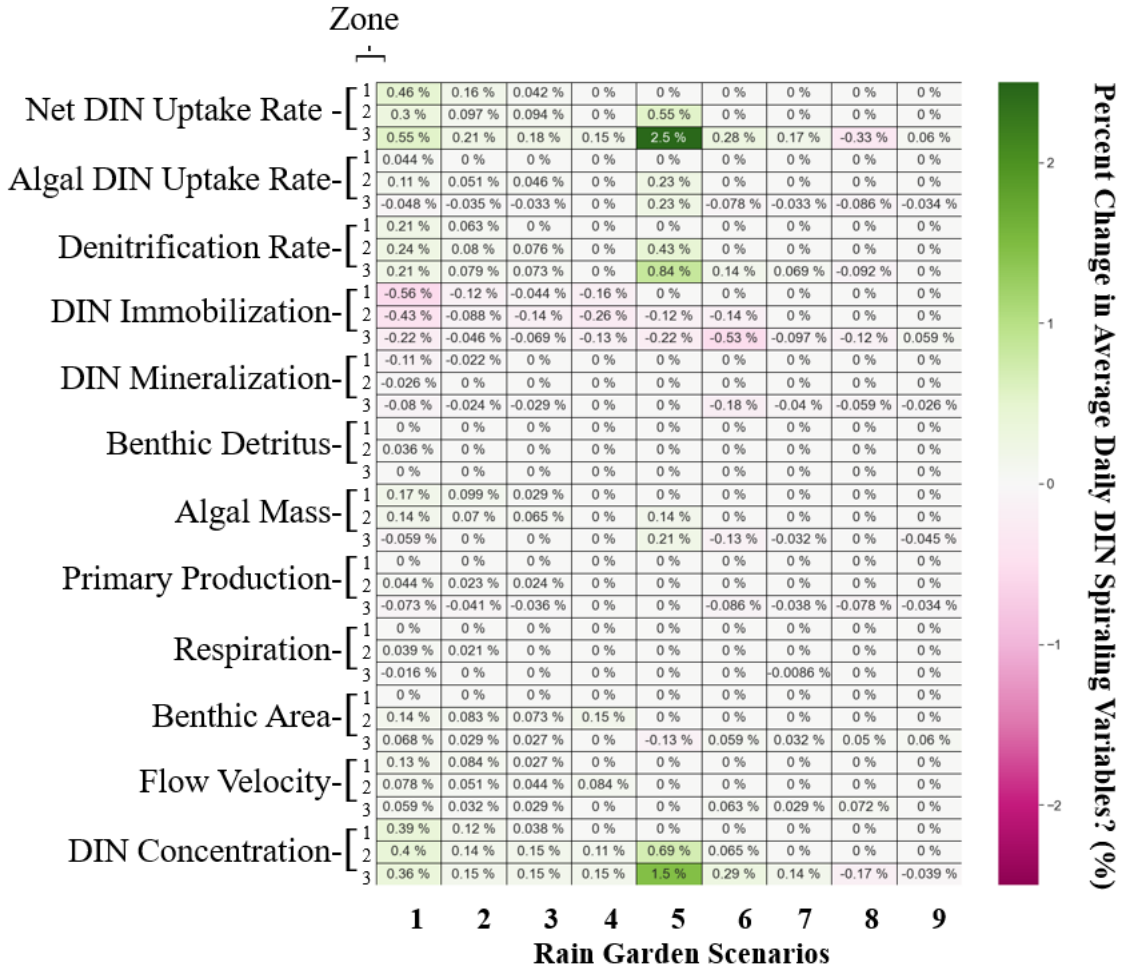


**Figure C-5:** Simulated percent changes in daily DIN spiraling variables at the three zones under the nine rain garden scenarios on a per hectare implemented basis. Raingarden scenarios are numbered at the bottom according to the subbasin where single 10 x 10-meter raingardens were implemented at all residential parcels. The numbers in brackets on the left indicate the zone.

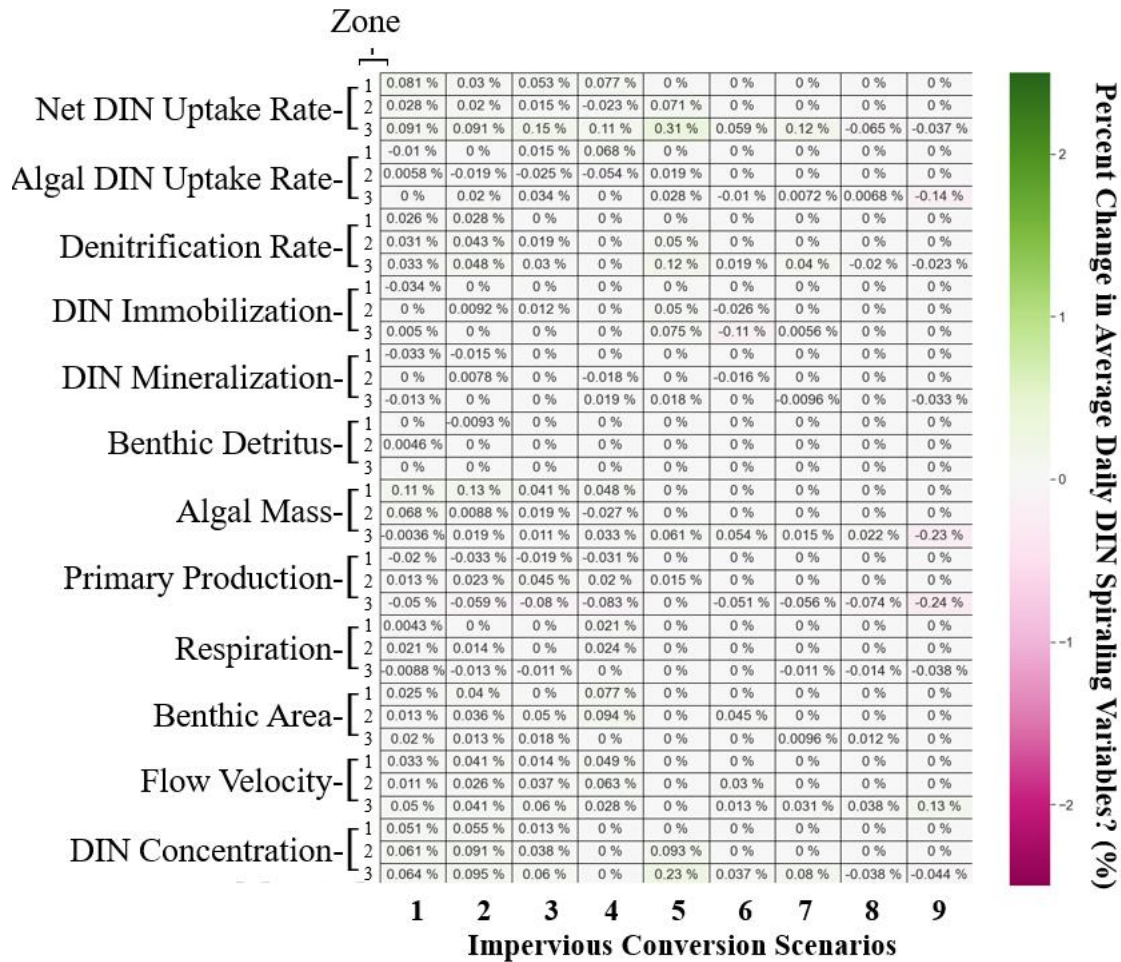


**Figure C-6:** Simulated percent changes in daily DIN spiraling variables at the three zones under the nine impervious conversions to green space scenarios on a per hectare implemented basis. Impervious conversion scenarios are numbered at the bottom according to the subbasin. The numbers in brackets on the left indicate the zone.

**Table C-1:** STOICMOD-SSHBS in-stream ecosystem parameters. Asterisks (\*) by the value indicate that it is a calibrated value. Otherwise, values were obtained by Lin et al. (2021) and Webster et al. (2016).

Variable	Description	Units	Value
$U_{\max,N}$	Max Algal Uptake of N	mgN/mgC/d	0.053
$U_{\max,P}$	Max Algal Uptake of P	mgP/mgC/d	0.00731
$k_{\text{half,algae,N}}$	Half saturation constant for algae N uptake	mgN/m <sup>3</sup>	14
$k_{\text{half,algae,P}}$	Half saturation constant for algae P uptake	mgP/m <sup>3</sup>	2
$k_s$	Algae Self-limitation coefficient	m <sup>2</sup> /mgC	0.0015
$\Phi_{\text{algae}}$	Algae Q10 coefficient	unitless	1.1*
$\Phi_{\text{detritus+heterotrophs}}$	Detritus and heterotrophic Q10 coefficient	unitless	1.3*
$\alpha$	Initial slope parameter for photosynthesis	unitless	0.12*
$G_{\max, \text{zone 1}}$	Maximum algae growth rate at zone 1	d <sup>-1</sup>	0.0035*
$G_{\max, \text{zone 2}}$	Maximum algae growth rate at zone 2	d <sup>-1</sup>	0.004*
$G_{\max, \text{zone 3}}$	Maximum algae growth rate at zone 3	d <sup>-1</sup>	0.0035*
$\sigma_{\text{algae}}$	Entrainment parameter for algae	unitless	0.5
$\sigma_{\text{detritus}}$	Entrainment parameter for detritus	unitless	0.4
$k_{\text{miners}}$	Maximum detritus decay rate for miners	d <sup>-1</sup>	0.01
$k_{\text{immobilization}}$	Maximum detritus decay rate for immobilizers	d <sup>-1</sup>	0.1
$k_{\text{half,I,N}}$	Half saturation constant for immobilizers N uptake	mgN/m <sup>3</sup>	90
$k_{\text{half,I,P}}$	Half saturation constant for immobilizers P uptake	mgP/m <sup>3</sup>	20
$r_{\text{detritus}}$	Respiration rate for detritus	d <sup>-1</sup>	0.08*
$r_{\text{miners}}$	Respiration rate for miners	d <sup>-1</sup>	0.05
$r_{\text{immobilizers}}$	Respiration rate for immobilizers	d <sup>-1</sup>	0.2

**Table C-2:** Minimum, mean, and maximum simulated uptake rates at each zone.

Daily Uptake (mg N/m <sup>2</sup> )	Zone 1			Zone 2			Zone 3		
	Min	Mean	Max	Min	Mean	Max	Min	Mean	Max
Algal	1	17	33	1	19	31	1	15	34
Denitrification	10	28	33	7	27	33	7	24	32
Immobilization	6	11	38	3	5	20	4	11	36
Mineralization	-9	-30	-52	-7	-20	-35	-9	-26	-45
Net DIN Uptake	-24	12	33	-8	21	35	-23	8	32

Daily Benthic Mass (mg/m <sup>2</sup> )	Zone 1			Zone 2			Zone 3		
	Min	Mean	Max	Min	Mean	Max	Min	Mean	Max
Algae	39	1278	5796	19	1509	5830	12	993	5526
Detritus	928	1562	3034	503	879	1653	914	1589	3051

**Table C-3:** Minimum, mean, and maximum benthic algae and detritus mass at each zone.

**Table C-4:** N inputs into the stream from the subbasin, total uptake from each zone reach, and the total % uptaken by the stream ecosystem under the status quo scenario.

Status Quo				
N Input from Subbasins (kg)	Zone 1 Uptake (kg)	Zone 2 Uptake (kg)	Zone 3 Uptake (kg)	% Uptake
23,620	23	124	55	0.86

**Table C-5:** N inputs into the stream from the subbasin, total uptake from each zone reach, and the total % uptaken by the stream ecosystem under the rain garden scenarios.

Subbasin	Rain Garden				
	N Input from Subbasins (kg)	Zone 1 Uptake (kg)	Zone 2 Uptake (kg)	Zone 3 Uptake (kg)	% Uptake
1	23,951	23	127	55	0.86
2	23,708	23	125	55	0.86
3	23,737	23	125	55	0.86
4	23,655	23	124	54	0.85
5	23,702	23	124	55	0.85
6	23,715	23	124	55	0.85
7	23,844	23	124	55	0.85
8	23,636	23	124	54	0.85
9	23,614	23	124	54	0.85

**Table C-6:** N inputs into the stream from the subbasin, total uptake from each zone reach, and the total % uptaken by the stream ecosystem under the green roof scenarios.

Subbasin	Green Roofs				
	N Input from Subbasins (kg)	Zone 1 Uptake (kg)	Zone 2 Uptake (kg)	Zone 3 Uptake (kg)	% Uptake
1	23,516	22	123	54	0.85
2	23,603	23	124	55	0.86
3	23,608	23	124	55	0.86
4	23,612	23	124	55	0.86
5	23,614	23	124	55	0.86
6	23,577	23	124	54	0.85
7	23,591	23	124	55	0.86
8	23,630	23	124	55	0.85

**Table C-7:** N inputs into the stream from the subbasin, total uptake from each zone reach, and the total % uptaken by the stream ecosystem under the impervious surface conversion scenarios.

Subbasin	Impervious Conversion				
	N Input from Subbasins (kg)	Zone 1 Uptake (kg)	Zone 2 Uptake (kg)	Zone 3 Uptake (kg)	% Uptake
1	24,072	23	128	55	0.86
2	23,744	23	125	55	0.85
3	23,760	23	125	55	0.85
4	23,666	23	124	54	0.85
5	23,715	23	124	55	0.85
6	23,712	23	124	55	0.85
7	23,860	23	124	55	0.85
8	23,652	23	124	54	0.85
9	24,059	23	124	54	0.84